Sol-Gel Synthesis and Properties of Nanoscopic Aluminum Fluoride

DISSERTATION

zur Erlangung des akademischen Grades
doctor rerum naturalium
(Dr. rer. nat.)
im Fach Chemie

eingereicht an der
Mathematisch-Naturwissenschaftlichen Fakultät I
Humboldt-Universität zu Berlin

von
M.Sc. (Chemistry) Gehan Eltanany

Präsident der Humboldt-Universität zu Berlin
Prof. Dr. Christoph Markschies

Dekan der Mathematisch-Naturwissenschaftlichen Fakultät I
Prof. Dr. Christian Limberg

Gutachter:

1. Prof. Dr. Erhard Kemnitz
2. Prof. Dr. Klaus Rademann

Tag der mündlichen Prüfung: 01. Oktober 2007

Abstract

Aluminum fluoride (HS-AlF_3) prepared via sol-gel synthesis route under non-aqueous conditions exhibits high surface area and an extremely strong Lewis acidity, comparable with some of the strongest known Lewis acids such as SbF_5 and ACF. The basis of its unusual properties is the sol-gel fluorination of aluminum alkoxide with anhydrous HF in organic solvents yielding first an amorphous catalytically inactive precursor with high surface area, which can be dried and eventually post-fluorinated to get HS-AlF_3. In this thesis, all steps of the synthesis route were thoroughly investigated. The results of these investigations together with detailed analysis of the obtained materials are reported and discussed.

HS-AlF_3 supported on Al_2O_3 with different HS-AlF_3 loadings was prepared by wet impregnation method. The properties of the HS-AlF_3/Al_2O_3 samples as Lewis acid catalyst were evaluated for $CHClF_2$ dismutation and $CBrF_2CBrFCF_3$ isomerization.

The preparation of AlF_yO_x via sol-gel method is also reported. AlF_yO_x prepared is amorphous and have high surface are up to 240 m^2/g.

Keywords:

Sol-gel synthesis, nano-alumnium fluoride, Lewis acidity, catalyzed halogen exchange, nano-aluminum oxide fluoride.

Zusammenfassung

Aluminiumfluorid (HS-AlF_3), das mit Hilfe des Sol-Gel-Verfahrens unter nicht-wässrigen Bedingungen hergestellt wird, weist eine extrem große Oberfläche und eine hohe Lewis-Acidität auf, die mit den stärksten bekannten Lewis-Säuren wie SbF_5 und ACF vergleichbar ist. Diese ungewöhnlichen Eigenschaften werden im Ergebnis einer neuen Sol-Gel-Synthese erhalten, die die Fluorolyse eines Aluminium-Alkoxids durch wasserfreien Fluorwasserstoff in organischen Lösungsmitteln zur Grundlage hat. Das zunächst in einer amorphen, katalytisch inaktiven Vorstufe mit großer Oberfläche gebildete Gel wird nach anschließender Trocknung mit gasförmigen Fluorierungsmitteln nachfluoriert, wobei die aktive Form des HS-AlF_3 erhalten wird. Im Rahmen der vorliegenden Arbeit wurden alle Schritte dieses Syntheseweges untersucht und die Ergebnisse einschließlich einer detaillierten Analyse der erhaltenen Materialien diskutiert.

Des Weiteren wurde HS-AlF_3 durch eine Imprägnierungs-Methode auf das Trägermaterial Al_2O_3 aufgetragen, wobei verschiedene Beladungen mit HS-AlF_3 getestet wurden. Die Eigenschaften des HS-AlF_3/Al_2O_3 als Lewis-Säure-Katalysator wurden mittels der Dismutierung von $CHClF_2$ und der Isomerisierung von $CBrF_2CBrFCF_3$ bestimmt.

Die Herstellung von AlF_yO_x mit Hilfe des Sol-Gel-Verfahrens ist ebenfalls beschrieben, wobei das Produkt amorph ist und eine große Oberfläche von bis zu 240 m^2/g aufweist.

Schlagwörter:

Sol-Gel Verfahren, Nano-Aluminiumfluorid, Nano-Aluminiumoxidfluorid, Lewis-Acidität, katalysierter Halogenaustausch.

Table of Contents

Acknowledgements

I wish to express my deep graditutude to my advisor Prof. Kemnitz. I would like to thank him for introducing me to an interesting research theme. I also appreciate his valuable time spent on deliberating and discussing this project with me and for closely following the work.

I am very grateful to Dr. St. Rüdiger and Dr. U. Groß for much helpful discussion, ideas, and advices throughout the study. Both of them have shown me some of the grandeur and enthusiasm involved in the quest to obtain accurate results.

I would like to thank Dr. G. Scholz for MAS-NMR measurements and for fruitful discussion. I am very grateful to Dr. Michael Feist for the thermal analysis and Mrs. S. Bäßler for the TPD and IR-PAS measurements and fluoride analysis.

I wish to express my gratitude to Dr. S. Coman, Dr. S. Troyanov, and Dr. Dimitrov. The discussions with them and the suggestions from them were very helpful. I extend my special thanks to former graduates Dr. K. Janmanchi, Dr. T. Krahl, Dr. Z. Li and Dr. H. Prescott for their help whenever I needed it. Their assistance made my research work easier to conduct and progress in smooth manner. I would like to thank all the members and former members in Prof. Kemnitz's group who have been helpful in so many different ways in completing my thesis.

I thank also the Deutsche Forschungsgemeinschaft (Ke 489/22-1;22-2) and European Commission Project FUNFLUOS (NMP3-CT-2004-505575) for the financial support. I am very grateful to the cooperation with the group of Prof. J. Winfield (Glasgow, UK), Dr. S. Schorder (University of Manchester, UK), and Prof. A. Tressand (Bordeaux, Fr).

And last, I would like to thank all my friends in the Humboldt University and my friends outside the Humboldt University. Special thanks for my family for their support and caring all the time.

List of Abbreviations, Acronyms, and Symbols

Å	angstrom
AlF_3	aluminum fluoride
Ar	argon
a.u	arbitrary units
BE	binding energy
BET	Brunauer-Emmett-Teller and their adsorption model
BJH	Barret-Joyner-Halenda and their adsorption model
°C	degree celsius
°C/min	degree celsius per minute
$CDCl_3$	chloroform-d
$CBrF_2CBrFCF$	1, 2-dibromohexafluoropropane
CF_4	tetrafluormethan
$CF_3CBr_2CF_3$	2, 2-dibromohexafluoropropane
CF_3CCl_3	1,1,1-trichlorotrifluoroethane
CH_2F_2	difluorometahne
CH_2FCF_3	1,1,1,2-tetrafluoroethane
$CHClF_2$	difluorochloromethane
$CClF_2CCl_2F$	1,1,2-trifluorotrichloroethane
CCl_2F_2	dichlorodifluoromethane
CNRS	Centre National de La Recherche Scientificue.
CO	carbon monoxide
DBP	dibromohexafluoropropane
DMSO-d_6	dimethyl-d_6 sulphoxide
DTA	differential thermal analysis
DTG	differential thermogravimetry
EDX	energy dispersive X-ray
FTIR	fourier transformation infrared spectroscopy
GC	gas chromatography
h	hour
HF	hydrogen fluoride
Hz	hertz
IC	ionic current
IR-CO	infrared radiation adsorption of carbon monoxide
IR-PAS	infrared radiation-photoacoustic spectroscopy
MAS NMR	magic angle spinning nuclear magnetic resonance
mg	milligram

µl	microliter
ml	milliliter
mm	millimeter
mol	mole
MS	mass spectrometry
N_2	nitrogen
NMR	nuclear magnetic resonance
PDF No	powder diffraction file number
ppm	part per million
Py	pyridine
S_{BET}	specific surface area calculated by BET method
STP	standard temperature and pressure
TEM	transmission electron microscopy
TG	thermogravimetric analysis
TPD	temperature-programmed desorption
UMIST	University of Manchester Institute of Science and Technology, UK
XAFS	X-ray absorption fine structure
XANES	X-ray absorption near edge structure
XPS	X-ray phtotoelectron spectroscopy
XRD	X-ray diffraction

Chapter 1

Introduction

Metal oxides are very common commodities, which are finding wide variety of uses including catalysts, supports for heterogeneous catalysts, sensors, etc. [1-6]. Although metal oxides doubtless are the most widely used compounds in industry, the interest in them became an additional push by the fast developing nano-technology. Evidently, the sol-gel synthesis in the meantime has been so widely developed that nano-metal oxides - either pure or organic-inorganic hybrid materials - are available now [7-8]. Hence thousands of papers related on nano-metal oxides appeared over the last decade and their number is still rising.

The contrary holds for metal fluorides, although they often exhibit properties superior to that of metal oxides. Beside other reasons, the lack of a powerful synthesis route as the sol-gel for metal oxides is one of the major reason for this situation. Metal fluorides have interesting optical, electrical, and magnetic properties, making them interesting for a wide variety of applications as optical components, ionic conductors, and ferroelectrics [8-15]. Aluminum fluoride, in particular, has a number of current and potential applications [16-25]. It is used, for example, as an additive to the molten electrolyte of the aluminum production cell in order to lower the melting point and increase the electrical conductivity. Another application which seems very promising is its utilization as a component of glasses [12, 14]. Moreover, among metal fluoride catalysts and catalyst supports for halogen exchange reactions, AlF_3 is one of the most important catalyst [19-25]. Halogen exchange reactions of halofluorocarbons are of interest for the production of hydrofluorocarbons (HFCs) as Freon-alternatives and in general for the synthesis of new fluorinated organic compounds to be used in pharmaceutics. The most prominent chlorine-fluorine exchange reactions are: (i) dismutation of CFCs and HCFCs, (ii) isomerization reactions, and (iii) fluorination reactions of halocarbons with gaseous HF. For heterogeneous Cl/F exchange, catalysts with strong Lewis acid sites are required. These sites are assumed to be catalytically active for the Cl/F exchange reactions [26]. For fluorination reactions which need very strong Lewis acidic sites, SbF_5 is the most common catalyst (SbF_5, Swarts reaction) [19]. However, it is very difficult to handle SbF_5 practically because it fumes strongly in the moist air due to its hygroscopic properties. Recently, aluminum chlorofluoride (ACF) has been found to be a strong solid Lewis acid as SbF_5. Nevertheless, the compound is extremely hygroscopic and this limits its application for technical reactions.

As stated above, aluminum fluoride has received great attention due to its great potential as catalyst in a range of Lewis acid catalyzed reactions including halogen exchange reactions. However, these applications are dependent on the phase structure of

AlF_3. Accordingly, various methods have been used to prepare AlF_3, such as gas phase fluorination of high surface area aluminum oxide with fluorine gas [27], hydrofluoric acid [28] HCFCs, CFCs, HFCs [29-31], liquid impregnation with hydrogen fluoride [32-33], by plasma fluorination of alumo-zeolites [34] or by decomposition of fluoroaluminates at temperatures higher than 460 °C [33].

More recently, a new novel sol-gel synthesis method for the preparation of high surface aluminum fluoride (HS-AlF_3) was developed [35-36]. This new development may be considered as a breakthrough not only in nano-aluminum fluoride synthesis but also for nano-metal fluorides in general. The preparation HS-AlF_3 is carried out under non-aqueous conditions. The method involves a sol-gel state in reaction of aluminum alkoxide ($Al(OR)_3$, R is, e.g., *CH_3, C_2H_5, C_3H_7 or C_4H_9*) dissolved in water free isopropanol with HF dissolved in non aqueous solvent to afford the fluorolysis of an Al-OR bond resulting in the formation of an Al-F-bond. In case of aluminium fluoride, this fluorolysis reaction is incomplete; hence, a second gas phase fluorination step is applied to get the pure high-surface-area of AlF_3. The aluminum fluoride prepared according to this method is X-ray amorphous, has a very high surface area and Lewis acidity comparable to that of SbF_5 and ACF [36].

It was found that HS-AlF_3 is able to catalyze the isomerization reaction of 1,2-dibromohexafluoropropane to 2,2-dibromohexafluoropropane with almost 100% conversion at room temperature [36-37]. This reaction is known to proceed only with the strongest Lewis acids as ACF and SbF_5 [38-40]. This catalytic activity provides strong evidence for the superior Lewis acidity of HS-AlF_3 prepared via the new sol-gel synthesis route.

As discussed above, the sol-gel synthesis of HS-AlF_3 is the first example for a direct sol-gel synthesis of nano-metal fluorides resulting in material with exciting properties which remarkably differ from that of classically prepared AlF_3-phases. Although the general reaction procedure was developed at the beginning of this work, practically nothing was really know about the influence of the synthesis parameters in the wet sol-gel-process as well as for the second gas-phase fluorination step necessary to get pure HS-AlF_3. Hence it was the objective of the present thesis to investigate in detail all these parameters and their influence on the materials properties since aluminum fluoride is the first material synthesized this way, and hence, no information from literature were available at that stage.

The most interesting properties of the nano-aluminum fluoride for catalytic applications which were in the focus of this thesis were:

- Surface area
- Porosity
- Particle size
- Performance (powder vs. supported material)
- Acidity (strength and concentration)
- Catalytic performance in selected probe reactions

Hence, the synthesis parameters under investigation were:

1. in the sol-gel-step
   - Concentration of the reaction systems
   - Temperature
   - Aluminum alkoxide precursor
   - Drying conditions
   - Aging
2. in the gas-phase post-fluorination step
   - Temperature
   - Fluorination agent
   - Partial pressure of the fluorination agent
   - Fluorination time
   - Fluorination agent concentration

Chapter 2

Literature Survey

This Literature survey covers topics that are related to sol-gel preparation of aluminum fluoride and metal fluorides in general. Because of its relevance the principles of sol-gel synthesis, which are typically investigated for metal oxides will briefly be reflected too. A review of preparation of crystalline AlF_3 phases as well as synthesis strategies towards high surface AlF_3 phases will be presented.

2.1 The sol-gel method

Sol-gel method is a wet-chemical synthesis used to prepare versatile materials with high surface areas at lower temperatures than those used by conventional methods [7, 41-42]. The approach is based on the hydrolysis and following condensation of metal alkoxides ($M(OR)_x$) or hydroxoalkoxides ($MO(OR)_x$) (or molecules having already metal-oxygen bonds), where R is an alkyl group (R = CH_3, C_2H_5, etc.) and M is a metal atom with the oxidation state x. The first step of these reactions is the nucleophilic substitution of the alkoxides groups (OR) by hydroxyl groups (OH) as shown in 2.1.

hydrolysis: $\equiv M{-}OR + H_2O \longrightarrow \equiv M{-}OH + ROH$ (2.1)

In the condensation reaction (2.2), M-O-M linkages are formed resulting in a three dimensional network "gel" with the liberation of water or alcohol. The gel state is described as a viscoelastic material composed of interpenetrating solid and liquid phases. There are many factors that influence the properties of the final products prepared using the sol-gel process including acidity of the hydrolysant, gelation conditions, hydrolysis ratio, solvent property, and drying conditions and procedures.

condensation: $\equiv M{-}OH + HO{-}M \equiv \longrightarrow \equiv M{-}O{-}M \equiv + XOH$ (2.2)

Through the sol-gel method, a good control of the sample morphology, texture, and chemical composition can be attained by monitoring the synthesis parameters. It is also possible to prepare materials in a wide variety of forms: ultra-fine powders, fibers, solids, aerogels, thin films, and bulk materials at ambient temperatures (Figure 2.1) [43]. Ambient processing conditions also enable encapsulation of numerous organic, organometallic, and biological molecules within these sol-gel derived inorganic matrixes and vice versa. The resulting properties of the material are determined by the nature of the dopant molecule. This synthetic approach is well recognized as an important direction for the design and synthesis of a wide range of novel materials, especially in the areas of photonics and

chemical sensors. In addition, this technique has been widely employed in the fields of catalysis, ceramics, coatings, and glasses industries.

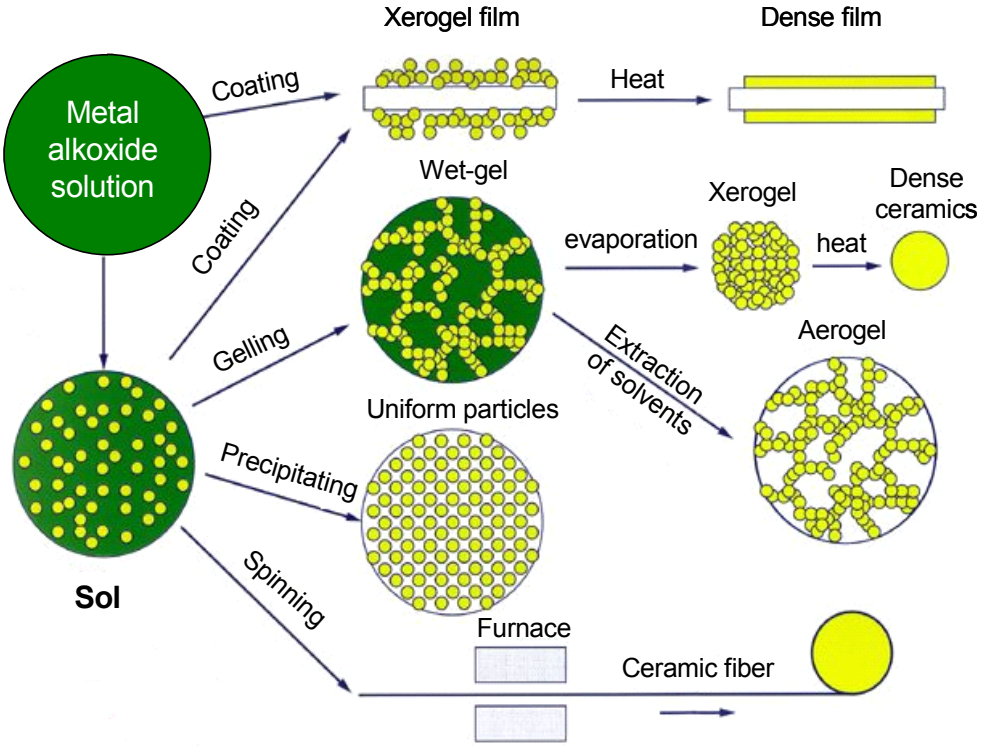

Figure 2.1. Sol-gel technologies and their applications [45].

Applications of sol-gel prepared metal oxides

The sol-gel process has been used to prepare high surface area materials such as Al_2O_3, MgO, ZrO_2, and TiO_2 [41-42, 44-47]. The very high surface area and mesoporosity associated with these materials make them attractive in the field of catalysis [41-53]. The most important characteristic of the sol-gel preparation of catalytic materials is its ability to (i) maintain high purity (because of the purity of the starting materials), (ii) change morphological characteristic such as surface area, pore volume, and pore size distribution, (iii) introduce several components in a single step, (iv) produce samples in different physical forms, and (v) vary the compositional homogeneity at a molecular level.

In coating industry, a great advantage with the sol-gel method is the possibility to use very large substrates. The homogeneous mixture of several components in liquid state makes it possible to vary the optical materials over a wide range of compositions at molecular level, hence, the optical properties of the materials are tailored, to change the refractive index [54]. Moreover, multi-core fibers or micro-structured fibers with gradients in the dopant

concentration or even mixed or multiple doping conditions can easily be produced using sol-gel process. Thin films or fibers can be produced directly from solution by techniques such as dip coating or spin drawing.

Another area where sol-gel techniques had widespread interest is the ceramic industry. Ceramic materials are normally synthesized by the direct reaction, in the solid state, of a mixture powders. For the reaction to proceed at reasonable rate, high mobility of the reactants and maximum contact surface between the reacting particles are necessary. The rates of these processes are enhanced by higher temperature and finer particle size. However, metastable phases are difficult to obtain and it is not possible to control the size and morphology of the solid particles. The sol-gel process allows preparation ceramic powders of high purity, fine spherical shape, narrow distribution of particle size, and homogeneity [7].

Sol-gel process is also important in the glass industry. Glasses doped with nanoparticles semiconductors or metals have been widely investigated for applications in nonlinear optics. Such materials are normally prepared by a traditional melt route. But the sol-gel process offers more advantages in terms of flexibility of composition and structure. It is also possible to fabricate titanium silicate glasses or graded-index optical fibers with more cost effective and with higher quality. Through the sol-gel process a wide range for the synthesis of glasses with novel composition is opened since melt-related problems such as liquid immiscibility, phase separation, or crystallization upon cooling, are now suppressed.

Inorganic fluorides

So far, sol-gel process for the preparation of inorganic oxides have been extensively studied and applied in numerous applications over the last thirty five years. However, in contrast to oxides, much fewer efforts have been made to study inorganic fluorides, oxyfluorides, and oxid/fluoride composites. Inorganic fluorides have interesting and useful optical, electrical, magnetic, and catalytic applications [9-19]. Because of the potential importance of these technologies, there is currently research of interest in developing new synthetic method of the fluorides. Many attempts were made to prepare metal fluorides glasses via sol-gel method, where an oxide gel is converted to fluorides with various kinds of fluorination agents. Sol-gel process offers many advantages for producing fluoride materials: (i) the level of purity can be controlled rather than being limited to a fluoride precursor, (ii) viscous sintering below the crystallization temperature should eliminate the

formation of crystalline defects, (iii) thin films, fibers, and monoliths can be made giving it broader range of applications.

Fujihara et al. reported the aqueous synthesis of $BaMgF_4$ particles [54]. They used mixture of barium, magnesium, and europium acetate in isopropyl alcohol. Trifluoroacetic acid and water was added to the solution to afford trifluoroacetate gel. By calcination at 600 °C, crystalline $BaMgF_4$ particles were obtained. A similar route was also employed to prepare $SrAlF_5$ [54]. Riman et al. reported the sol-gel synthesis of amorphous ZBLA glass, which is an acronym to denote the fluoride component of zirconium, barium, lanthanum, aluminum, and sodium. First a porous oxide gel containing zirconium, barium, lanthanum, aluminum was prepared followed by fluorination with HF [13]. Another attempt was made to prepare SiO_2-MgF_2 composite. MgF_2 sol was prepared by the reaction of HF with methanolic aqueous H_2O_2 and $Mg(OCH_3)_2$. MgF_2 sol and silicon alkoxide sol were then mixed together to yield nanoparticles dispersion in an amorphous matrix. After calcination SiO_2-MgF_2 composite is obtained [55]. Following these initial publications, several more amorphous and crystalline metal fluorides were reported [56-57].

An interesting synthesis route for the preparation of high surface metal fluorides was developed by Kemnitz and co-workers [35]. In the first step, a metal alkoxide in non aqueous solvent is fluorinated with anhydrous HF to yield the metal alkoxide fluoride gel. A gas phase fluorination is then applied to get the amorphous metal fluoride. This new development has proved to have a great potential for the preparation of many metal fluorides, fluorometallates and related systems, which can be used as bulk materials for, e.g., catalysis, pressed to transparent optical materials, or for preparing thin metal fluoride coatings on different materials [58-62].

2.2 Aluminum fluoride structure and catalytic activity

The structural phases of aluminum fluoride are very diverse, all of which form a series of MF_3 modifications (Figure 2.2a-e). The most known and well characterized with reliable synthetic and structural data available phases of AlF_3 are α- and β-AlF_3 [56-61].

α-AlF_3 is prepared by passing gaseous hydrogen fluoride over anhydrous $AlCl_3$ at 800 °C. It is the most thermodynamic stable phase of aluminum fluoride and is made of AlF_6 octahedra three dimensionally linked together. α-AlF_3 adopts a rhombohedrally form of the ReO_3 structure at room temperature (Figure 2.2a). At approximately 460 °C, it undergoes reversible phase transition to the cubic α-ReO_3 structure. In the high-temperature cubic phase, all the AlF_6 octahedra are connected via bridging (corner shared) fluorine atoms with

Al-F-Al bond angles of 180°. Whereas in the low-temperature rhombohedral phase, the octahedra are tilted along their 3-fold axis, resulting in zigzag chains of octahedra, Al-F-Al bond angles of 157.9°. Theoretical investigation of the surface of α-AlF_3 showed that the surface of α-AlF_3 is terminated by a layer containing two F^- ions which form a zigzag chain across the surface and mask the Al^{3+} ions from the surrounding environment [60]. These results are also in agreement with the experimental results that the perfect α-AlF_3 surfaces are chemically inert and do not act as a Lewis acid catalyst.

The *β*-AlF_3 phase (Figure 2.2b) has a more open structure of the hexagonal tungsten bronze (HTB) type, where the corner sharing rings of six AlF_6 octaherdra form hexagonal channels running along the c-axis [61-62]. The surface structure along the channels in c direction is wave-shaped with Al atoms on the top of the waves. As a result of this open structure, the density of *β*-AlF_3 is to great extent lower than that of α-AlF_3. *β*-AlF_3 shows moderate catalytic activity. A recent model presented by the group of Harrison et al showed that *β*-AlF_3 contains co-coordinatively unsaturated five-fold aluminum ions at the surface, which gives explanation for its catalytic properties.

In addition to α- and *β*-AlF_3 phases, there are also other metastable phases, which have been described in the literature, all of which built of octahedral AlF_6 units sharing only corner [61-64]. These new meta-stable phases of AlF_3, designated as θ, *η*, κ, have been synthesized via different routes [61-64]. *η*-AlF_3 (Figure 2.2c) has a structure similar to *β*-AlF_3 phase. The density of *η*-phase is lower than α- and *β*-AlF_3. θ-AlF_3 phase resembles to a great extent the pyrochlore structure (Figure 2.2d) and its microporous nature is similar to that of *β*-AlF_3 and *η*-AlF_3. Another phase is κ-AlF_3 (Figure 2.2e). It has linear channels running though the crystal comprised of five, four and three rings of corner-shared AlF_3 octahedra.

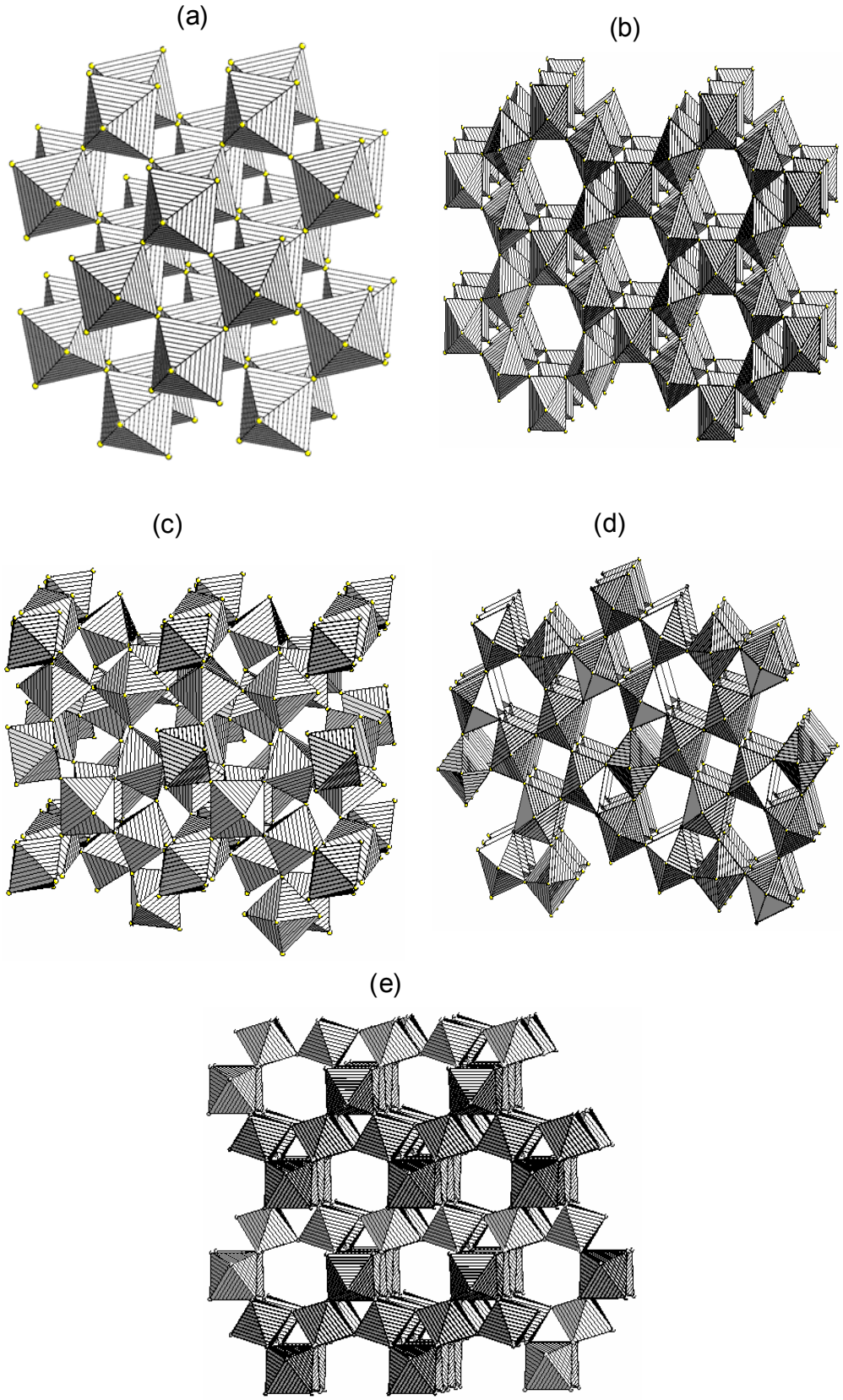

Figure 2.2. Crystal structures of (a) α-AlF_3, (b) *β*-AlF_3, (c) *η*-AlF_3, (d) θ-AlF_3, (e) κ-AlF_3.

The summary of some preparation routes for the aluminum fluorides is provided in Figure 2.3 [61-64]. All the metastable phases of aluminum fluoride undergo irreversible phase change to α-AlF_3 in the temperature range of 450 to 650 °C.

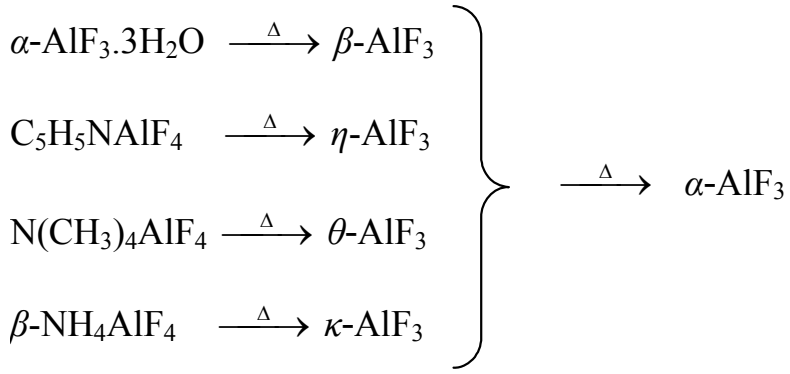

Figure 2.3 Preparation of meta-stable AlF_3 and their phase transition.

It has been reported that the meta-stable phases of AlF_3 (θ, η, κ, β) owing to their open structure, possess interesting catalytic activity for halogen exchange reactions. However, the catalytic activity is to great extent dependent on the phase structure of AlF_3 [10]. Hence, an aluminum fluoride with open structures is more likely to possess an excellent catalytic activity than the thermodynamically more stable forms because it deviates from the close packed structure. Accordingly, several attempts were made to produce such modifications of aluminum fluoride, especially synthesis procedures at low temperature [61]. One of the common method for preparation of aluminum fluoride is the treatment of γ-Al_2O_3 with HF or fluorocarbons at moderate temperature [61], however, as the fluorination proceeds, the surface area drops significantly, reaching the size of traditionally prepared AlF_3.

Recently, high surface AlF_3 (190 m^2/g) was prepared by plasma treatment of alumo-zeolites with NF_3 [35, 65]. However, the catalytic activity in the $CHClF_2$ dismutation of the plasma AlF_3 is similar to those found in β-AlF_3.

A new non-aqueous synthesis route based on sol-gel method to X-ray amorphous aluminum fluoride having high surface areas and high Lewis acidity (HS-AlF_3) was developed in our group. This development may be considered as a breakthrough in metal fluoride synthesis. In a first step, aluminum alkoxide dissolved in non-aqueous solvent is treated with anhydrous HF to get an amorphous catalytically inactive material precursor. The resulting precursor is then fluorinated in a second step with fluorination agent such as CCl_2F_2 to yield high surface area aluminum fluoride (HS-AlF_3).

2.3 Scope and outline

As discussed in the proceeding chapter, the synthesis of HS-AlF_3 is governed by a variety of parameters which affect its overall quality. Even the characterization of the HS-AlF_3 has been made just partly, however, the synthesis parameters influencing the HS-AlF_3 properties have not at all been investigated systematically.

Therefore, the main objectives of the present PhD-thesis were:

(i) to study the effect of synthesis parameters on the HS-AlF_3 samples properties. These factors are: concentrations, sol-gel fluorination temperature, nature of alkoxides, solvents, nature of fluorinating agent, its concentration, and temperature regime. In order to gain more insight into the structure of the HS-AlF_3 samples, the samples were investigated using various techniques (XRD, XPS, XANES, EXAFS, MAS-MNR, IR). The catalytic active sites were investigated by using in-situ IR-CO, IR-PAS of pyridine adsorbed and ammonia TPD. The gained information will be summarized and combined to describe the correlation between bulk and surface structure and catalytic activity.

(ii) to elucidate the preparation of HS-AlF_3 supported on various alumina and modified alumina by impregnation method. The factors which influence the surface area and catalytic activity were optimized. The results will provide reference for the future preparation of supported metal fluoride catalysts as well as nano metal fluorides.

(iii) to modify the synthesis method of HS-AlF_3 using an aqueous HF with varied HF/Al ratios. Several factors which influence the performance of the HS-AlF_3 samples were evaluated. Moreover, it will be demonstrated that this synthesis can result in the formation of AlF_xO_y, which are not known so far.

Chapter 3

Experimental Section

A description of the techniques and equipments used in this work is given in this Chapter. Samples prepared in this thesis were characterized for structure, texture, acidity, and catalytic activity.

3.1 Sample preparation

Sol-gel, wet impregnation and post fluorination methods were used in the preparation of the samples. The details concerning the preparation process are given in chapters 4, 5, and 7.

3.2 Methods

Freeze-drying

Freeze-drying involves the removal of water or any other solvents from a frozen product by sublimation. This method is advantageous for mild drying and conservation of sensitive products [67].

The sol-gel was dried using a Christ Alpha 2-4 freeze-dryer (LDC-1M control system). The sol-gel (400 ml) was placed in the freeze drier, frozen by liquid N_2, and dried in the freeze drier chamber for 48 h. The chamber was then evacuated (4×10^{-2} mbar) and freeze-drying process was started. At the end of the drying process, the temperature and the pressure were -25 °C and 0.1 mbar, respectively.

Microwave-assisted drying

In comparison to conventional air drying and freeze-drying, microwave drying provides a better option for the removal of solvents due to its volumetric heating mechanism [68].

In these studies a microwave digestion system (MARS 5 Express, CEM Corporation) with a 300 W maximum at a frequency of 2.45 GHz was used. The oven has a single magnetron that operates using contentious power up to 100% of the maximum power. The internal pressure and temperature were monitored by a transducer and a fiber optic probe, respectively. About 50 ml of the sol-gel was placed in closed Teflon container for microwave hydrothermal process. Microwave-assisted drying was performed under primary vacuum and argon flow[1].

[1] Microwave drying experiments was performed in the group of A. Tressaud, CNRS, Bordeaux

Plasma enhanced fluorination (PEF)

The plasma treatment was carried out at 13.56 MHz in a S.E. 80 Barrel Plasma Technology System using CF_4 gas[2]. The sample was placed on a sample holder in the center of the chamber. The sample was then subject to degassing cycles using Edwards E2M40-type pump equipped with a liquid nitrogen condenser to trap the residual gases. CF_4 gas was introduced in the inner part of the chamber and then dissociated by electron impacts occurring between the two electrodes (Figure 3.1). The neutral species and the radicals diffused from this plasma zone to the center of the reactor where they reacted with the sample. The plasma treatment was carried out at 90 °C for 1 h.

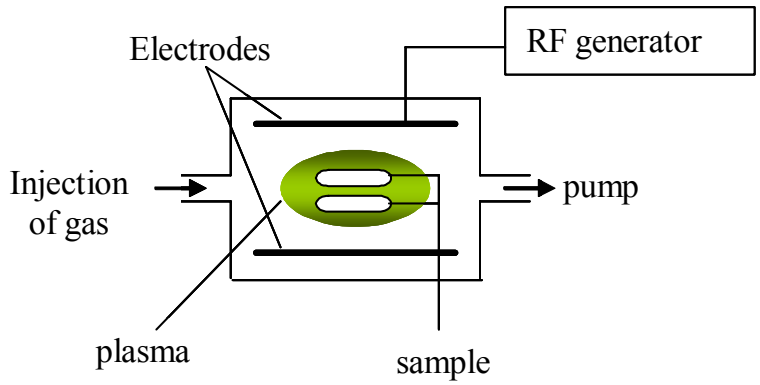

Figure 3.1 schematic diagram of plasma fluorination.

Elemental analysis

C, N, H, contents were determined by LECO CHNS-932 element analyzer. Approximately 2 mg of the sample was placed inside a silver capsule and was dropped into the *CHNS-932* furnace kept at 1050 °C, where it was completely combusted. Infrared detection was used to measure the weight percent of carbon and hydrogen, while nitrogen was measured using thermal conductivity detection.

The fluoride content was determined as followes: about 0.2-0.5 g of the samples were dissolved by melting in a mixture of 0.5 g of K_2CO_3 and 0.5 g of Na_2CO_3 in a platinum crucible for 30 min [69]. After cooling down, the obtained mixture was dissolved in water. The fluoride content in the aqueous solution was determined with an F^- sensitive electrode (FSE).

[2] Plasma fluorination experiments were performed by the group of A. Tressaud, CNRS, Bordeaux.

N_2 adsorption-desorption experiments

The specific surface area, pore size distribution, and pore volume of the samples were determined using nitrogen as an adsorbate at -196 °C using Micromeritics ASAP 2020 volumetric adsorption analyzer. The sample was loaded and outgassed in vacuum at 200 °C for 10 h before the measurements to remove the physically adsorbed water from the pores. The specific surface areas were determined according to the BET method [70]. The determination of the pore size distribution and pore volume were calculated via Barret-Joyner-Halenda (BJH) method [71].

Scanning electron microscopy (SEM)

The powder samples were mounted on double-sided adhesive carbon tape and coated with a 20 nm thick gold layer in an EMITECH K 500 sputtering equipment operated at 25 mA and under vacuum conditions better than 10^{-1} mbar. The SEM analyses were performed using Jeol JSM-60460 (Tokyo, Japan) features with EDX (Röntec).

Transmission electron microscopy (TEM)

For the preparation on the sample grid, the sample was grounded into fine powder and suspended in methanol. The powder was then dispersed onto the grid, by dipping the grid into the suspended solution. The dried grid was loaded into the sample chamber. The analysis was conducted under high vacuum. TEM experiments were carried out using Hitachi H-8110 electron microscope operated at 200 kV (LaB6 gun) with energy dispersive X-ray detector.

Thermal analysis

Thermal analysis (TG and DTA) was performed with a Netzsch STA 429 TG/DSC instrument combined with mass spectrometer, Netzsch STA 409 C skimmer-coupled system. Measurements were performed by heating in nitrogen flow from room temperature to 600 °C at a constant heating rate of 10 °C/min using Al_2O_3 as a reference. A DTA-TG sample-holder system (Pt/PtRh10 thermocouple) was used.

X-ray diffraction (XRD)

X–Ray powder diffraction (XRD) patterns of all the samples were obtained using CuKα (λ = 1.5418 Å) radiation with a Seiffert RD7 (Freiburg, Germany) diffractometer operated at 40 kV and 35 mA. Samples were placed into the samples cell and the patterns

were recorded over a range of 2θ angles from 5° to 65° with 0.05 steps and 10 s counting time per step. The crystalline phases were determined by comparing the obtained patterns with the PDF databank [72] for the known compounds.

X-ray photoelectron spectroscopy (XPS)

XPS spectra were recorded on a KRATOS Axis Ultra system operating, with monochromatized Al Kα radiation, at a pressure below 10^{-9} mbar[3]. Before recording the spectra, sample was outgassed under a pressure of 10^{-9} mbar to minimize the surface contamination. Survey spectra and high resolution scans of the Al 2p, F 1s, O 1s, photoemission lines and the valence band were recorded. Survey scans with a resolution of 0.5 eV and a pass energy of 80 eV were recorded to analyze the elemental surface composition. Additionally, high-resolution scans of the most interesting emission features were carried out with an energy grid of 0.1 eV and pass energy of 20 eV. Data acquisition times were approximately 20 min for a survey and 10 minutes for a high-resolution region scan. The obtained XPS spectra were analyzed using CASAXPS [73]. The binding energy data collected were corrected and referred to a C1s binding energy of 284 eV [74].

X-ray absorption fine structure (XAFS)

Al K-edge XAFS spectra were recorded at SOXAFS station 3.4 of the Synchrotron Radiation Source (SRS) at Daresbury Laboratory, UK. A double-crystal YB_{66} monochromator was used with the second crystal being detuned to 80% of the maximum of the Bragg peak to monochromatize the beam [75]. Higher harmonics were rejected using C/Si bilayer mirror and a Cr coated toroidal mirror was applied to focus the beam. Samples were mounted on a multi-sample stage using double-sided adhesive tape. Spectra were collected under high vacuum conditions (10^{-6} mbar) at room temperature. Spectra were taken at photon energies from 1500 to 1850 eV. Typical data acquisition times were approximately 1 h per spectrum.

F K-edge XAFS spectra were recorded at station 5U.1 of SRS at Daresbury Laboratory, UK. Undulator radiation was monochromatized using an SX700 type monochromator with a plane grating of 1200 lines/mm. All measurements were performed at room temperature after evacuating the chamber to better than 10^{-5} mbar.

[3] XPS and XAFS experiments were performed by the group of S. Schörder, UMIST, Manchester.

Liquid ^{19}F nuclear magnetic resonance (NMR)

Samples for ^{19}F studies were dissolved in $CDCl_3$ and measured in NMR tubes. The spectra were recorded on a Bruker AV 400 spectrometer at larmor frequency of 376.5 MHZ. ^{19}F chemical shifts were referenced to $CFCl_3$ (0 ppm) and deviation to ±1 ppm.

Solid state nuclear magnetic resonance (MAS NMR)

All MAS NMR spectra were measured on a Bruker AVANCE 400 spectrometer.

^{27}Al MAS NMR

^{27}Al MAS NMR spectra were recorded ($\nu_L(^{27}Al)$ = 104.2 MHz) using an excitation pulse lengths of about $\pi/9$. All ^{27}Al spectra were collected using 2.5 mm rotors at a spinning rate of 25 kHz. 1 M aqueous solution of $AlCl_3$ was used as reference for the chemical shift of ^{27}Al. The recycle delay was chosen as 1 s and the accumulation number was 16384, necessary for the highly disordered samples.

^{19}F MAS NMR

^{19}F MAS NMR spectra were recorded at $\nu_L(^{19}F)$ = 376.5 MHz and excitation pulses length of a 2 μs using 2.5 mm probe. The samples were characterized at room temperature at a spinning speed from 25 to 30 kHz to reduce most of the ^{19}F dipolar interactions and to obtain high-resolution spectra. Chemical shifts of fluorine resonance were recorded relative to C_6F_6 as a secondary standard (δ_{iso}= -166.61 ppm against $CFCl_3$).

FTIR measurements

FTIR measurements were conducted on a Perkin-Elmer 2000 spectrometer in transmission mode. About 200 mg of CsI was pressed with 2 mg of the samples, and then the samples were measured at room temperature in 4000 to 200 cm^{-1} wavenumber range.

Temperature programmed desorption of ammonia (NH_3-TPD)

NH_3-TPD technique was employed to characterize the acid strength distribution. Experiments were carried out in a fixed bed flow reactor in a temperature range of 80-500 °C. Before the TPD experiment, the sample (200 mg) was outgassed for 1h in a flow of argon (10 ml/min) to desorb the gases from the surface. The sample was then cooled down to 120 °C and exposed to a stream of NH_3. The excess of NH_3 was eliminated by heating

under argon at 120 °C for an hour. After cooling to 80 °C, the TPD program (10 °C/min, up to 500 °C, held for 30 min) was started. Desorbed NH_3 was monitored continuously via IR spectroscopy (FT-IR System 2000, Perkin-Elmer), absorbed in acid and its total amount determined by titration with sodium hydroxide.

FTIR- photoacoustic analysis (IR-PAS)

IR-PAS of pyridine was used to determine the nature of acid sites present (Lewis and Brønsted). Sample (100 mg) was outgassed at 150 °C for 15 min in the flow of nitrogen (35 ml/min), and then 60 µl pyridine was injected into the sample tube. The sample was purged with nitrogen for another 15 min to remove the physisorbed pyridine. The Spectra were recorded at room temperature over a wavenumber range of 4000-400 cm^{-1} using a Perkin-Elmer system 2000 equipped with a MTEC detection cell.

IR of adsorbed carbon monoxide (IR-CO)

IR-CO measurements were recorded on Nicolet 5700 from thermoelectron equipped with a MCTA detector and an extended KBr beam splitter, resolution 4 cm^{-1}.

Pellets preparation: A self-supporting wafer (20-50 mg) was pressed from the samples inside a glove box into self supporting pellet (area 2 cm^2, pressure 1.5 tons, time 5 min).

In situ activation: The sample wafer was evacuated in an *in situ* IR cell at 300 °C for 6h and then 80 torr of CHF_3 was introduced into the IR cell. After 30 min, the CHF_3 gas was removed. Subsequently, the sample was evacuated for another 1 h at 300 °C to remove any adsorbed CHF_3.

CO adsorption: The adsorption of CO with different surface coverage was performed at the liquid nitrogen temperature (-196 °C) using a loop of known volume (1.76 cm^3) and a pressure of ca. 5-20 torr. After each dose, the samples were degassed for 1 h to remove the weakly adsorbed CO and a spectrum was recorded. The procedure continued until no new features were observed in the spectrum. Spectra of the catalyst wafers were taken before and after CO adsorption[4].

Gas chromatography (GC)

For identifying the organic reaction products from catalytic experiments, a Shimadzu GC-17A gas chromatograph with flam ionization detector (FID) was used. The different products were separated in PONA (crosslinked methylsiloxane) capillary column (50 m by

[4] IR-CO measurements were performed with incorporation with the group of A.Vimont, CRNS, Caen.

0.2mm, film thickness of 0.5 μm) with N_2 as carrier gas. Heating program was applied. The initial column temperature was 60 °C and remained at this temperature for 3 min followed by an increase of the temperature (10 °C/min) to 200 °C, which was held at this temperature for 11 min. The retention times for the organic products, CHF_3, $CHClF_2$, $CHCl_2F$, and $CHCl_3$ were determined as 2.6, 2.7, 3.0, and 4.5 min, respectively.

3.3 Catalytic reaction measurements

Gas-phase reaction: Dismutation of $CHClF_2$ and CCl_2F_2:

$$3\ CHClF_2 \longrightarrow 2\ CHF_3 + CHCl_3$$

$$5\ CCl_2F_2 \longrightarrow CClF_3 + 3\ CCl_3F + CCl_4$$

The dismutation of $CHClF_2$ or CCl_2F_2 was performed in a continuous-flow fix-bed tube-type reactor with inner diameter of 5 mm under external heating. Approximately 1 g of the sample was placed at the central position of the reactor onto silver wool plug. The reactor was heated in a cylindrical resistance oven equipped with a temperature controller. The flow of the $CHClF_2$ (5 ml/min) or CCl_2F_2 (7 ml/min) and N_2 (20 ml/min) was controlled by mass flow controllers and the temperature at the inlet was controlled automatically using a thermocouple. The reaction products effluent from the reactor was analyzed by on-line gas chromatography.

Liquid-phase reaction: Isomerization of $CBrF_2CBrFCF_3$

$$CBrF_2CBrFCF_3 \longrightarrow CF_3CBr_2CF_3$$

Inside a glove box, 20 mg of the sample was placed in a 10 ml flask equipped with a magnetic stirrer. The flask was then sealed with rubber septum cap. $CBrF_2CBrFCF_3$ (300 μl) was added via the septum using a syringe and the mixture was stirred at ambient temperature for 2 h. The yield of the target product was analyzed by ^{19}F NMR spectroscopy (solvent: $CDCl_3$).

Liquid-phase reaction: Isomerization of CCl_2FCClF_2

$CClF_2CCl_2F \longrightarrow CCl_3CF_3$

For CCl_2FCClF_2 isomerization, the same procedure as mentioned above was followed. In general, 20 mg of the sample is placed in 10 ml V-shaped flask provided with magnetic stirrer. Then 300 µl of CCl_2FCClF_2 was added and the mixture was stirred at ambient temperature for 2 h. The yield of the target product was analyzed by ^{19}F NMR spectroscopy (solvent: $CDCl_3$).

3.4 Chemicals

Solids	
Aluminum (Al)	99.9%, Sterm
Aluminum *tert*-butoxide ($Al(O^tBu)_3$)	99.9%, Alderich
Aluminium triisopropoxide ($Al(O^iPr)_3$)	99.8%, Aldrich
Cesium Iodide (CsI)	99.9%, Chempur
α-aluminum oxide (α–Al_2O_3)	Saint-Gobain
γ-aluminum oxide (γ-Al_2O_3)	Strem Chemicals
γ-aluminum oxide (γ-Al_2O_3)	Alfa Aesar
Liquids	
1-butanol	99.9%, Aldrich
Chloroform-d	99.5%, Chemotrade
1,2-dibromohexafluoropropane	99.5%, Fluorochem
Methanol	99%, Aldrich
Hydrofluoric acid	95%, Merck
2-propanol	99.5%, Aldrich
Pentane	99%, Aldrich
Pyridine	99%, Merck
tertahydrofuran	99.8%, Ferak
1,1,2-trichlorotrifluoroethane	Fluorochem
Gases	
Argon	4.8, Air Liquid
Dichlorodifluoromethane	Solvay Fluor
Difluorochlromethane	Solvay Fluor
Difluoromethane	99.7%, Alderich
Fluorine	1.8, Messer-Griesheim
Hydrofluoric acid	Solvay Fluor
Nitrogen	5.0, Air Liquid
Propane	3.5, Messer-Griesheim
1,1,1,2-tetrafluoroethane	Solvay Fluor

Chapter 4

Preparation of HS-AlF_3

4.1 Introduction

Catalysts with very strong Lewis acid sites are extensively used in fluorochemicals manufacture and in petrochemical processes. Aluminum fluoride (AlF_3) with high BET surface area has received a great attention due to its great potential as catalyst in these applications. However, its activity and selectivity depends very much on its structure and surface area. Consequently, various methods have been used to prepare AlF_3, which led to various crystalline phases.

Recently, a new facile method for the preparation of high-surface-area aluminum fluoride (HS-AlF_3) via a non-aqueous sol-gel synthesis route was developed in the group and has been reported [35-36, 81]. The first step is liquid phase fluorination of $Al(OR)_3$/solvent (R is *CH_3, C_2H_5, C_3H_7 or C_4H_9*) with non-aqueous HF solution in organic solvent. A gel is immediately formed up on HF/solvent addition. Thus, this step resembles to a great extent the hydrolysis step in the well known sol-gel reaction for metal oxide preparation. The fluorination reaction involves the substitution of OR groups by F and may be considered as fluorolysis.

hydrolysis: $\equiv M{-}OR + H_2O \longrightarrow \equiv M{-}OH + ROH$

fluorolysis: $\equiv M{-}OR + HF \longrightarrow \equiv M{-}F + ROH$

During the fluorination reaction, a proton goes to the leaving OR group. Following the protonation of the alkoxy groups, an alcohol splits off and Al-F bonds form. As the number of Al-F groups increases, they bridge with each other and a network of $Al(F,OR)_6$ octahedra is formed (scheme 4.1).

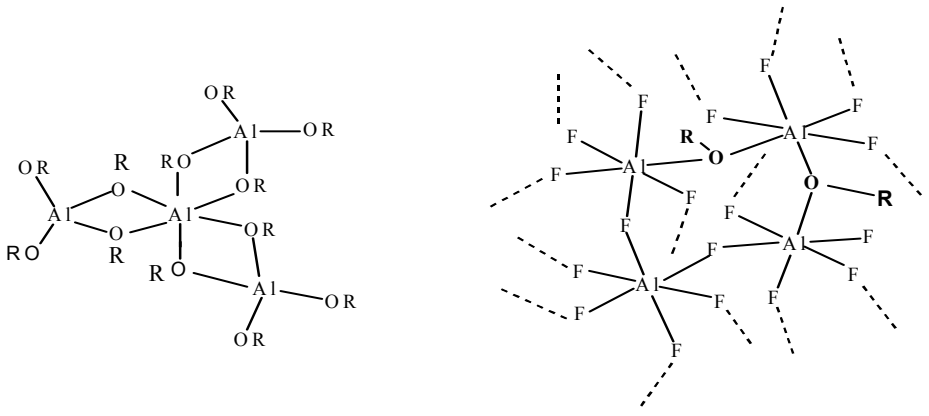

Scheme 4.1 Structure model (left) $Al(^{i}OPr)_3$ and (Right) aluminum alkoxide fluoride ($Al(F,OR)_6$).

After drying in vacuum, aluminum alkoxide fluoride (precursor) is formed. Even if an excess of HF is employed, a total OR against F exchange can not be achieved. The resulting precursor has a high surface area (430 m^2/g), a F/Al ratio ranging from 2 to 2.7, and high carbon content (30%). Thus, a second fluorination step is applied to get the HS-AlF_3. The resulting HS-AlF_3 has very high specific surface area combined with extremely high Lewis acidity [36, 40]. Despite this, little is known about the detailed synthetic parameters, which affect HS-AlF_3 properties.

Thus, the main focus of the present chapter is to investigate all synthesis parameters which have or might have an influence on HS-AlF_3 properties. In the first step of the synthesis, comprising a sol-gel fluorination of an aluminum alkoxide under anhydrous conditions followed by removal of the solvent yielding a dry Al-F-gel (HS-AlF_3 precursor), the main variables of influence are the respective concentrations, the temperature and time schedules, and the nature of alkoxide and solvents used. The second step comprises a final fluorination of the dry Al-F-gel with a gaseous fluorinating agent at elevated temperatures yielding HS-AlF_3, where the nature of fluorinating agent, its concentration and the temperature regime applied are the principle factors of influence. All these factors mentioned have been varied and tested for their influence on the final properties of HS-AlF_3, measured in terms of BET surface area, XRD, and catalytic activity in dismutation of $CHClF_2$ or CCl_2F_2 and isomerization of $CBrF_2CBrFCF_3$. Details of the surface and bulk characterization as well as the nature of the acid sites and catalytic behavior of HS-AlF_3 will be discussed thoroughly in chapter 5.

4.2 Preparation of HS-AlF_3

The general procedure will be described briefly: (i) Water free isopropanol was added to $Al(O^iPr)_3$ and stirred. Then, a stoichiometric amount of HF dissolved in non-aqueous solvent was added to the mixture while stirring. A translucent gel was formed immediately after the addition of the HF solution. The sol-gel was aged at room temperature for 24 h prior to drying. The final gel was evaporated under vacuum at 70 °C to obtain the dry Al-F-gel (precursor).

(ii) Activation (fluorination) process of the dry Al-F-gel was performed in a continuous-flow fixed-bed tube-type reactor. The reactor consisted of nickel tube with an inner diameter of 5 mm located inside an electrical furnace. The desired amount of the sample was placed in the center of the reactor onto silver wool plug. The reactant gases

and the diluent N_2 were controlled by mass flow controllers and the temperature of the tube was automatically controlled using a thermocouple.

Catalytic activities of HS-AlF_3 samples were tested for dismutations of CCl_2F_2 (eq. 4.1) and $CHClF_2$ (eq. 4.2) and for isomerizations of $CF_2BrCFBrCF_3$ (eq. 4.3) and CCl_2FCF_2Cl (eq. 4.4).

$$5\ CCl_2F_2 \longrightarrow CClF_3 + 3\ CCl_3F + CCl_4 \quad (4.1)$$

$$3\ CHClF_2 \longrightarrow 2\ CHF_3 + CHCl_3 \quad (4.2)$$

$$CBrF_2CBrFCF_3 \longrightarrow CF_3CBr_2CF_3 \quad (4.3)$$

$$CClF_2CCl_2F \longrightarrow CCl_3CF_3 \quad (4.4)$$

The dismutations of CCl_2F_2 and $CHClF_2$ are considered to be catalyzed by medium strong Lewis acid sites, whereas isomerizations of $CF_2BrCFBrCF_3$ and CCl_2FCF_2Cl require catalysts with very high Lewis acidity such as SbF_5 or ACF [38-39]. These isomerization reactions proceed at room temperature only under the catalytic action of aluminum chlorofluoride (ACF), whereas with SbF_5 elevated temperature are needed (80 °C).

4.3 Rseults and discussion

4.3.1 Step 1: dry Al-F-gel preparation

The first step of preparation aims to synthesize the dry Al-F-gel, an amorphous solid, which still contains some remaining alkoxide groups and high amounts of solvents. The formation of dry Al-F-gel via a wet gel is summarized in eq. 4.5.

$$Al(O^iPr)_3 + x\ HF/ROH \longrightarrow AlF_x(OR)_{3-x}.yROH \longrightarrow AlF_x(OR)_{3-x}.zROH + y\text{-}z\ ROH \quad (4.5)$$

$$y >> z$$

Since the dry Al-F-gel formed is an intermediate in the preparation of HS-AlF_3, its properties are also of importance for the final properties of HS-AlF_3. However, there is no direct method to relate its quality with respect to HS-AlF_3 property. Because of the amorphicity, XRD techniques are not applicable, MAS NMR is not as informative as necessary for the evaluation of dry Al-F-gel quality, and high vacuum methods alter its properties. Therefore, parameters influencing this step were varied and the resulting material was fluorinated (activated) in a second step to get HS-AlF_3. The properties of the

obtained materials were then compared with each other and also with the properties of HS-AlF_3 prepared according to [36].

Gel formation

Effect of Al:HF ratio

To examine the influence of HF to $Al(O^iPr)_3$ molar ratio on HS-AlF_3 properties, experiments with HF/Al ratios of 2, 3, 4, and 5 were performed. As it is shown in Table 4.1, as the HF concentration increased from HF/Al = 2 to HF/Al = 5 carbon content decreased from 38 to 6%. After fluorination with $CHClF_2$, the residual alkoxide groups and solvents were removed, as indicated by low carbon content in the samples. Table 4.1 shows also the effect of HF/Al ratio on the surface area and crystallite structure of the resulting HS-AlF_3. It is observed that HF/Al ratios from HF/Al = 2 to HF/Al = 3 had minor influence on the surface area of AlF_3. However, excessive amount of HF (up to HF/Al = 5) led to a smaller surface area (33 m^2/g). All products were X-ray amorphous, whereas HF/Al = 5 resulted already in a weakly crystalline product, which was therefore not further investigated.

Table 4.1: Effect of HF: $Al(OiPr)_3$ molar ratio on HS-AlF_3 surface properties

Sample	HF/ Al ratio	C % of dry Al-F-gel	Properties of HS-AlF_3		
			C %	S_{BET} (m^2/g)	XRD
1	2	38	0.8	275	amorphous
2	3	27	0.2	250	amorphous
3	4	18	0.6	182	amorphous
4	5	6	0.5	33	weakly crystalline

Effect of temperature

In all standard experiments the liquid phase sol-gel fluorination step was carried out at room temperature. A sol-gel was obtained and the final product (after drying and fluorination with $CHClF_2$) gave a surface area of 250 m^2/g (sample 1, Table 4.2). Since it is known from the literature that $Al(O^iPr)_3$ has a tetrameric structure at room temperature,

this tetrameric structure transfers to trimeric structure at elevated temperature. Hence, experiments have been carried out at (i) -70 °C and (ii) 70 °C, respectively.

In (i), $Al(O^iPr)_3$/isopropanol solution was cooled down to -70 °C, then HF/Et_2O solution was added (sample 2). Samples prepared in this way showed almost identical surface area (225 and 229 m^2/g, respectively) with sample 1 (Table 4.2). Moreover, to test the effect of the $Al(O^iPr)_3$ structure on the final properties of HS-AlF_3, in a different experiment, the sol-gel was prepared by heating $Al(O^iPr)_3/^iPrOH$ solution at 130 °C (under reflux) for 1 h before rapidly cooling to -70 °C (sample 3*). The last entry in Table 4.2 corresponds to an experiment where $Al(O^iPr)_3$ was first melted at 140 °C, then ^iPrOH was added to the melt (sample 4**). After cooling down the solution to room temperature, HF/Et_2O was added to the solution. In this way (samples 3* and 4**), the tetrameric $Al(O^iPr)_3$ is transformed into the trimeric form, what results obviously in a less open structure as indicated by the decrease in the surface area.

Table 4.2: Effect of liquid phase fluorination temperature on surface area of HS-AlF_3

Sample	Sol-gel temp (°C)	C Content (%)		S_{BET} (m^2/g)
		bf	af	
1	20	37	0.3	250
2	-70	29	0.4	225
3*	-70	27	0.6	140
4**	20	29	0.7	156

* kept under reflux for 1 h before cooling down to -70 °C

** prepared by melting $Al(O^iPr)_3$ at 140 °C

bf– before fluorination, af– after fluorination with $CHClF_2$

Influence of solvent

It became clear that a remarkable amount of solvent is sticked at the precursor, probably via the pre-formed Lewis-sites. This might be a substantial factor during gel-formation. Therefore, the effect of various solvents on the final properties of HS-AlF_3 was investigated. In addition to isopropanol, dioxane, methanol, THF, toluene, pentane, and butanol were also tested. Under all conditions, a fluorination with HF/Et_2O or

HF/isopropanol took place resulting in a sol or gel. Gel was formed when the solvents used were isopropanol, dioxane, pentane, and butanol, whereas just a sol was formed with toluene, methanol, and THF. In all the experiments, the Al-F-sol or the wet Al-F-gel obtained was dried in vacuum at 70 °C to get dry Al-F-gel. The obtained materials were fluorinated to get HS-AlF_3.

As seen in Table 4.3, samples show slight differences in the surface area, implying that the solvents used has no remarkable influence on the texture properties of HS-AlF_3. The catalytic activity for $CHClF_2$ dismutation (96-99%) provided supporting evidence that the solvents used have slight or no effect on the final properties of the HS-AlF_3. The highest surface areas were obtained when the solvents employed were isopropanol or butanol (about 309 m^2/g) while the lowest were obtained when methanol was used as a solvent (198 m^2/g).

Table 4.3: Effect of solvents on the HS-AlF_3 properties

$Al(OiPr)_3$ / Solvent	C Content (%)		S_{BET} (m^2/g)	Conversion of $CHClF_2$ (%) at 50 °C
	bf	af		
methanol	4	0.2	198	96
isopropanol	27	0.3	250-309	98
butanol	31	0.5	305	98
toluene	26	0.2	269	98
THF	6	0.7	229	99
pentane	7	0.8	256	99
dioxane	27	0.5	223	99

bf– before fluorination, af– after fluorination with $CHClF_2$

Preparations with other alkoxides

Besides $Al(O^iPr)_3$, Al-methoxide ($Al(OMe)_3$) and Al-tert-butoxide ($Al(O^tBu)_3$) were also tested for their suitability for HS-AlF_3 preparation. $Al(OMe)_3$ was dissolved in methanol and $Al(O^tBu)_3$ was dissolved in butanol before the addition of the HF solution. Under all conditions the sol-gel fluorination took place, irrespective of the tetrameric structure of aluminum alkoxide $[(Al(O^iPr)_3]_4$, the dimeric derivative $[(Al(O^t(Bu)_3]_2$ or the structure of $Al(OMe)_3$ (presumably polymeric structure).

Dry Al-F-gels prepared from $Al(O^tBu)_3$ as well as from $Al(OMe)_3$ were activated with $CHClF_2$ resulting in a HS-AlF_3 similar to that prepared from Al-isopropoxide (Table 4.4). HS-AlF_3 prepared from $Al(O^tBu)_3$ showed slightly higher surface area (321 m^2/g) and higher isomerization activity (≈ 100%) than those prepared from $Al(O^iPr)_3$ or $Al(OMe)_3$, whereas HS-AlF_3 prepared starting from $Al(OMe)_3$ showed the lowest catalytic activity for 1,2-DBP (≈ 90%) and the smallest surface area (196 m^2/g). These results indicate that the type of the alkoxide used has an effect on the final properties of HS-AlF_3, but only of minor importance.

Table 4.4: HS-AlF_3 prepared from $Al(OMe)_3$ and $Al(O^tBu)_3$

Al-alkoxide	Solvent	C Content (%)		S_{BET} (m^2/g)	1,2-DBP isomer. activity (%)
		bf	af		
$Al(O^i(Pr)_3$	^{i}PrOH	27	0.3	250-309	> 90
$Al(O^t(Bu)_3$	*n*-butanol	28	0.3	321	≈ 100
Al $(OMe)_3$	methanol	9	0.7	198	≈ 90

bf– before fluorination, af– after fluorination with $CHClF_2$
1,2-DBP isome.– $CBrF_2CBrFCF_3$ isomerization

Effect of wet-gel work-up procedures

Drying procedure

Drying temperature: To study the effect of the drying temperature, a wet Al-F-gel, prepared from $Al(O^iPr)_3/^i$PrOH and HF/Et_2O, was dried in vacuum at one part at 50 °C and another part at 70 °C. The weight loss curves of the vacuum drying experiments (Figure 4.1) show only slightly different kinetics with faster drying rate at 70 °C. According to elemental analysis, both dried samples had a residual carbon content of about 27%, and in thermal analysis their characteristic TG/DTA curves (shown in chapter 5, Figure 5.1) were almost identical, with additional weight losses of 47.8% (dried at 50 °C) and 47.4% (dried at 70 °C).

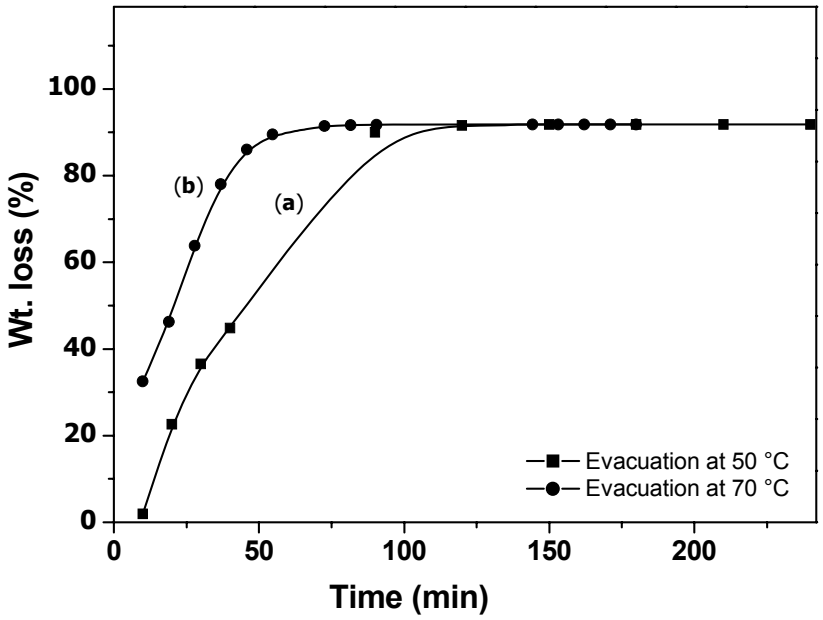

Figure 4.1 Weight loss of wet gel under vacuum at (a) 50 °C (b) 70 °C.

Drying methods: In all the standard experiments, the wet Al-F-gel was dried in vacuum at 70 °C. For comparison the wet gel was dried using Freeze-dryer and Microwave-assisted drying techniques. The resulting materials were then fluorinated with $CHClF_2/N_2$ to get HS-AlF_3. Regardless of the drying methods, the surface areas were almost similar (Table 4.5). All BET/N_2 adsorption-desorption isotherms were of type IV, representing a mesoporous character (not shown here), and all samples were X-ray amorphous. Therefore, in all experiments discussed here, the dry Al-F-gel was prepared by vacuum drying the wet-gel at 70 °C.

Table 4.5: Effect of drying method on the properties of HS-AlF_3

Sample	Drying method	C Content (%)		S_{BET} (m^2/g)
		bf	af	
1	vacuum at 70 °C	27	0.4	250
2	freeze-dryer	24	0.4	219
3	microwave	12	0.4	259

bf– before fluorination, af– after fluorination with $CHClF_2$

Effect of gel aging

To study the effect of gel aging, wet sol-gel was divided into 4 parts, was aged for 1 (fresh gel), 7, 90 and 120 days at room temperature, respectively. After aging, the samples were dried and fluorinated to get HS-AlF_3.

$CBrF_2CBrFCF_3$ (1,2-DBP) conversion, $CHClF_2$ conversion, and surface area of the samples are reported in Table 4.6. Although only minor differences in the catalytic activity for $CHClF_2$ dismutation (97-98%) were observed by aging the wet Al-F-gel from 1 to 120 days, remarkable differences were observed in the surface area values and 1,2-DBP isomerization. The 1,2-DBP isomerization was reduced as the aging time increased, the most active sample is the one from the fresh Al-F-gel (≈ 90%) while the lowest activity was showed for that aged for 120 days. Obviously, some ordering processes take place with time in the wet gel connected with a shrinking of the wet gel by expel of alcohol [82]. This is indicated by the reduced carbon content of the gel, although all HS-AlF_3 samples were X-ray amorphous. This means that in order to obtain a large surface area and a high catalytic activity, the wet sol-gel should be worked up in fresh state.

Table 4.6: Effect of wet gel ageing on the surface properties of HS-AlF_3

Sample	Aging time/days	C content (%)		S_{BET} (m^2/g)	1,2-DBP isomer. activity (%)
		bf	af		
1	1	33	0.3	249	≈ 90
2	7	31	0.3	217	63
3	90	29	0.3	176	20
4	120	26	0.6	170	6

bf– before fluorination, af– after fluorination with $CHClF_2$

1,2-DBP isome.– $CBrF_2CBrFCF_3$ isomerization

4.3.2 Step 2: dry Al-F-gel activation

The aim of the post-fluorination step is to convert the dry Al-F-gel into an HS-AlF_3, a high surface area and extremely Lewis acidic amorphous form of AlF_3. To accomplish this, the organic constituents of the dry Al-F-gel, alkoxide groups and/or alcohol, have to be

removed under moderate conditions preserving the very high structural disorder of the dry Al-F-gel.

All discussed results presented in the following section were obtained starting with dry Al-F-gel prepared from $Al(O^iPr)_3/^iPrOH$ and HF/Et_2O only. The gel obtained in the fresh state was dried at 70 °C under vacuum.

Calcination

To gain more information about the dry Al-F-gel and its reactivity, to see if calcination can already remove the organic with the high surface area being preserved and Lewis acidity developed, dry Al-F-gel samples were calcined in air without any fluorination agent at 220 °C for 2 h, or under nitrogen at 160, 220, and 350 °C for 2 h.

Table 4.7 shows that heating the samples up to 350 °C in N_2 flow resulted in removal of almost all the remaining alkoxide groups and/or solvents, as indicated by low carbon content in the samples (0.2 %). However, the surface area was drastically decreased. The decrease in the surface area with increasing the calcination temperatures is probably due to some ordering processes which take place in the amorphous material. In term of catalytic activity, all the samples showed no catalytic activity for $CHClF_2$ dismutation or 1,2-DBP isomerization. A comparison of the IR-photoacustic spectra of adsorbed pyridine on the sample calcined at 350 °C and on HS-AlF_3 prepared via activation with $CHClF_2$ as described in reference [36] indicates that, in principle, there are Lewis acidic sites on the calcined sample surface similar to HS-AlF_3, but of much lower concentration. The catalytic activity and TPD results suggest that precursor heated in N_2 at 350 °C has lower amount and less strong sites than at HS-AlF_3.

Table 4.7: Effect of calcination on the precursor structure

Sample	Temp. (°C)	Atmosphere	C Content (%)		S_{BET} (m^2/g)	XRD phases
			bc	ac		
1	160	N_2	32	15.5	530	amorphous
2	220	N_2	32	5.1	334	amorphous
3	350	N_2	32	0.2	130	amorphous

bf– before calcination, af– after calcination

Post-fluorination

Activation with gaseous fluorocarbon compounds

A post-fluorinating treatment of the dry Al-F-gel at moderate temperature with gaseous CCl_2F_2 was shown to be very effective for obtaining highly Lewis acidic HS-AlF_3 [35-36]. At lower temperature, the reaction of dry Al-F-gel with CCl_2F_2 starts with liberation of ROH. In the range of 200-250 °C propene is formed together with diisopropylether. At about 300 °C, the dismutation products (CCl_4 and $CClF_3$) can be found together with $COCl_2$ (eq. 4.6), resulting from the fluorination reaction of CCl_2F_2 with dry Al-F-gel [36]. Therefore, various commercially available fluorination agents have been tested: CCl_2F_2, $CHClF_2$, CH_2F_2, and CH_2FCF_3.

$$AlF_x(O^iPr)_{3-x} \cdot y\ ^iPrOH \xrightarrow{CCl_2F_2} AlF_3 + y\ ^iPrOH + z\ C_3H_6 + {}^iPrO^iPr + COCl_2 \quad (4.6)$$

$$y + z = 3 - x$$

Typically, the reactions were carried out as described in section 4.2. The temperature was step-wise increased, held at each respective temperature as long as the GC showed changes. Since both CCl_2F_2 and $CHClF_2$ undergo dismutation reactions under the catalytic action of strong Lewis acids, progress of the activating treatment can be followed up monitoring the composition of the exhaust from the tube reactor. The temperature was slowly increased until maximum dismutation was detected.

Fluorination with CCl_2F_2

Heating the dry Al-F-gel in a flow of CCl_2F_2:N_2 (7:20 ml/min), dismutation of CCl_2F_2 starts at about 300 °C reaching after a short time 96% conversion, indicating a complete transformation of the dry Al-F-gel into HS-AlF_3. The resulting HS-AlF_3 is very active in the isomerization of 1,2-DBP (≈ 90%). However, activation with CCl_2F_2 combines the drawbacks of a long fluorination time (about 12 h), and the problems derived from use of CCl_2F_2 [83]. By increasing the temperature to 400 °C the fluorination time is reduced, but surface area and catalytic activity drops significantly (Table 4.8).

Table 4.8: Activation with CCl_2F_2: Effect of temperature on the surface area of HS-AlF_3

Sample	Final temp. (°C)	Fluorination time (h)	C Content (%)		S_{BET} (m^2/g)	1,2-DBP isomer. activity (%)
			bf	af		
1	300	12	27	0.3	186	≈ 90
2	350	10	27	0.3	156	≈ 83
3	400	7	27	0.4	71	not active

bf– before fluorination, af– after fluorination with $CHClF_2$

1,2-DBP isome.– $CBrF_2CBrFCF_3$ isomerization

Fluorination with $CHClF_2$

With the more reactive $CHClF_2$, fluorination can be expected to take place at a lower temperature. Tests have been carried out by varying both activation temperature and $CHClF_2/N_2$ ratio.

Fluorination temperature: The data in Table 4.9 illustrate the effect of fluorination temperature on the surface area and catalytic activity of the resulting HS-AlF_3. Several trends can be observed from this Table.

Table 4.9: Activation with $CHClF_2$: Effect of fluorination temperature on HS-AlF_3 properties

Sample	Final temp. (°C)	C Content (%)		S_{BET} (m^2/g)	F Content (%)	Conversion of $CHClF_2$ (%)	1,2-DBP isomer. activity (%)
		bc	ac				
1	160	27	15.4	540	41	0	0
2	220	27	1.2	254	45	4	0
3	270	27	0.6	249	66	99	> 90
4	300	27	0.3	178	66	96	38
5	350	27	0.4	155	66	93	26
6	270	27	0.5	110	59	≈ 90	0

bf– before fluorination, af– after fluorination with $CHClF_2$

1,2-DBP isome.– $CBrF_2CBrFCF_3$ isomerization

Comparing samples 1 to 5, it is clear that the higher the fluorination temperature the lower the carbon content and the higher the fluorine content approaching that of AlF_3. The

low carbon contents found (0.3-0.4%) and the high F contents (66%) indicate complete fluorination. The measured and calculated F content of AlF_3 is 66 % and 67.7%, respectively. Above 250 °C, a decrease in the surface area and 1,2-DBP isomerization activity as well as coke formation were observed. These findings are obviously due to the fact that coke is formed at the most active sites of the HS-AlF_3 surface, which blocks the sites and part of the pores, resulting in smaller surface area and lower catalytic activity for 1,2-DBP isomerization.

Heating the dry Al-F-gel at 220 °C in N_2 only resulted in amorphous products with high surface area and low carbon content, which are not active in dismutation of $CHClF_2$ (see sample 2, Table 4.7). However, after prolonged heating (≈ 5 h) in $CHClF_2/N_2$ at 270 °C, these samples became active in dismutation, but remained inactive in 1,2-DBP isomerization (sample 6 in Table 4.9). Obviously oxide formed becomes, at least partly, fluorinated under these conditions.

$CHClF_2$ concentration: Another factor that can affect the properties of HS-AlF_3 is the concentration of $CHClF_2$, which was studied using various $CHClF_2$:N_2 ratios, namely, 3:20, 5:20, and 7:20 ml/min. Although there are no differences in the residual carbon content and only small differences in the surface area were observed, however, the time needed for complete fluorination (i.e., for reaching a dismutation activity of 98% conversion) differs significantly (Table 4.10). Furthermore, high amounts of $CHClF_2$ (7 ml/min) led to coke formation, which causes blocking of the active sites and decreasing the activity in 1,2-DBP isomerization.

Table 4.10: Effect of $CHClF_2$ concentration on HS-AlF_3 formation (T = 250 °C)

Sample	$CHClF_2$ flow (ml/min)	N_2 flow (ml/min)	C Content (%)		Time needed to reach 98% dismutation	S_{BET} (m^2/g)	1,2-DBP isomer. activity (%)
			bf	af			
1	3	20	27	0.3	14	176	17
2	5	20	27	0.3	8	249	> 90
3	7	20	27	0.4	7	206	21

bf– before fluorination, af– after fluorination with $CHClF_2$

1,2-DBP isomer.– $CBrF_2CBrFCF_3$ isomerization

Fluorination with CH_2FCF_3 and CH_2F_2

HFCs (hydrofluorocarbons) have attracted considerable attention recently since they are the major CFC-alternative refrigerants. They have no chlorine and have zero ozone-depletion potential. Among all HFCs, CH_2FCF_3 and CH_2F_2 are the most frequently used once because they are less expensive and provide excellent properties.

Experiments with CH_2FCF_3 and CH_2F_2 were carried out at 200, 250, and 300 °C, using admixtures with N_2 in a ratio of HCFC/N_2 as 5/20 ml/min. From Table 4.11, it is noticed that the samples fluorinated with CH_2FCF_3 have slightly higher surface area than the samples fluorinated with CH_2F_2. With both fluorination agents, increasing the fluorination temperature resulted in a decrease of the surface area.

Moreover, at 300 °C coke formation was observed with both fluorinating agents, and under all conditions tested no catalytically active material was obtained. However, upon additional treatment with $CHClF_2$ for 2-3 h at 280 °C, 98% dismutation activity was reached and also moderate activity for 1,2-DBP isomerization was obtained. These experiments show that both CH_2FCF_3 and CH_2F_2 are not suitable as fluorination agents for HS-AlF_3 preparation. Obviously, because of the lower stability due to the higher hydrogen content these compounds are more likely to undergo decomposition, i.e., coke formation, at temperatures needed for fluorination activities.

Table 4.11: Activation with CH_2FCF_3 and CH_2F_2

Sample	Fluorinating agent	Temperature. (°C)	C Content (%)		S_{BET} (m^2/g)
			bf	af	
1	CH_2F_2	200	27	0.8	218
2	CH_2F_2	250	27	0.6	180
3	CH_2F_2	300	27	3.6	130
4	CH_2FCF_3	200	27	0.5	276
5	CH_2FCF_3	250	27	0.4	270
6	CH_2FCF_3	300	27	0.2	138

bf– before fluorination, af– after fluorination

Plasma fluorination of $AlF_x(O^iPr)_{3-x}$ precursors

Fluorination was performed using CF_4 as fluorination agent. Sample was heated at 100 °C for 90 min. The material obtained has high carbon content (11%). The high carbon content on the fluorinated sample could be attributed to remaining alkoxide groups. Thus, the sample did not show any catalytic activity for dismutation of $CHClF_2$ or isomerization of 1,2-DBP. After prolonged heating (≈ 2 h) in $CHClF_2/N_2$ at 270 °C, sample showed high catalytic activity for both test reactions. These results imply that plasma fluorination is not suitable (under these fluorination conditions) for preparation of HS-AlF_3.

Fluorination with F_2

There are several reasons to investigate elemental fluorine as activating agent. It is very strong fluorination agent, thus, the fluorination reaction should proceed at lower temperatures, preserving the high distortion and surface area better than with fluorocarbon activation. In addition, unlike fluorocarbons, F_2 cannot decompose forming coke.

Sol-gel was dried in microwave at 90 °C for 1h, then fluorinated with elemental F_2. The activation reactions were performed with varied F_2/Ar mixtures (100%, 50%, and 10% F_2) in a heated tube type reactor. Fluorination was performed at 80-225 °C for 5 h[5]. The results are shown in Table 4.12.

Table 4.12: Catalytic activity for $CHClF_2$ dismutation and 1,2-DBP isomerization

sample	C content		Conversion $CHClF_2$ (%)			S_{BET} (m^2/g)
	bc	af	200°C	100°C	50°C	
1 (100% F_2)	13	0.0	99	≈ 100	≈ 100	329
2 (50% F_2)	13	0.0	≈ 100	≈ 100	≈ 100	n.d.
3 (10% F_2)	13	0.0	98	≈ 100	68	n.d.

bf– before fluorination, af– after fluorination with HF

n.d.– not determined

The product, named HS-AlF_3/F_2, showed high catalytic activity for $CHClF_2$ dismutation (100% conversion) at even 100 °C (Table 4.12). In addition, HS-AlF_3/F_2

[5] Fluorination with elemental fluorine was performed by the group of A. Tressaud, CNRS, Bordeaux.

samples displayed also high surface area (329 m^2/g), which are similar to HS-AlF_3 prepared by $CHClF_2$ activation. These results imply that elemental F_2 or Ar diluted F_2 can also be used successfully as fluorination agent.

Activation with gaseous HF

One of the problem which results from fluorination with gaseous fluorocarbons is the coke formation. HF is an ideal fluorination agent since it can not be decomposed forming coke. In addition, its fluorinating activity is higher than that of fluorocarbon compounds, thus the fluorination (activation) reaction should proceed at lower temperatures, preserving the high distortion and higher surface area in the formed AlF_3. To test this hypothesis, fluorination with HF was studied by varying the fluorination temperature, the fluorination time as well as the HF concentration. The products obtained from these experiments are denominated HS-AlF_3-HF. The results are shown in Table 4.13.

Fluorination temperature: The fluorination temperature range studied was from100 to 250 °C, using a HF concentration of HF:N_2 of 1:20 ml/min for 4 h. As it can be seen from Table 4.13, sample 1 to 4, increasing the fluorination temperatures from 100 to 250 °C reduced the surface area significantly. Below 120 °C, high amount of carbon contents are retained, which is attributed to the presence of residual alkoxyl groups.

HF concentration: The influence of HF concentration was studied by varying HF:N_2 ratio from 1:20 to 5:1 at 120 °C for 4 h (Table 4.13, samples 2 and 5 to 8). It can be seen that the values of surface areas were decreased as the HF concentration increase, reaching only 55 m^2/g for the highest HF concentration.

Fluorination time: To further study the effect of fluorination time, samples were fluorinated for 4, 6 or 9 h using HF:N_2 ratio of 1:20 ml/min at 120 °C. Long fluorination time caused a decrease in the surface area from 420 to 90 m^2/g (Table 4.13, samples 2, 9, 10).

Such decrease in the surface area by increase the fluorination temperature, fluorination time, and HF concentration may be due to the fact that the reaction enthalpy of HF is high. This results in releasing a high amount of heat in a short time. This induces structural rearrangement and reduction in the surface area. Thus, low HF concentration and low temperatures are advantageous in order to complete removal of the volatile organic material and to obtain a HS-AlF_3-HF with high surface area.

Table 4.13: Effect of temperature HS-AlF_3-HF properties

Sample	HF flow (ml min^{-1})	N_2 flow (ml min^{-1})	Fluorination time (h)	Temp. (°C)	C Content (%)		S_{BET} (m^2/g)
					bf	af	
1	1	20	4	100	27	11.8	447
2	1	20	4	120	27	0.3	420
3	1	20	4	160	27	0.2	303
4	1	20	4	250	27	0.2	124
5	2	20	4	120	27	1.2	125
6	5	20	4	120	27	1.2	9 0
7	5	5	4	120	27	0.6	89
8	5	1	4	120	27	0.5	55
9	1	20	6	120	27	1.2	125
10	1	20	9	120	27	1.2	90

bf– before fluorination, af– after fluorination with HF

Catalytic activity and surface area: In terms of surface area, HS-AlF_3-HF is at least as good as HS-AlF_3 prepared by $CHClF_2$ or CCl_2F_2 activation. However, it was not comparably active in the catalytic test reactions, showing only 4 % conversion in $CHClF_2$ dismutation. A direct comparison of the NH_3-TPD curves of HS-AlF_3-HF and HS-AlF_3 shows that HS-AlF_3 is by far superior to HS-AlF_3-HF as solid acid (see chapter 5, Figures 5.22). This can be explained assuming that excessive HF is adsorbed at the most active and the strongest Lewis acid sites, which become blocked and are not accessible to reactants (c.f. chapter 5, Figure 5.15c). As a consequence, additional treatment by which the adsorbed HF should be removed was looked for and tested.

By subsequent treatment with N_2 at 250-280 °C, the catalytic activity of the resulting material (denominated HS-AlF_3-HF + N_2) could be improved. HS-AlF_3-HF + N_2 obtained showed almost 100% activity for $CHClF_2$ dismutation and high activity in 1,2-DBP isomerization (56%), indicating that the adsorbed HF is removed. These results were confirmed from IR-photoacustic of adsorbed pyridine (c.f. chapter 5, Figure 5.15d).

Direct fluorination of aluminum alkoxide

An attempt was made to prepare aluminum fluoride by fluorination of $Al(O^tBu)_3$. The sample was heated in a $CHClF_2$/HF (5/20 ml/min) flow. Heating started from room

temperature and increased in step of 50 °C to 250 °C. The dismutation of $CHClF_2$ started at 250 °C and after short time reached almost 99 %. However, the resulting material did not show any catalytic activity for isomerization of 1,2-DBP. In addition, the sample had much lower surface (67 m^2/g) than HS-AlF_3 (250-309 m^2/g).

4.4 Summary

In order to understand the influence sample preparation on catalytic performance of HS-AlF_3, different preparation routes were chosen. It was found that the concentration and composition of the aluminum alkoxide do not affect remarkably the final properties of HS-AlF_3. However, it turns out that a certain content of remaining organics in the precursor stage is a sufficient pre-condition to obtain finally a very Lewis acidic high surface area AlF_3 material. Meanwhile sol-gel fluorination temperature and aging treatment of sol-gel has a profound effect on the performance of HS-AlF_3.

Several fluorination agents were used such as CCl_2F_2/N_2 or $CHClF_2/N_2$, CH_2F_2/N_2, CH_2FCF_3/N_2, and HF/N_2. It was found that fluorination temperature and fluorination agent concentration were found to have great influence on the HS-AlF_3 properties.

Samples prepared by fluorinating the precursor with CCl_2F_2/N_2 or $CHClF_2/N_2$ exhibited high surface area and high catalytic activity for the probe reaction used.

HS-AlF_3 samples prepared using HF/N_2 as a fluorination agent showed only slight catalytic activity in dismutation of $CHClF_2$ (4% conversion). However, after heating the samples in N_2 flow, the catalytic activity was attained.

Chapter 5

Characterization of HS-AlF_3

5.1 Introduction

Surface and bulk characterizations are an important source of information for compound identification. Samples prepared in this thesis were characterized for structure, texture, acidity, and catalytic activity. Thus, to elucidate the texture of the samples prepared, surface area, pore volume, and pore size distribution were analyzed using N_2 adsorption-desorption techniques. To characterize a solid acid in terms of acid nature and acid strength, a combination of NH_3-TPD technique, and FTIR of adsorbed CO and pyridine were used. FTIR, MAS-NMR, and XRD for bulk characterization, were used. Other techniques such as XPS, XAFS, and SEM were also used to characterize the samples.

All measurements were performed on HS-AlF_3, which was prepared by fluorination of the precursor with $CHClF_2/N_2$, HS-AlF_3-HF (prepared by fluorination of the precursor with HF/N_2), and dry Al-F gel ($AlF_x(O^iPr)_{3-x}$, i.e., precursor).

5.2 Bulk characterization

Thermal analysis

Thermal analysis was used to study both physical and chemical properties changes occurring in HS-AlF_3 and its precursor on heating. From the thermal analysis curve, it is possible to determine the chemical changes or physical transitions resulting from the change of temperature. Thus, phase change for example from amorphous HS-AlF_3 (amorphous) to crystaline α-AlF_3 can be determined.

Thermal analysis comprises a group of techniques in which the properties of materials are studied as they change with temperature whilst the substance is subjected to a controlled temperature program. The program may involve heating or cooling (dynamic), or holding the temperature constant (isothermal), or any combination of these. Two of the major thermal analysis techniques are thermogravimetry (TG) and differential thermal analysis (DTA).

The basic principle in TG is to measure the mass loss or gain of a sample as a function of temperature while the substance is subjected to a controlled temperature program. The first derivative of the mass loss (dm/dT) can be also plotted as an alternative mode of presentation against temperature, and gives a rise to DTG curve. Information about the endothermicity or exothermicity of the process can be also determined by DTA.

Additionally, when mass spectrometry (TG-MS) or IR spectroscopy (IR-TG) techniques are coupled, the volatile products released during the thermal analysis treatment can be identified.

Results

Dry Al-F-gel: TG and DTA profiles of the Al-F-gel dried at 70 °C (precursor 1) and the Al-F-gel dried at 50 °C (precursor 2) in vacuum are presented in Figure 5-1A-B. The two precursors showed nearly identical behavior with total weight loss between 46.7-47.3%. Below 500 °C, three different processes of weight loss were identified in the TG experiments.

For precursor 1 (Figure 5.1A), the first weight loss takes place between 40 and 130 °C. This step represents about 12% from the total weight loss and is most probably due to the Elimination of weakly bonded isopropanol, probably at Lewis acid sites on aluminum. The second weight loss is attributed to the decomposition of the residual alkoxide (OR) groups; in this zone the main weight loss (25 %) occurs. This process is strongly endothermic with maximum at 160 °C as shown in the DTA profiles. During the last stage (from 200 to 500 °C), an additional 9% loss of the initial weight is attributed to water removal [36]. This behavior can be explained by either the condensation of alkoxide groups and formation of Al-O-Al bonds together with propene as shown in 5.1 and 5.2 or condensation of alcohol (5.3).

$$\text{-Al-OR- + -Al-OR-} \longrightarrow \text{-Al-O-Al- + ROR} \quad (5.1)$$

$$C_3H_8OC_3H_8 \longrightarrow 2\,CH_2 = CHCH_3 + H_2O \quad (5.2)$$

$$\text{R-OH + H-OR} \longrightarrow H_2O + \text{ROR} \quad (5.3)$$

$$R = {}^{i}Pr$$

At 557 °C an exothermic reaction takes place without any additional weight loss due to the transformation of the amorphous phase to crystalline material, identified from XRD analysis as α-AlF_3 (PDF file number 77-252). If there is Al_2O_3, is most likely amorphous and therefore is not possible to identify from XRD.

The thermal behavior of precursor 2 is similar to that of the precursor 1, a total loss of 47% from the initial weight was observed from 40-600 °C (Figure 5.1B). At 551 °C, the amorphous material undergoes phase transformation to α-AlF_3.

Based on these results, it can be affirmed that the main part of the decomposition process occurs on the temperature range between 40 and 200 °C. These significant similarities in the

thermal analyses of the precursors 1 and 2 are a strong indication that indeed evacuation temperature (at 50 and 70 °C) does not affect the structure of the dry Al-F-gel.

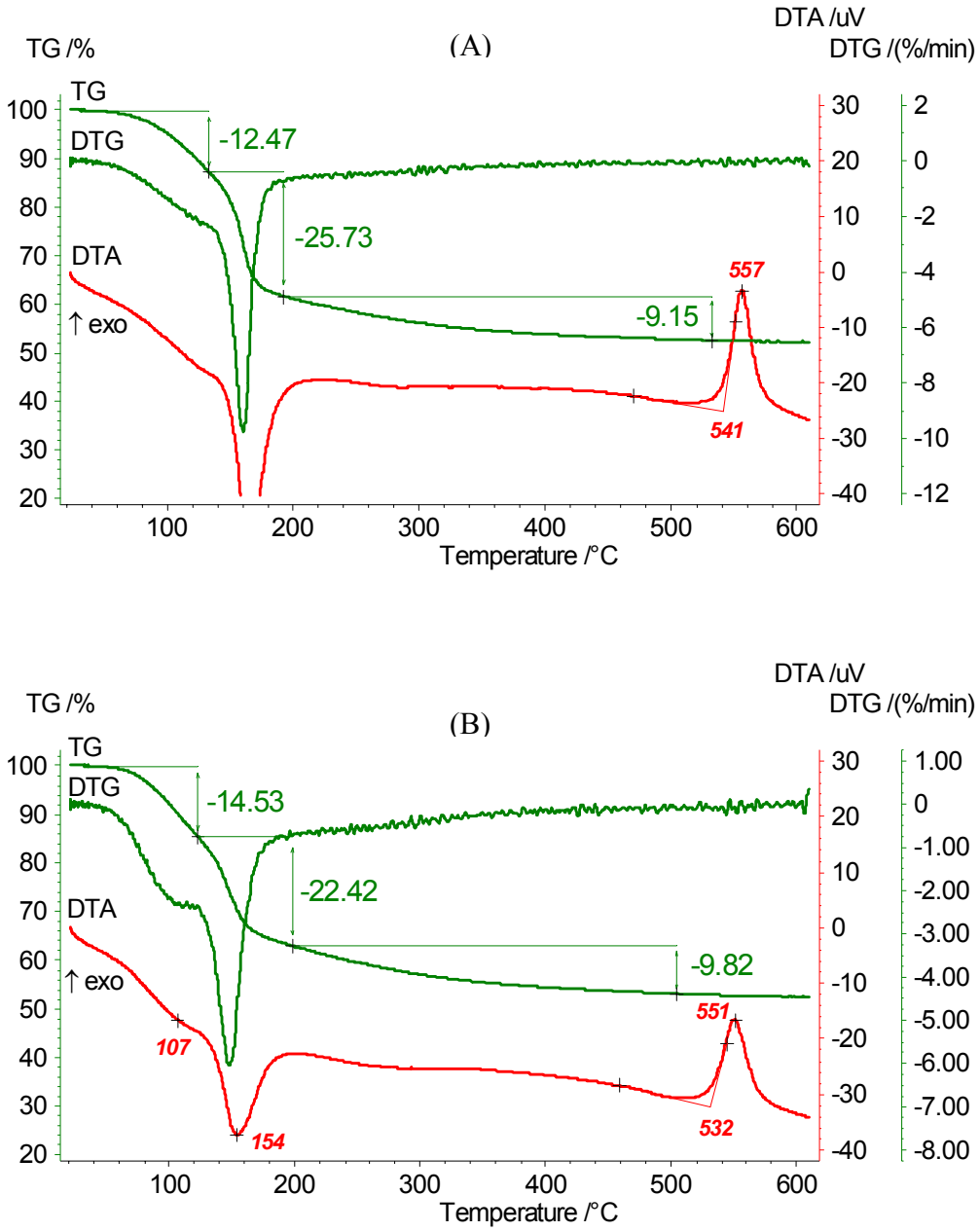

Figure 5.1 TG/DTA of (A) Al-F-gel dried at 70 °C (B) Al-F-gel dried at 50 °C.

HS-AlF₃: Thermal analysis of the HS-AlF_3 was also performed (Figure 5.2). The TG plot reveals a continuous mass loss of about 10 wt% over the whole temperature range. Taking into account the combination of DTA and mass spectrometric (MS), the mass loss can be divided into two steps: Below *ca.* 200 °C there is an endothermic loss of water, indicated by *m/z* peak at 18 (H_2O^+) for H_2O or 17 (OH^+), which may be physisorbed on the surface

(moisture air), when the sample was exposed to air before loading in the TA cell. In the seconds step, between 200 and 500 °C, a mass loss is observed, during which both water and the remaining ROH, which is adsorbed on the strong Lewis acid sites, are detected (*m/z* peak of $C_2H_5O^+$).

At about 534 °C, an exothermic effect in DTA curve due to the crystallization of HS-AlF_3 without further mass loss at about 534 °C was observed; the final decomposition residue was α-AlF_3 (PDF file number 77-252). These results are representative of all HS-AlF_3 samples; likewise, all the materials showed almost the same thermal behavior after post-fluorination with $CHClF_2$ or HF.

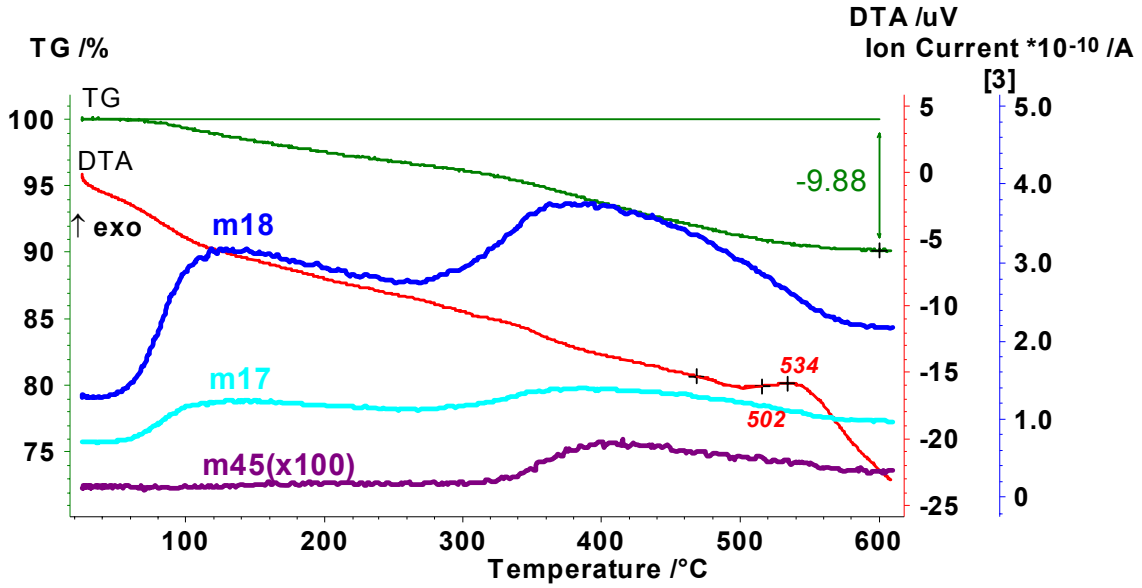

Figure 5.2 DTA/TG-MS of HS-AlF_3 with ion current (IC) curves for (A) *m/z* 18 (H_2O^+), *m/z* 17 (OH^+), and *m/z* 45 ($C_2H_5O^+$).

X-ray diffraction (XRD) studies

X-ray diffraction (XRD) is mainly used to identify and characterize unknown crystalline materials. However, in this work, it was used to see if the HS-AlF_3 and precursor samples prepared are amorphous.

XRD depends on the constructive interference of X-rays at crystal lattice planes. The requirements for constructive interference are given by the Bragg equation ($n\lambda = 2\,d \sin\theta$) with n is an integer and is the order of the diffracted beam, λ is the wavelength of the incident of monochromatic X-ray beam, d is the distance between adjacent planes of atoms (the d-spacings), and θ is the angle of incidence of the X-ray beam [84]. This equation relates the spacing between the crystal planes, d, to the particular Bragg angle, θ, at which

reflections from these planes are observed. The diffractograms are measured as a function of the 2θ angle and thus enable to identify phases by calculating the d spacing of the lattice.

X-ray amorphous materials such as oxide glasses and HS-AlF_3 as described here are at the opposite extreme from crystalline materials, they do not have a regularly repeating structure (ordered crystal structure). Their scattering patterns displays broad, low intensity peaks characteristic of the average local atomic environment.

Results

The XRD patterns of the precursor, HS-AlF_3, HS-AlF_3-HF, and HS-AlF_3 heated at 600 °C are shown in Figure 5.3a-d.

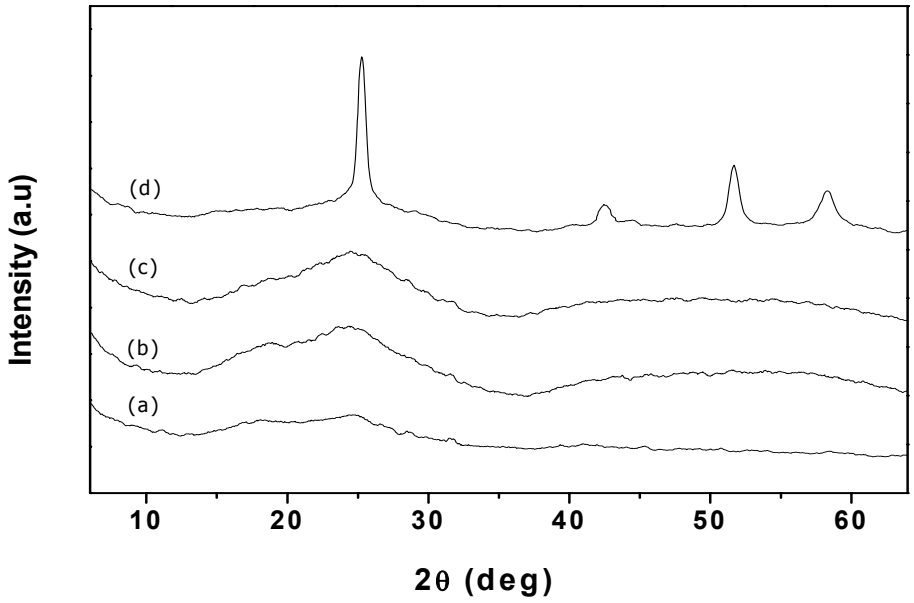

Figure 5.3 XRD patterns of (a) precursor, (b) HS-AlF_3, (c) HS-AlF_3-HF, (d) HS-AlF_3 heated at 600 °C.

Only broad weak diffraction signals with very low intensity were observed in the XRD patterns for precursor (Figure 5.3a), HS-AlF_3 (Figure 5.3b), and HS-AlF_3-HF (Figure 5.3c), pointing toward the absence of a long rang ordering owing to the presence of the bulky and randomly disturbed alkoxy groups at the sol-gel fluorination stage that prevented the formation of crystalline AlF_3 during fluorination. Similar diffractograms were obtained for all the HS-AlF_3 preparations. Only by heating the HS-AlF_3 samples, at about 600 °C, crystallization takes place to α-AlF_3 phase (Figure 5.3d), in consistent with the PDF file number 77-252 [79].

Infrared spectroscopy (IR)

To further investigate the framework of the HS-AlF_3 and HS-AlF_3-HF samples, FTIR of calcined samples was performed to clarify whether OH^- or residual alkoxide groups or both are present in the network. For comparison, FTIR was also carried out on the starting material $Al(O^iPr)_3$, precursor, α-AlF_3 and *β*-AlF_3 as reference samples.

IR is based on interaction of infrared light with matter. In order of this interaction to occur, molecular vibration must cause a change in the dipole moment of the molecule. When the frequency of the electromagnetic field matches the frequency of the oscillation of the dipole moment, IR radiation can be adsorbed, exciting a vibrational transition. The parameters of the bands such as frequency, intensity, and shape refer to certain structural properties. Hence, IR absorption bands can be used to get information about the structure properties of any material including the amorphous ones. The dipole moment of Al-F bond is very high, giving rise to very intense bands in IR.

Crystalline α-AlF_3 consists of a three dimensional network of AlF_6 units, sharing corner fluoride ions. It is known that an isolated octahedral ion $[AlF_6]^{3-}$ has six fundamental vibration, of which ν_1, ν_2, and ν_5 are active in the Raman spectrum, whereas ν_3 and ν_4 are IR active. AlF_3 typically are built from AlF_6 octahedra by the bridging chains or nets of different orders, thus the bonds corresponding to the stretching vibration of AlF_6 octahedra have more complex contours. This leads to electron density re-distribution, giving rise to nonequivalent (in the strength) Al-F bonds.

In the IR spectra of anhydrous AlF_3, the asymmetric stretching vibration bands ν_3 lie in the region 660 cm^{-1}; the deformation bands ν_4 are in the region 360 cm^{-1}. The hydrated forms of AlF_3, on the other hand, have at least two additional broad bands around 3400 cm^{-1} (ν_{O-H}) and 1650 cm^{-1} (δ_{H-OH}) due to stretching and deformation modes of crystallization water [85].

Results

The FTIR spectra of HS-AlF_3 and HS-AlF_3-HF samples as well as the crystalline α-AlF_3 and *β*-AlF_3 are shown in Figures 5.4 a-d and 5.5a-d.

In Figure 5.4a-d, at the left part of the spectra at higher wave numbers CH_3 and CH absorption bands at 2800-3000 cm^{-1} (ν_{C-H}) are characteristic of the alkoxide and of such remaining groups in the precursor. Also, solvating isopropanol contributes to these absorptions and to the broad bands at 3300-3700 cm^{-1}. In the spectral range of 950-1300 cm^{-1}, CO vibrations are characteristic. The right part of the spectra is indicative of the metal-

oxygen and metal-fluorine valence vibrations from 360-700 cm^{-1}, respectively, followed by the C-C frame absorptions of the organic constituents. The spectra of the amorphous products, i.e., HS-AlF_3 and HS-AlF_3-HF show a strong but very broad band arround about 667 cm^{-1}, which is assigned to the Al-F stretch of corner-sharing AlF_6 octahedral and weaker deformation vibration at about 360 cm^{-1}.

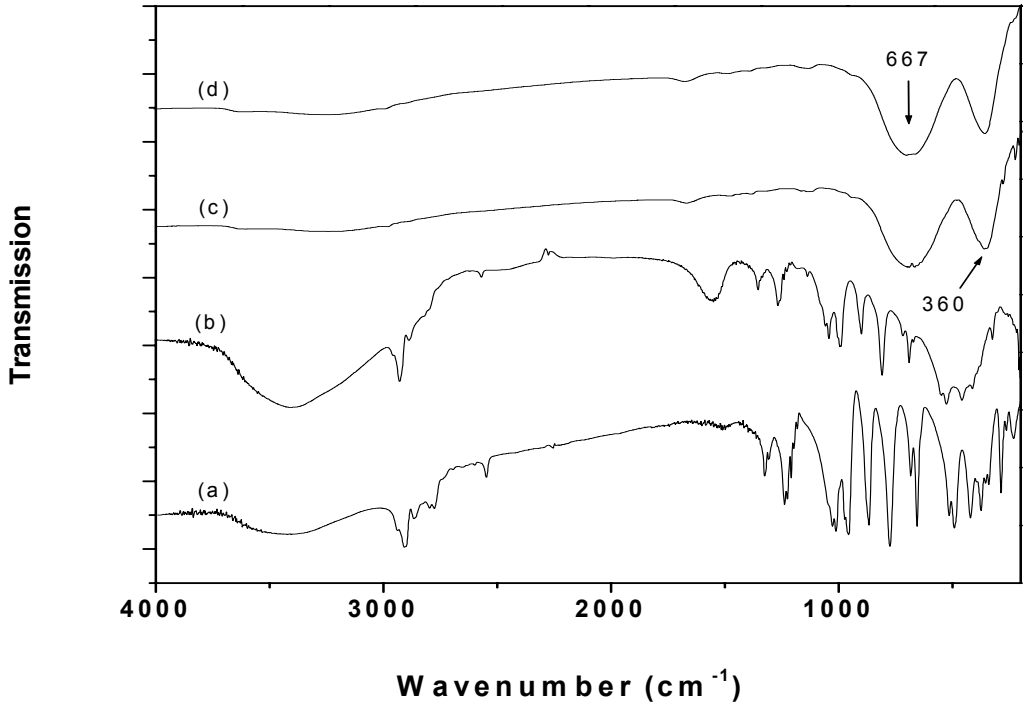

Figure 5.4 FTIR spectra of (a) $Al(O^iPr)_3$, (b) precursor, (c) HS-AlF_3, (d) HS-AlF_3-HF.

Comparing the IR spectra of HS-AlF_3 and HS-AlF_3-HF with the crystalline β-AlF_3 and α-AlF_3 phases, it is clear that the spectra of HS-AlF_3 and HS-AlF_3-HF samples (Figure 5.5a-b) are quite different from those of crystalline β-AlF_3 and α-AlF_3. Both β-AlF_3 (Figure 5.5c) and α-AlF_3 (Figure 5.5d) have two intense, sharp bands at 667 and 360 cm^{-1} (stretching and deformation bands, respectively). An additional a weak band at 547 cm^{-1} is observed for α-AlF_3. The position of this band is slightly shifted in case of β-AlF_3 due to the different connectivities of the AlF_6 octahedra and different lattice structure (HTB structure). It has been found that β-AlF_3 has two types of octahedral and different local geometries (differences in Al-F-Al angles). The bands observed for the amorphous HS-AlF_3 and HS-AlF_3-HF are very broad. The broadness of absorption bands found in HS-AlF_3 and HS-AlF_3-HF is directly related to the enormous degree of structural disorder present in these samples due to statistic distribution of bond lengths and angles.

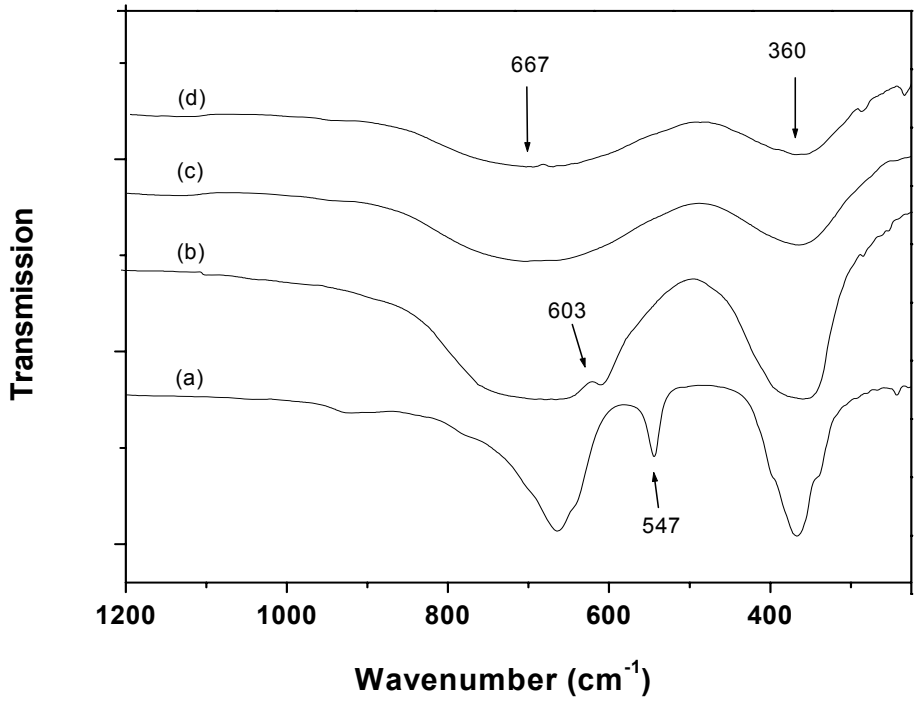

Figure 5.5 FTIR spectra of (a) α-AlF_3, (b) *β*-AlF_3, (c) HS-AlF_3, (d) HS-AlF_3-HF.

MAS-NMR

Since the long range disorder of amorphous HS-AlF_3 and HS-AlF_3-HF samples precludes the use of diffraction techniques for identification the structure, nuclear magnetic resonance (NMR) was used. Moreover, the progress in NMR with magic angle spinning (MAS) made studies of these amorphous samples possible.

NMR probes molecules by recording the interaction of radiofrequency electromagnetic radiation with the nuclei placed in a strong magnetic field. The method is based on the Zeeman Effect.

After applying Fourier transformation, NMR spectroscopy gives a spectrum of the resonance signals of nuclear spins as function of the frequency of electromagnetic radiation. When the spin system is saturated, relaxation processes have to occur which return nuclei from higher to lower energy states in order to enable continuous excitation. There are two elementary types of relaxation processes: Spin-Lattice and Spin-Spin relaxation.

The line width of the NMR signal is inversely proportional to the Spin-Spin relaxation time. The faster the relaxation the broader is the NMR signals. Spinning the sample at the magic angle θ (θ = 54.7°) with respect to the direction of the magnetic field, helps to reduce

the solid state interactions (e.g. dipole-dipole interaction, anisotropies in chemical shifts, quadrupole interaction) and the broad lines become narrower.

From previous studies, according to the MAS NMR of the starting material $[Al(O^iPr)_3]_4$, the Al atom is tetrahedrally and octahedrally coordinated (see chapter 4, scheme 4.1) [36]. During the first fluorination process, F substitutes for $-O^iPr$ groups to form octahedrally surrounded but distorted Al sites of the type $Al(F,O)_6$ [36]. The coordinative state depends on the relative F contents or in another word HF/Al ratio. In the second fluorination step, the remaining $-O^iPr$ groups are replaced by F to form amorphous AlF_3 with Al coordinated by F only (scheme 4.1).

^{27}Al MAS-NMR

The ^{27}Al MAS NMR spectra of HS-AlF_3 and HS-AlF_3-HF samples as well as of the crystalline α-AlF_3 and *β*-AlF_3 reference samples are shown in Figure 5.6a-d. The position of the ^{27}Al signal for HS-AlF_3 (Figure 5.6c) is similar to that arising from the crystalline α-AlF_3 (Figure 5.6a) and *β*-AlF_3 (Figure 5.6b), which indicates that the basic structural units in HS-AlF_3 involve AlF_6 octahedra. Only one signal at -15.5 ppm was observed for HS-AlF_3, which is attributable to six-fold coordinated Al with F. The signal is rather broad and asymmetric, which is typical of second order quadrupole broadening and disorder effects. In addition to that, a large sideband manifold is present, indicating that the aluminum sites in the sample have a larger quadruple coupling constant (QCC) compared with the aluminum sites in α-AlF_3 and *β*-AlF_3 [34]. The larger QCC is indicative of a more distorted aluminum environment for HS-AlF_3. The ^{27}Al MAS spectrum of HS-AlF_3-HF showed almost identical behavior to that of HS-AlF_3 (Figure 5.6d).

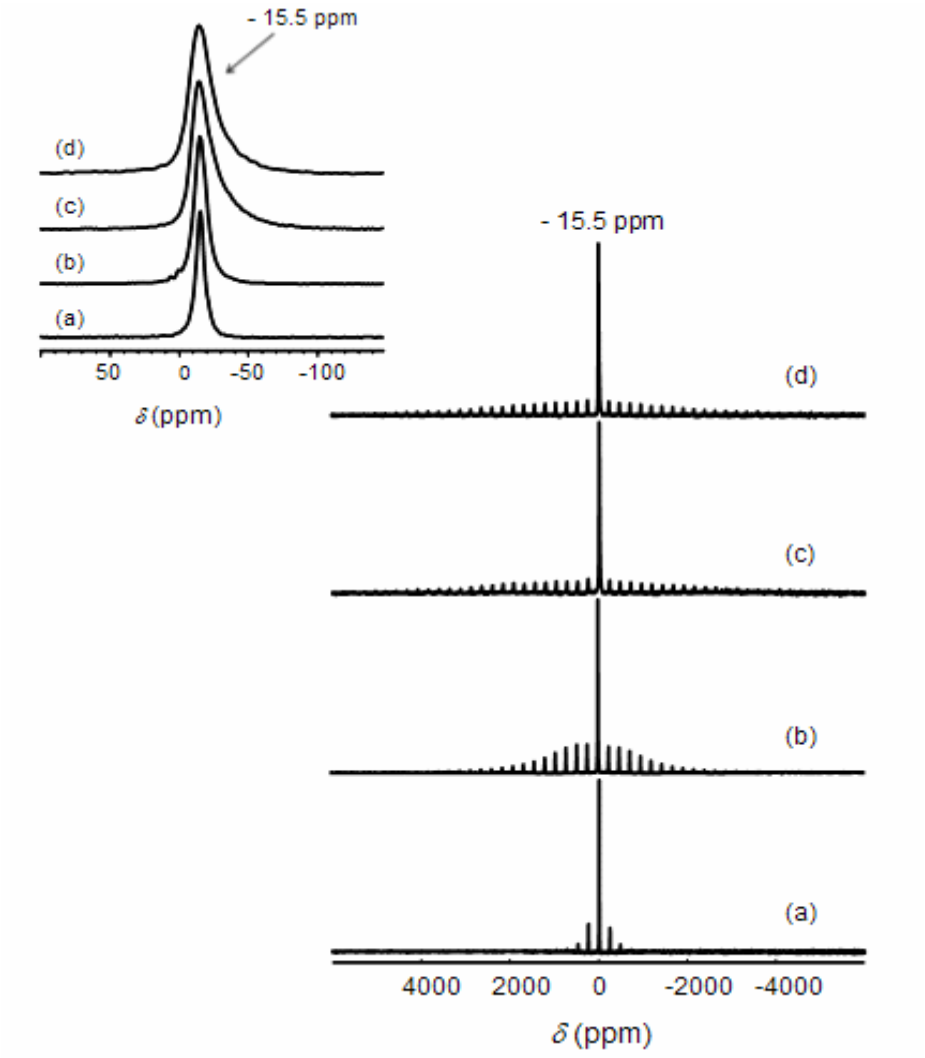

Figure 5.6 ^{27}Al MAS NMR spectra of (a) α-AlF_3, (b) *β*-AlF_3, (c) HS-AlF_3, (d) HS-AlF_3-HF (ν_r = 25 KHz).

^{19}F MAS-NMR

Solid-state ^{19}F MAS NMR was used to study the fluorine coordination species of the same samples. Figure 5.7a-d illustrates the ^{19}F MAS NMR spectra obtained for α-AlF_3, *β*-AlF_3, HS-AlF_3-HF, and HS-AlF_3. The ^{19}F spectra of α-AlF_3 (Figure 5.7a) and *β*-AlF_3 (Figure 5.7b) are identical and resonant at -172 ppm, whereas the ^{19}F signal for HS-AlF_3 (Figure 5.7c) is shifted to higher field with maximum at -164 ppm. These signals correspond to the Al-F-Al linkages in octahedrally coordinated AlF_3. They closely resemble to that reported for fluorinated γ-Al_2O_3 (main signal at -168 ppm) [86], and to that of ACF, the most distorted aluminum fluoride known with main signal at -162 ppm [87]. The ^{19}F MAS NMR spectrum of HS-AlF_3-HF, prepared by fluorination of the dry precursor with HF, i.e., with

HF blocking the strong Lewis acid sites, is almost similar to that of HS-AlF_3 and to HS-AlF_3+HF (main signal at 165.8 ppm) [36], the signal is shifted slightly to -166 ppm (Figure 5.7c). These results imply that the fluorine atoms of the physically adsorbed HF cannot be distinguished from the chemically bound ones by MAS-NMR.

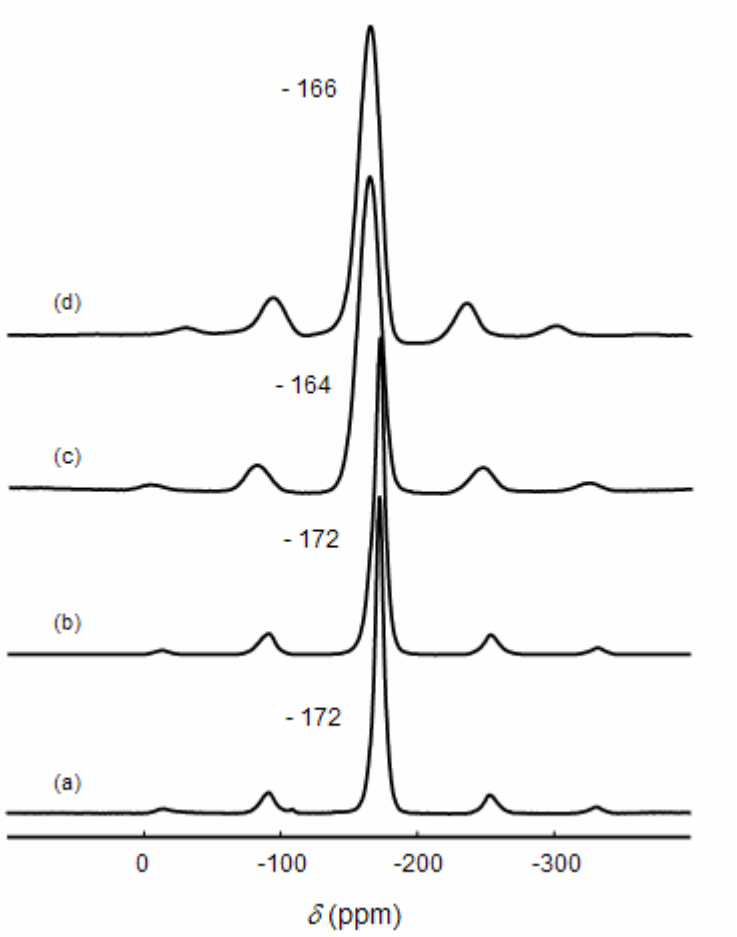

Figure 5.7 ^{19}F MAS NMR spectra of (a) α-AlF_3 (ν_r = 30 KHz), (b) *β*-AlF_3 (ν_r = 30 KHz), (c) HS-AlF_3 (ν_r = 25 KHz), (d) HS-AlF_3-HF (ν_r = 20 KHz).

5.3 Surface characterization

X-ray photoelectron spectroscopy (XPS)

Photoelectron spectroscopy is based on the external photoelectron effect. The relation governing the interaction of a photon with a core level electron is described by the following equation: $Ek = h\nu - BE - \varphi_s$, with Ek being the kinetic energy of the ejected photoelectron, $h\nu$ is the energy of the incoming photon, BE is the binding energy of the emitting electron from the core level, and φ_s is the spectrometer work function. The fact that all elements

show unique binding energies, identification of the elements and quantification of surface compositions in HS-AlF_3 and its precursor can be directly obtained from XPS.

Results

Changes in the chemical environment of an atom may be followed by changes in the photoelectron energies. From XPS, information about the chemical state of aluminum and fluorine in HS-AlF_3 and precursor can also be obtained.

Al(2p) spectra for HS-AlF_3 and precursor samples are illustrated in Figure 5.8. As it can be seen, the deconvoluted Al(2p) spectrum of the precursor is only one peak centered at binding energy (BE) of about 75.6 eV, which is typical for Al^{3+} in AlF_3. However, this BE is lower than Al(2p) of edge-shared regular AlF_6 octahedra found in the crystalline AlF_3 modifications (75.9 eV). This behavior can be explained as following: precursor has high carbon content (about 30%), i.e., remaining of –O^{i}Pr and/or solvents, which are less electronegative than F. Therefore, they withdraw less electron density from the Al atoms, resulting in shifting the BE of Al(2p) to a lower value. For HS-AlF_3, the deconvoluted Al(2p) spectrum is composed of two peaks located at around 75.1 and 76.2 eV, respectively. The one at high BE is characteristic for crystalline α-AlF_3, while the other is significantly lower. These results indicate the presence of two different Al sites in HS-AlF_3.

The F(1s) BE in HS-AlF_3 is comparable with that of α-AlF_3 (686 eV), indicating that the chemical environment of F^- ions in the samples are almost similar (Figure 5.8). In the AlF_3 crystalline phases, F atoms are always 2-fold coordinated by Al, with Al-F bond lengths and Al-F-Al angles are similar between 132 and 180° [71]. The F 1s binding energy is unlikely to vary significantly as a result of these modest bond angle variations. Whereas lower BE was observed for the precursor (685.6), which is due to the presence of the residual electropositive –O^{i}R groups. The presence of –O^{i}R groups screens the F core hole and results in decrease in the BE of the F 1s electrons.

In the O(1s) XPS spectra, relatively broad and less intensive peaks were observed for both samples (precursor and HS-AlF_3, Figure 5.8). From The BE values, it can be concluded that HS-AlF_3 and the precursor materials contain oxygen containing compounds like alkoxide, alcohol, adsorbed H_2O and/or hydroxyl groups [89-90]. The latter two are less probably, however, it is not possible to give a clear designation although contributions around 534 eV in the spectrum of the precursor material could be due to adsorbed water whereas the BE equals to 532 eV could be probably due to the remaining alkoxide groups

and/or isopropanol. However, as already stated it is not possible to distinguish between alkoxides, alcohols, hydroxyl or adsorbed water species in the precursor material by XPS spectra.

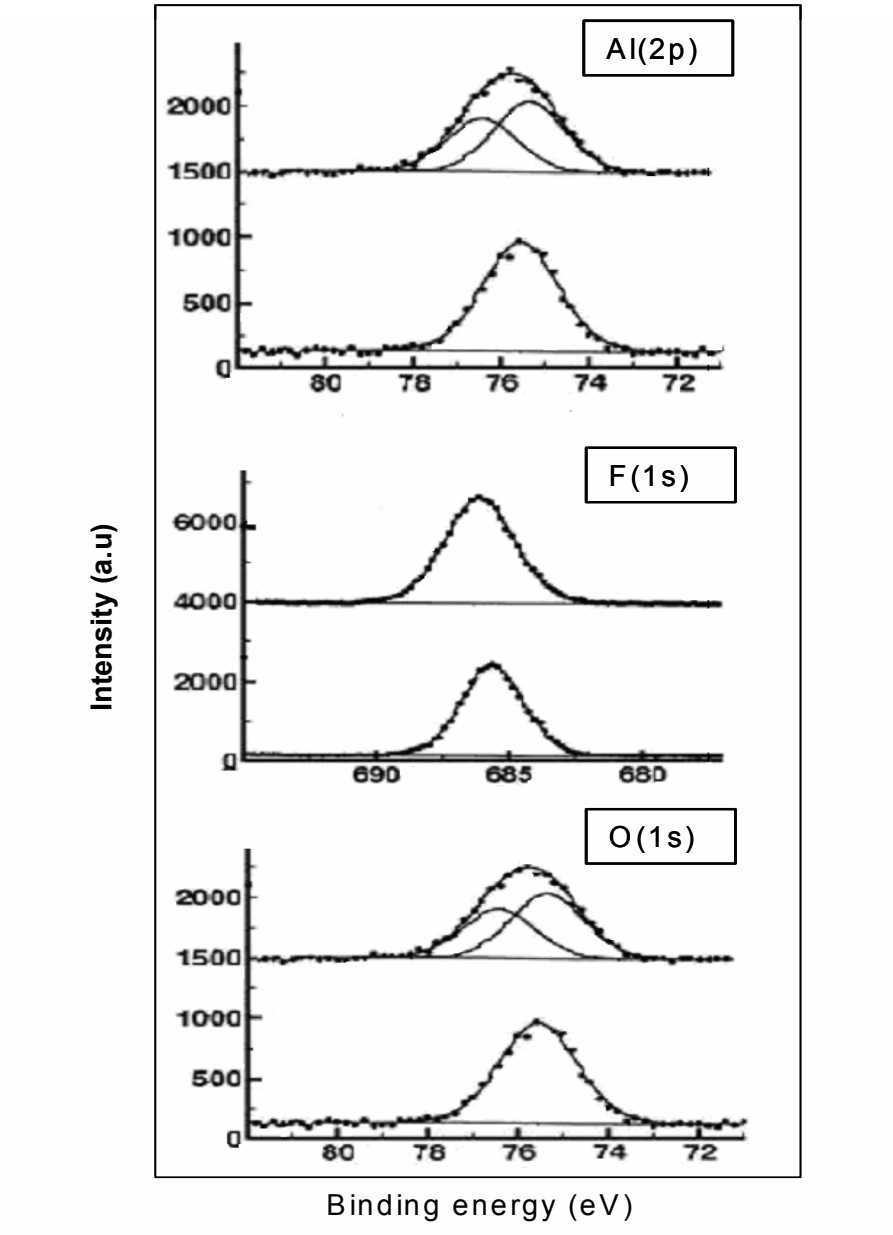

Figure 5.8 Al(2p), F(1s), and O(1s) XPS data of the (a) precursor and (b) HS-AlF_3.

X-ray absorption fine structure is (XAFS) studies

XAFS is based upon energy transitions between different electronic states in atoms or molecules. These energy transitions are due to absorption of X-rays by an atom at energies near and above the core-level binding energies of an atom. X-ray absorption is recorded as a function of the incident X-ray energy. If X-ray energy is higher than the binding energy of

the core electron (K-edge: 1s electrons are excited, L-edge: 2s or 2p, M-edge: 3s, 3p or 3d), an increase in the adsorption occurs (adsorption edge).

XAFS are usually separated in two regions: The X-ray absorption near edge structure (XANES) and the extended X-ray absorption fine structure (EXAFS). The XANES region is dominated by the local atomic resonance and multiple scattering at neighboring atoms (≈ 50 eV above the core level energies). From the absorption profile near an absorption edge, information about the oxidation state and the geometry around metals in the compounds can be obtained. The EXAFS fine structure (i.e., interference pattern) region is determined by single and multiple scattering events at neighboring atoms. In addition, if there is disorder in the investigated sample, the position of the neighboring atoms will not be defined and different interference patterns are generated. Simulation of experimental EXAFS spectra can be used to determine the distance between the adsorber and backscatters, the coordination number of the adsorber atom and disorder [88]. Hence, the type, number and distance of the nearest neighbors atoms and structural disorder can also be determined. The method does not require crystalline material; hence, it is allows to investigate the amorphous HS-AlF_3 and the precursor structures.

Results

Figure 5.9 shows the Al K-edge XANES spectra of four samples with well-defined Al coordination: two references samples (crystalline α-AlF_3 and *β*-AlF_3), HS-AlF_3 precursor, and HS-AlF_3. It can be seen that there are strong similarities between all the samples, especially the energy position of the adsorption edge, which is characteristic for Al^{3+}. At higher kinetic energies, α-AlF_3 and *β*-AlF_3 showed intense amplitude of the spectra due to multiple-scattering caused by the ordered local structure, whereas precursor and HS-AlF_3 showed weaker EXAFS oscillations caused by the disorder of the first Al-F coordination shell.

The F K-edge XANES spectra of the above samples are shown in Figure 5.10. Two well-defined near edge features (marked $4a_1$ and $2b_2$) of XANES spectra of the reference compounds were observed, whereas the XANES spectra of HS-AlF_3 and precursor do not exhibit a clear split resonance. According to the literatures, F K-edge XANES can be interpreted in terms of the local F-Al-F binding angle. Hence, local structure with different F-Al-F geometries will have different energies of the unoccupied $4a_1$ and $2b_2$ orbitals. Highly distorted structures as in HS-AlF_3 and precursor will not show a clear split between the resonances from the unoccupied $4a_1$ and $2b_2$ orbitals.

In addition, based on EXAFS Al K-edge fitting analysis, the coordination numbers of HS-AlF_3 and the precursor were found to be 5.3 and 5.8, respectively. These results imply that HS-AlF_3 contains distorted AlF_6 octahedra together with five-fold coordinated Al-species (AlF_5) or even four-fold coordinated Al-species (at least on the surface), which is possibly the reason for its high Lewis acidity.

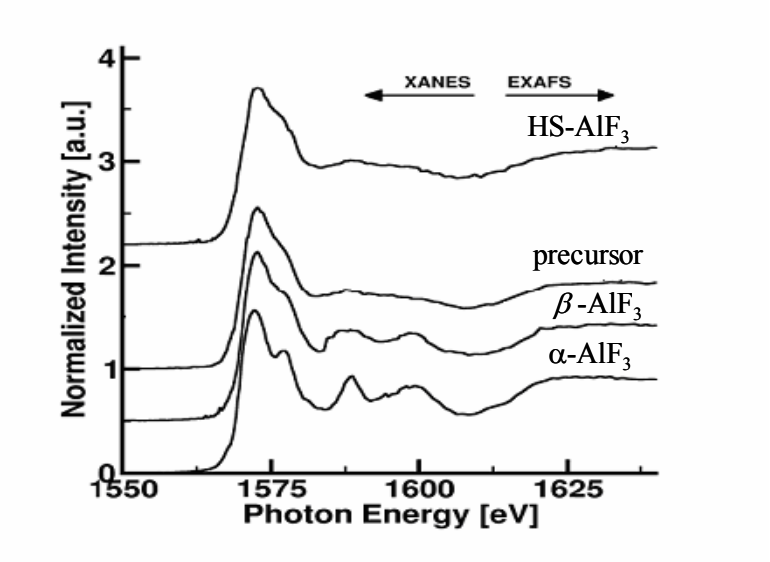

Figure 5.9 Al K-edge XANES spectra of precursor and HS-AlF_3, and two reference materials α-AlF_3 and β-AlF_3.

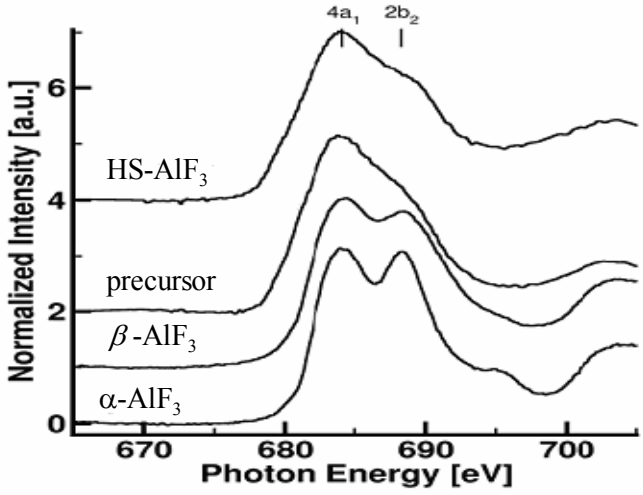

Figure 5.10 F K-edge XANES spectra of precursor and HS-AlF_3, and two reference materials α-AlF_3 and β-AlF_3.

N_2 adsorption-desorption

Adsorption of N_2 was used to gain information about surface area and porosity of HS-AlF_3, HS-AlF_3-HF, and precursor samples. Adsorption-desorption of probe molecules on surfaces of solid samples are commonly used methods for characterization of porous materials. Information about the porosity of the materials can be obtained from the shape of the hysteresis loop of the adsorption-desorption isotherms. According to IUPAC classification six types of isotherms and four types of hysteresis loops can be distinguish [91-92].

The total surface area of the sample can also be calculated when the area (cross section) of the adsorbed molecule is known (N_2 = 16.2 Å^2). The most widely used technique for estimating the surface area, is the so called BET method. This method is developed by Brunauer, Emmett, and Teller in 1938 [77].

Results

Table 5.1 shows the surface area, pore volume, and the average pore diameter of precursor, HS-AlF_3, and the HS-AlF_3-HF samples. Precursor had a higher surface area than HS-AlF_3-HF, and HS-AlF_3. The difference in the surface area is due to different treatment/fluorination temperature used.

Table 5.1: Texture properties of the precursor, HS-AlF_3, and HS-AlF_3-HF

Sample	Fluorination (treatment) temperature/time (°C/h)	Texture properties BET/N_2		
		S_{BET} (m^2/g)	V_p[a] (cm^3/g)	d_p[b] (Å)
precursor	100/2	602	0.29	31
HS-AlF_3	250/8	250	0.59	68
HS-AlF_3-HF	120/4	420	0.35	33

a– BJH desorption cumulative pore volume of pores between 17.0 and 3000.0 Å diameter
b– average pore diameter by BET

N_2 adsorption-desorption isotherms of HS-AlF_3, prepared by fluorination of the precursor with $CHClF_2$ and HS-AlF_3-HF are presented in Figure 5.11. Samples exhibited similar isotherms (type IV), which are typical of mesoporous solids according to IUPAC classification [91-92]. The hysteresis loops, owing to the capillary condensation associated

with the mesopores can be ascribed to type H1. Large mesopores were observed in HS-AlF_3 samples, indicated by closing the hysteresis loop at P/P_0 values of ca. 0.5. Small mesopores were found for HS-AlF_3-HF samples, whose desorption step is displaced to a lower P/P_o value. The shape of the isotherms suggests that the samples have "ink-bottle" pores or voids between close-packed spherical-like particles [91].

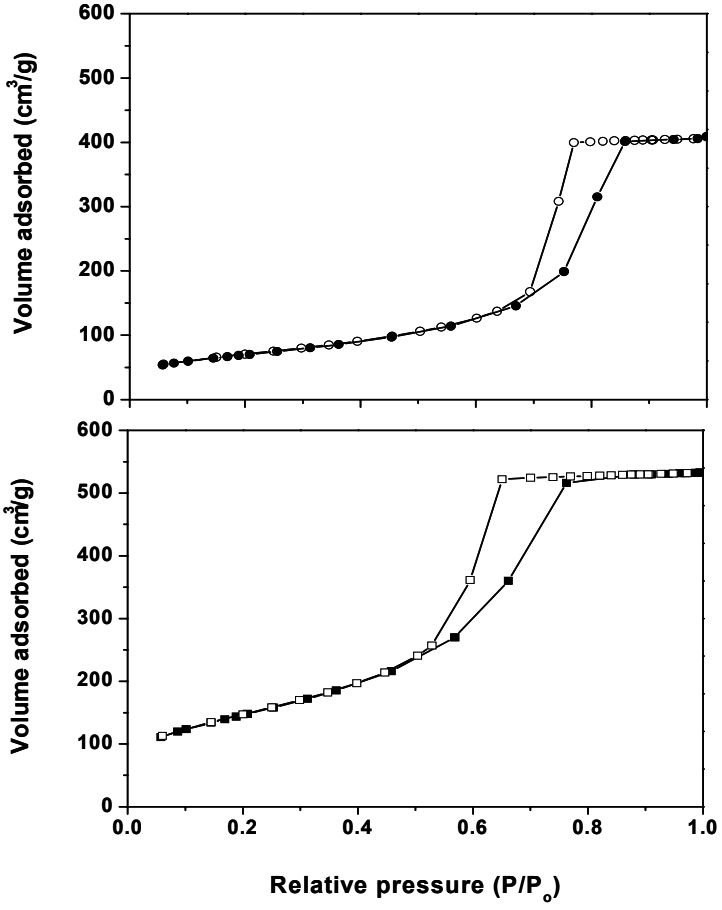

Figure 5.11 N_2 adsorption/desorption isotherms of HS-AlF_3-HF (top) and HS-AlF_3 (bottom).

The mesopore size distributions of HS-AlF_3-HF and HS-AlF_3 are shown in Figure. 5.12. The pore size distribution from desorption branch of the isotherm is calculated by the BJH methods. The pore diameters of HS-AlF_3, HS-AlF_3-HF and HS-AlF_3 samples were centred at about 52 and 108 Å, respectively. The HS-AlF_3 had pores with slightly higher pore volumes than that of HS-AlF_3-HF.

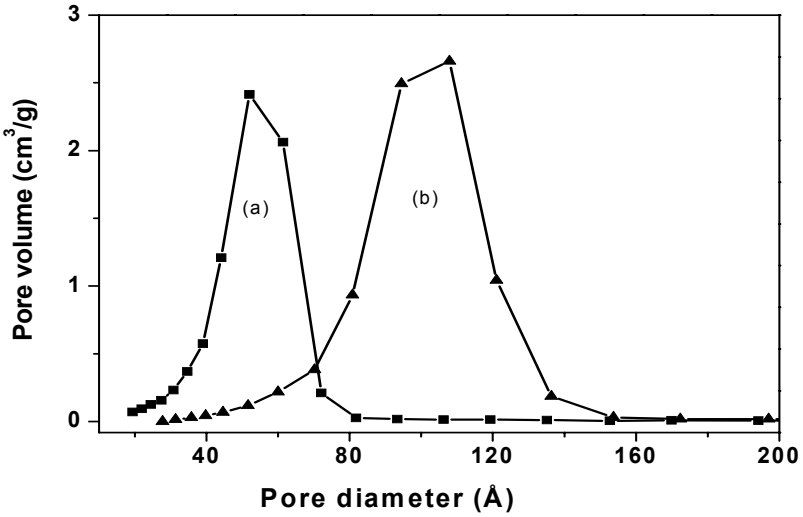

Figure 5.12 Pore size distribution of (a) HS-AlF_3-HF, (b) HS-AlF_3.

Scanning electron microscopy (SEM)

The SEM analysis are performed to determine the morphology of the precursor and HS-AlF_3 samples and in order to see how the morphology of the precursor and how its change with fluorination.

In SEM, electrons are generated from an electron gun enter the surface of the sample and generate many low energy secondary electrons. An image of the sample surface can thus be constructed by measuring the secondary electron intensity as a function of the position of the scanning primary electron beam. In addition to low energy secondary electrons, backscattered electrons and X-rays are also generated by primary electron bombardment. The intensity of backscattered electrons can be correlated to the atomic number of the element within the sampling volume. Hence, some qualitative elemental information can be obtained. In addition, the analysis of the characteristic X-rays emitted from the sample by energy dispersive X-ray (EDX) gives more quantitative elemental information.

Results

The morphology of the HS-AlF_3 and the precursor at the micrometer scale as determined from SEM comprises disordered aggregated form, which differs from the crystalline α-AlF_3. These aggregates consist of particles which are mesoporous and XRD amorphous (Figure 5.13). Energy dispersive X-ray (EDX) indicated the presence of fluorine, aluminum, and oxygen in the precursor ($AlF_x(O^iPr)_{3-x}$) and HS-AlF_3. The presence of oxygen in HS-AlF_3 could

be attributed to the presence of water when the sample was exposed to air prior to measurements.

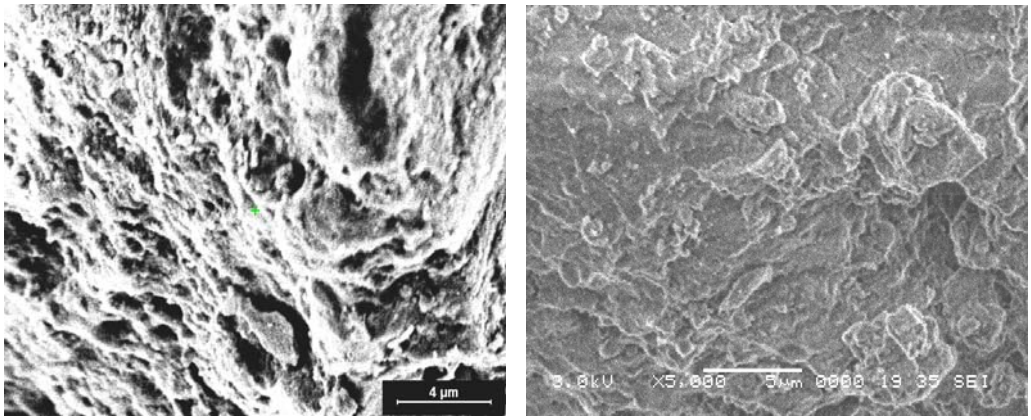

Figure 5.13 SEM images (left) HS AlF_3 and (right) precursor.

Acidity measurements

The catalytic activity of a large group of catalysts used in isomerization, halogen exchange, cracking, hydrocraking, dehydration of alcohols, polymerization of alkenes, and other process is due to the acidity of their surface. The catalytic activity of HS-AlF_3 indicates the existence of very strong Lewis acid sites on the surface. Base molecules such as ammonia and pyridine are, in principle, good probes for the study of acid sites and have been often used for such studies. Carbon monoxide (CO) makes useful probe molecules because it is less basic than ammonia and pyridine; it would presumably be held only by stronger acid sites.

IR-PAS of pyridine adsorption

Pyridine has a lone pair of electrons on the nitrogen atom. Therefore, it is expected to coordinate to Lewis acid sites and to be protonated to Brønsted acid sites as shown in Figure 5.14 [93-99].

Figure 5.14 Schematic representation of interaction of pyridine with Lewis (L) and Brønsted acid sites (B).

All these forms can be identified by studying the changes in the ring vibration of pyridine and other bands in the region of 1700 cm^{-1} to 1400 cm^{-1} as shown in Table 5.2 [100-101].

Table 5.2: IR vibration of pyrdines bands in the region of 1700 cm^{-1} to 1400 cm^{-1}

Mode	Class	$Py_{(gas)}$	Py-Lewis sites (cm^{-1})	Py- Brønsted sites (cm^{-1})
ν_{19b}	B_2	1438	1447-1464	1535-1550
ν_{19a}	A_1	1492	≈ 1490-1485	≈ 1490-1485
ν_{8b}	B_2	1570	1634-1600	1640
ν_{8a}	A_1	1586	1600-1580	1600-1580

Data taken from reference [29]

The ring vibrational modes ν_{19b} and ν_{8a}, are the most sensitive vibrations with regards to the nature of intermolecular interactions via the nitrogen lone pair. The formation of coordinated species Py on Lewis acid sites leads to the appearance of IR bands near 1620-1600 cm^{-1} (ν_{8a}) and 1447-1464 cm^{-1} (ν_{19b}), while the formation of pyridinium ions, pyH^+, on protonic sites gives a rise to characteristic bands at 1640 cm^{-1} and 1540 cm^{-1}.

The observation of a band at about 1540 cm^{-1} is a unique indication of Brønsted acidity of the sample under investigation. This band is due to the combined C-C stretching and in-plane C-H and N-H bending modes and, therefore, cannot be present in coordinately bound Py since the N^+-H bending motion is involved in the vibration. Hence there must be a proton transfer to the nitrogen in order to observe this band [100].

While the band around 1540 cm^{-1} does not change in the wavenumber upon varying the acidity of the solid, the band characteristic for coordinatively bound pyridine shift to higher wavenumber as the strength of the interaction increases.

Results

The spectra measured after pyridine adsorption at 150 °C on HS-AlF_3, HS-AlF_3 treated with HF/N_2 (named HS-AlF_3 + HF), HS-AlF_3-HF (prepared by activation of the precursor with HF), and HS-AlF_3-HF heated in N_2 (HS-AlF_3-HF + N_2) are shown in Figure 5.15a-d.

The IR spectra of Py/HS-AlF_3-HF (Figure 5.15b) and Py/HS-AlF_3 + HF samples (Figure 5.15c) are essentially the same, but differ significantly from Py/HS-AlF_3 (Figure 5.15a).

While, HS-AlF_3 shows the dominance of very strong Lewis acid sites, indicated by the bands at 1454 cm^{-1} and about 1490 cm^{-1} with an intensity ratio of 3:1, in the IR-PAS of Py/HS-AlF_3+HF and of Py/HS-AlF_3-HF the intensity ratio is quite the opposite, and protonation of pyridine on Brønsted acid sites is observed indicated by the strong broad band at about 1545 cm^{-1} [36]. Brønsted acid sites result from the reaction of HF molecules with strong Lewis acid sites according to: Lewis acid + F–H → Lewis site··· F^{-}····H^{+}. Figure 5.15d gives additional evidence of enhancement of the Lewis acidity after heating HS-AlF_3-HF under N_2 or $CHClF_2$. The band at 1545 cm^{-1} was vanished and only bands characteristic of Py adsorbed on Lewis acid sites, between 1620 and 1600 cm^{-1} and between 1450 and 1440 cm^{-1} were observed, leading to the conclusion that HS-AlF_3-HF + N_2 sample, possesses predominantly Lewis acid sites. No evidence was found for a band at 1540 cm^{-1}, indicating that there are no Brønsted sites on the surface [100].

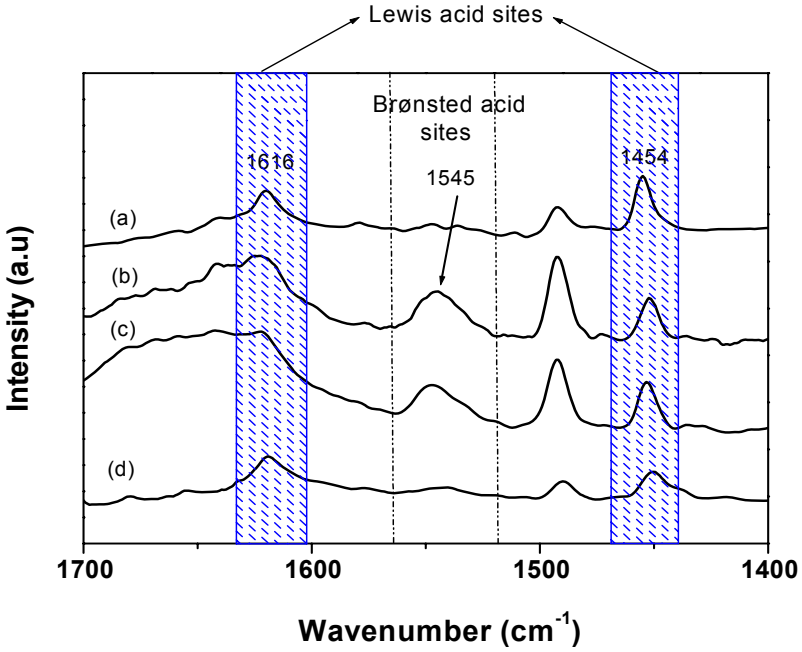

Figure 5.15 pyridine adsorption on (a) HS-AlF_3 (b) HS-AlF_3 + HF, (c) HS-AlF_3-HF, (d) HS-AlF_3-HF+N_2.

IR-CO adsorption

CO shows basic behavior due to the presence of an electron lone pair. The vibrational spectrum of CO adsorbed on exposed surface cations in coordinative unsaturation presents a band falling at higher frequencies than the free gaseous CO (ν_{CO} = 2143 cm^{-1}). The

interaction involves the σ (non-bonding) orbital of CO (Figure 5.16), which donates an electron to the cation and forms a bond with σ character [101-104].

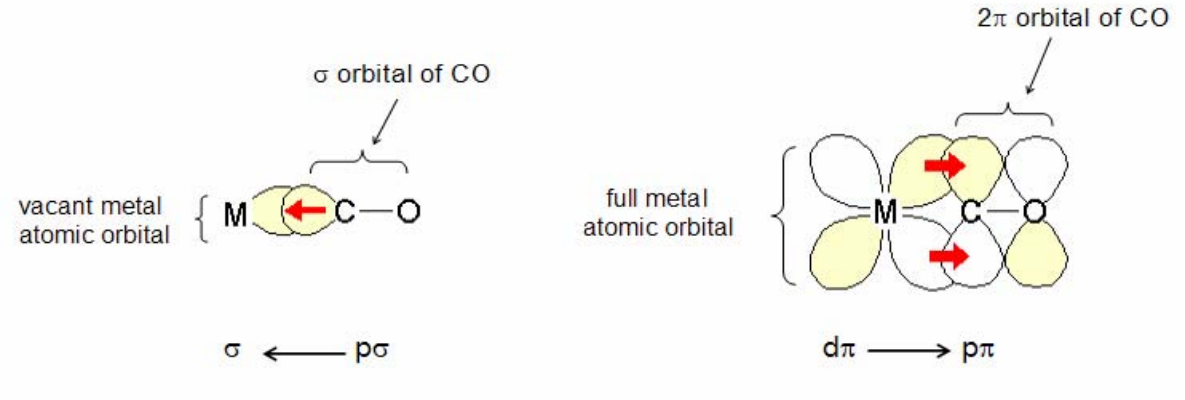

Figure 5.16 σ donation and π backdonation between d orbitals of transition metal and π^* of CO orbitals.

If the cation possesses d orbitals fully or partially occupied, an interaction between these d orbitals and unoccupied π^* CO orbitals could occur through the π back donation from metal or cation to CO. This back donation will lead to strengthening of the interaction due to the formation of stable metal-carboxyl bonds and gives rise to a decrease of bond order and, consequently, the CO stretching [103].

In case of HS-AlF$_3$, however, there are no d-electrons. Hence, the σ interaction prevails. This results in a reduced contribution of anti-bonding character of the CO bond making the bond stronger, which is observed as a large blue shift CO stretching IR band, as illustrated in Figure 5.17.

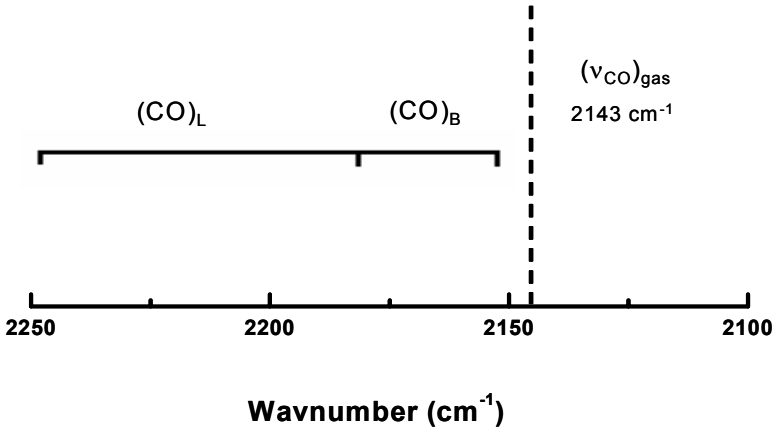

Figure 5.17 Spectral ranges for CO adsorbed on Lewis ((CO)$_L$) and Brønsted ((CO)$_B$) acid sites.

The blue shift of its IR band increases with increasing strength of the CO bond. When CO is adsorbed on Brønsted acid sites, a red shift of the stretching band of the acidic OH band is observed with a small blue shift of the CO stretching band. Therefore, it is possible to distinguish between Lewis and Brønsted acid sites using IR-CO.

Results

Figures 5.18-5.21 show typical IR spectra in the 2300-2000 cm^{-1} region CO-stretching-region, of CO adsorbed on β-AlF_3 (β-AlF_3 reacts as Lewis acid), HS-AlF_3, HS-AlF_3-HF, and precursor. All these figures show arrays of curves representing the respective spectra for graduates CO bondings.

Thus, in Figure 5.18 of HS-AlF_3 upon adding the first portion of CO, two partially overlapping bands (2235-2218 and 2183-2175 cm^{-1}) were observed, which grow in a different way upon increasing the CO dosing. Both bands have higher frequency than the free CO molecules and are assigned to CO bonded to Lewis acid sites of different strength. At the lowest coverage, only the band at 2235 cm^{-1} appeared and with increasing the surface coverage, the intensity of the band increased and the frequency shifted to lower wavenumber at 2218 cm^{-1}. This band is attributed to CO σ-bonded to very strong cationic Lewis acid sites, not observed before for Lewis acid catalyst (Al^{3+} ← CO complex with Al^{3+}_{cus} coordinated to F^- ligands). The second band at 2183-2175 cm^{-1} appeared only when the first band nearly reached its maximum intensity, i.e., when all the strongest Lewis acid sites are completely covered by CO. This band is assigned to CO species interacting with medium strong Lewis acid sites [103-104]. With further increasing the surface coverage, the intensity of the band increases and the frequency shift to lower wave number (2175 cm^{-1}).

For β-AlF_3 (Figure 5.18 top), at low coverage rate a small shoulder at 2220 cm^{-1} is observed (strong acid sites), which is shifted to 2179-2165 cm^{-1} at higher coverage rates. This band corresponds to medium strong Lewis acid sites. This clearly shows that the majority of the acidic centres on the surface of β-AlF_3 is of medium strength, but only a few very acidic centres are also present. These results imply that the Lewis acidity of HS-AlF_3 is higher than β-AlF_3.

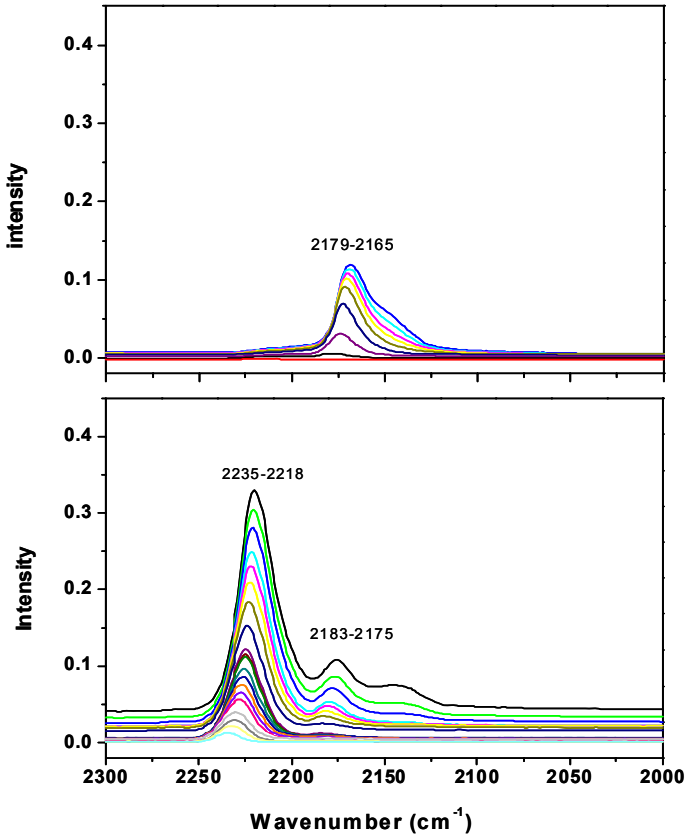

Figure 5.18 IR spectra of CO adsorption on (bottom) HS-AlF_3 and (top) β-AlF_3.

Comparing the IR spectra of CO adsorbed on HS-AlF_3-HF and HS-AlF_3 (Figure 5.19), it is clear that there is a down shift (≈ 15 cm^{-1}) of all the vibrational frequencies of CO adsorbed on HS-AlF_3-HF. CO adsorbed on HS-AlF_3-HF gave again two bands: one minor band at 2220 cm^{-1} (strongly Lewis acidic sites) with low intensity and one major band at 2169 cm^{-1}, assigned to Brønsted acid sites or very weak Lewis acid sites [103-104]. This is obviously because HF is adsorbed on the strongest Lewis acid sites and blocking them, which can be seen in IR-CO data and indicated by NH_3-TPD (Figure 5.22).

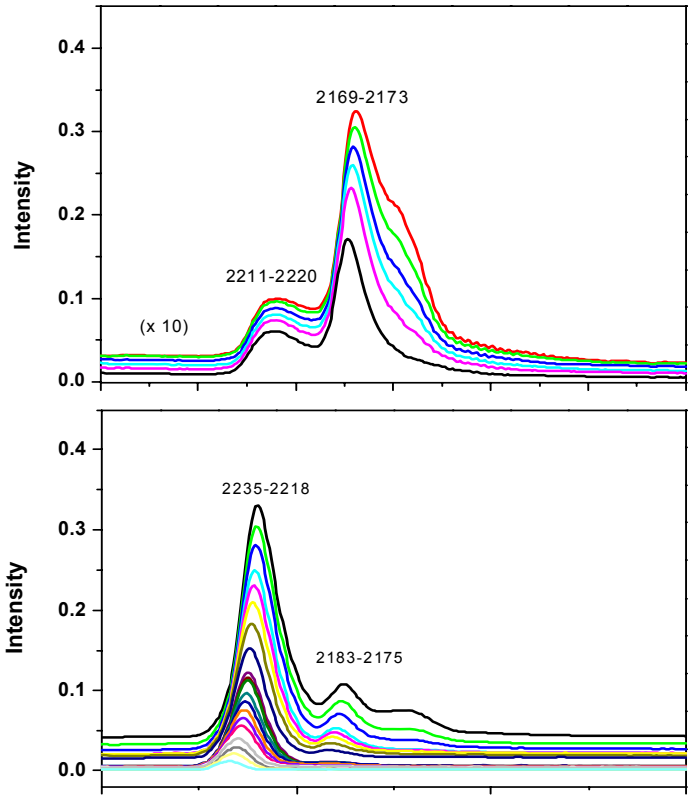

Figure 5.19 IR spectra of CO adsorption on (bottom) HS-AlF$_3$ and (top) HS-AlF$_3$-HF.

Figure 5.20 shows typical IR spectra of CO adsorbed on HS-AlF$_3$ precursor (top) and HS-AlF$_3$ (bottom). Whereas the band maxima do not differ markedly from those of HS-AlF$_3$, which is an indicative of the existence of strong and medium Lewis acid sites, these relative intensities differ markedly. Higher intensity of the low frequency (2183-2180 cm^{-1}) was observed and also the total intensity is lower compared with HS-AlF$_3$. This implies that there are some Lewis acid sites on the surface of the precursor but in smaller amount and with lower strength.

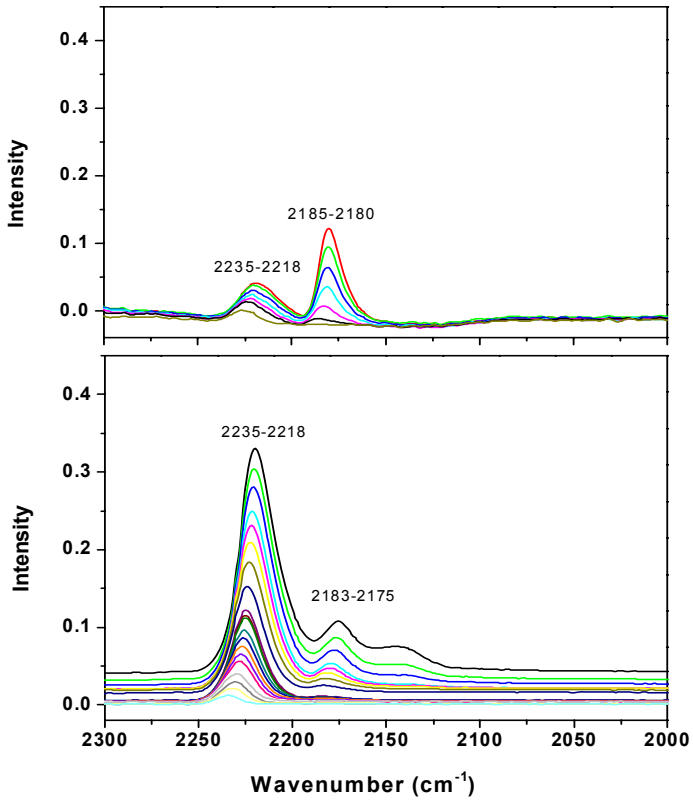

Figure 5.20 IR spectra of CO adsorption on (bottom) HS-AlF$_3$ and (top) precursor.

NH$_3$-TPD

The knowledge of the strength and amount of acid sites on HS-AlF$_3$ is also very important for understanding activity and selectivity for catalytic reactions. Temperature programmed desorption (TPD) of basic molecules is to characterize the acid strength and acid amount on the catalyst surface [105-109]. Ammonia, pyridine, n-butylamine are extensively used as basic probe molecules. Since a base is more stable on stronger sites, the basic molecules at weaker sites will be desorbed earlier when raising the temperature. Thus, the temperature of the TPD peaks can indicate the acid strength. Ammonia was used because of its small molecular size (ω_m = 0.16 nm^2), stability at high temperature, and strong basicity (p$K_a \approx 9.2$) [36-37, 40, 62, 109].

Results

In NH_3-TPD profile of HS-AlF_3, the abscissa denotes the temperature, while, the normalized (per unit weight of the sample) NH_3 desorbed per degree temperature increments is indicated in the ordinate. The strength of acid sites is indicated by the temperature in the desorption profile; the higher the temperature, the stronger the acid sites.

Figure 5.21 shows NH_3-TPD profiles of HS-AlF_3. The ammonia TPD profile was fitted by Gaussian deconvolution using four peaks in order to get more information about the acid strength distribution of HS-AlF_3. The use of these peak fit profiles was not based on peak assignment to specific acid sites, but only to help to characterize the acid strength distribution. As shown in Figure 5.21 HS-AlF_3 shows four peaks (deconvoluted peaks) with maxima at 227, 326, 392, and 500 °C, respectively, assigned to weak (227 °C), medium (326 and 392 °C) and strong (500 °C) acidity, respectively, related to the maximum desorption temperature.

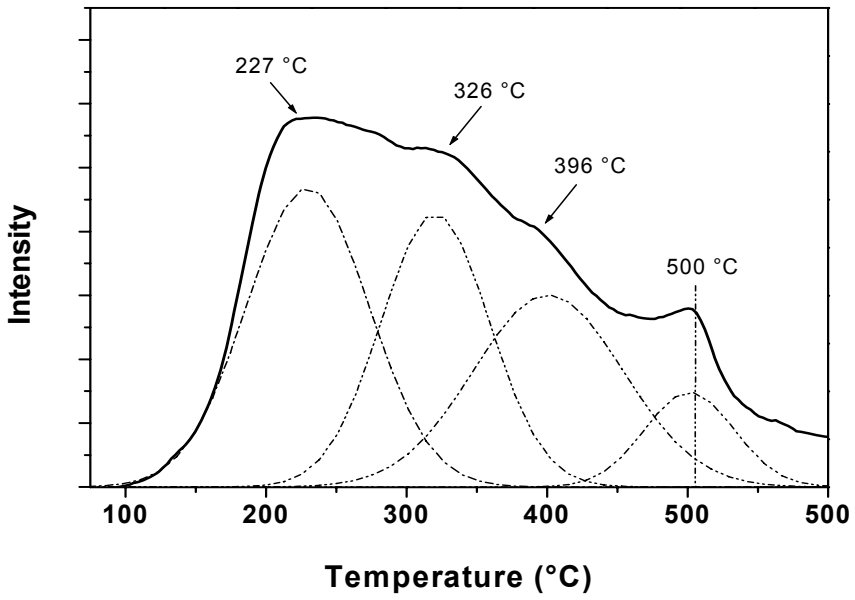

Figure 5.21 NH_3 temperature-programmed desorption profiles of HS-AlF_3.

Figure 5.22a-b compares the differences between the profiles of NH_3-TPD of HS-AlF_3-HF and HS-AlF_3. This direct comparison of the NH_3-TPD curves of HS-AlF_3-HF and HS-AlF_3 shows that HS-AlF_3 (Figure 5.22a) is by far superior to HS-AlF_3-HF (Figure 5.22b) as solid acid. HS-AlF_3.HF showed only one broad desorption peak with maximum at 209 °C, attributed to weak acid sites. This shows again that excessive HF blocks the strongest Lewis acid sites [36].

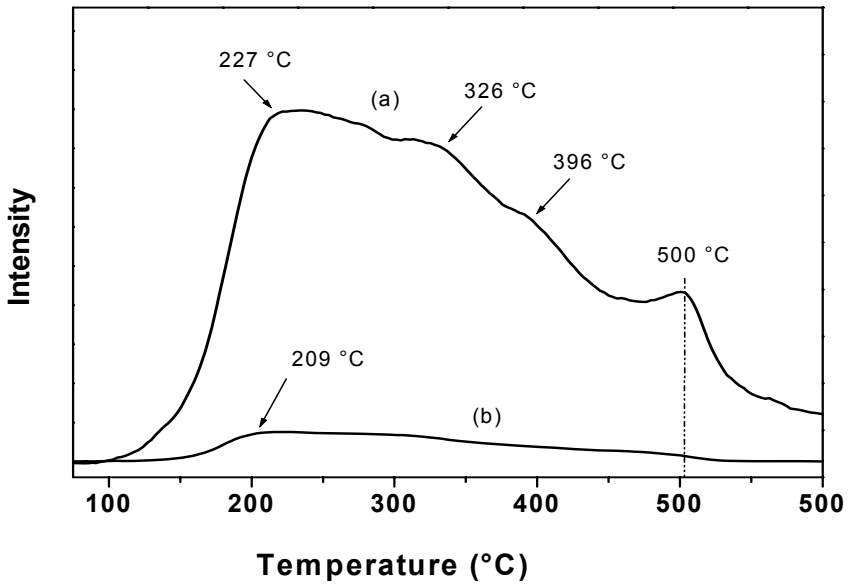

Figure 5.22 NH_3 temperature-programmed desorption profiles of (a) HS-AlF_3, (b) HS-AlF_3-HF.

5.4 Catalytic behavior

In the following section, a comparative catalytic study of selected HS-AlF_3 samples will be presented and discussed. In order to compare HS-AlF_3 samples prepared from different precursors, they were tested under similar conditions. Dismutation activities were studied at 300, 250, 100, and 50 °C, whereas isomerizations tests were performed at room temperature for 2h.

According to the data given in Table 5.3, the dismutations of CCl_2F_2 (eq. 4.1) and $CHClF_2$ (eq. 4.2) proceed over all HS-AlF_3 preparations giving a rise to almost 100% conversion even at temperatures as low as 50 °C. This conversion is much higher than that obtained for β-AlF_3 [35]. The relatively high reactivity of HS-AlF_3 as compared to *β*-AlF_3 and amorphous AlF_3 evidences its high Lewis acidity. The presence of the more acidic sites on the HS-AlF_3 surface compared to β-AlF_3 and amorphous AlF_3, was also demonstrated by the NH_3-TPD measurements [35-36].

Table 5.3: Dismutations of $CHClF_2$ and CCl_2F_2 over HS-AlF_3

Catalyst	Fluorination agent	Dismutation of $CHClF_2$ (%)			Dismutation of CCl_2F_2 (%)		
		250 °C	100 °C	50 °C	300 °C	100 °C	50 °C
HS-AlF_3	CCl_2F_2/N_2 or $CHClF_2/N_2$	99	99	99	96	96	96
HS-AlF_3-HF-N_2	$HF/N_2 + N_2$	97	≈ 100	≈ 100	95	95	≈ 95
*HS-AlF_3	$CHClF_2/N_2$	≈ 100	≈ 100	≈ 100	97	97	97
**HS-AlF_3	$CHClF_2/N_2$	96	96	96	94	94	94
β-AlF_3	$CHClF_2/N_2$ or CCl_2F_2/N_2	96	96	84	93	49	0

* HS-AlF_3 prepared from $Al(O^tBu)_3$

* HS-AlF_3 prepared from $Al(OMe)_3$

The results of the isomerization reactions catalyzed by HS-AlF_3 are given in Table 5.4. For $CF_3CFBrCF_2Br$ isomerization (eq. 4.3), all HS-AlF_3 samples were very active and produced the target product with 90-98% selectivity, but expect for HS-AlF_3-HF+N_2 with a somewhat lower activity (57%). HS-AlF_3 was also successful for isomerizing CCl_2FCClF_2 (eq. 4.4) at room temperature, with 17% selectivity.

Samples prepared from $Al(O^tBu)_3$ had higher catalytic activity for the isomerization of CCl_2FCClF_2, reaching 71% conversion. The main products were CCl_3CClF_2 (56%) and CCl_3CF_3 (15%). Obviously, because of its high Lewis acidity, dismutation reaction of CCl_3CF_3 into CCl_3CClF_2 and CCl_2FCF_3 takes place, [110]. As the Cl-F exchange of CCl_3CF_3 over HS-AlF_3 takes place, the amount of this isomer is small and the main product is CCl_3CClF_2, however, this could not be confirmed here. In contrast, *β*-AlF_3 was not at all able to catalyze these isomerization reactions.

Based on the above results, it can be concluded that HS-AlF_3 prepared from $Al(O^tBu)_3$ is slightly more active for isomerization $CF_3CFBrCF_2Br$ than the corresponding HS-AlF_3 catalysts prepared from $Al(O^iPr)_3$ and $Al(OMe)_3$. Although the conversion of $CF_3CFBrCF_2Br$ over HS-AlF_3 prepared from $Al(O^tBu)_3$ is relatively comparable to those prepared from $Al(O^iPr)_3$ and from $Al(OMe)_3$, the yield (isomerization activity) of

CCl_2FCClF_2 is much higher; this could be a result of the difference in the surface area (Chapter 4, Table 4.4) and the presence of very strong acid sites on the surface.

The isomerization of CCl_2FCClF_2 with HS-AlF_3 prepared from $Al(O^iPr)_3$ or $Al(O^tBu)_3$ was ≈ 100%, when the reaction was made at 50 °C.

Table 5.4: Isomerizations of $CF_3CFBrCF_2Br$ and CCl_3CF_3 over HS-AlF_3

Catalyst	Weight (mg)	$CBrF_2CBrCF_3$ isomerization (%)	CCl_2FCF_2Cl isomerization (%)
		2 h	2 h
HS-AlF_3	20	> 90	17
HS-AlF_3-HF + N_2	20	57	13
*HS-AlF_3	20	98	71
**HS-AlF_3	20	≈ 90	11
β-AlF_3	20	0	0

* – HS-AlF_3 prepared from $Al(O^tBu)_3$,

** – HS-AlF_3 prepared from $Al(OMe)_3$

5.5 Summary

The results obtained can be summarized as following:

HS-AlF_3 precursor, HS-AlF_3, and HS-AlF_3-HF are amorphous like materials. Only when they are heated up to about 600 °C phase transformation to α-AlF_3 takes place. FTIR and MAS NMR showed that HS-AlF_3 and HS-AlF_3-HF are highly distorted; the degree of distortion is similar to those found for ACF, the most distorted aluminum fluoride known.

Adsorption of probe molecules on differently prepared HS-AlF_3 revealed differences in their surface acid properties. When pyridine was adsorbed on HS-AlF_3 and HS-AlF_3-HF+N_2 only bands indicative of pyridine adsorbed on Lewis acid sites were observed. However, adsorption of pyridine on HS-AlF_3-HF confirmed the presence of Brønsted acid sites, whereas HS-AlF_3 precursor showed in principal Lewis acidic sites, however, with low concentration. These results were also supported from IR-CO.

All HS-AlF_3 samples prepared are mesoporous solids with very high surface area. Under appropriate preparation conditions, HS-AlF_3 samples showed high catalytic activity for

dismutations of CCl_2F_2 and $CHClF_2$ and isomerization of $CBrF_2CBrCF_3$ with almost 100% conversion in all the reactions.

Chapter 6

Supported HS-AlF_3

6.1 Introduction

Unsupported HS-AlF_3 was introduced in chapter 4. It was shown that unsupported HS-AlF_3 has very high surface areas and very high Lewis acidity comparable with SbF_5 and ACF and higher than $AlCl_3$ [35-36, 40]. The advantage of this HS-AlF_3 is that it is chemically robust and does not undergo hydrolysis reactions at temperatures below 500 °C, thus it could be an alternative to today used Lewis acidic catalysts (ex. SbF_5, ACF). However, because of the sol-gel synthesis route, HS-AlF_3 has powder form and hence, all investigations and characterizations have been performed using powder materials of HS-AlF_3.

In practical applications, however, material with a certain mechanical stability and shape is necessary in order to be used as catalyst for catalytic reactions under both, liquid phase and gaseous steady flow conditions. Since a post-processing of powdered material has several disadvantages, the deposition/immobilization of HS-AlF_3 on a suitable support maintaining its exciting Lewis acidic properties would be a great advantage. Although a variety of supports are available, there are several restrictions originating from the sol-gel synthesis route of HS-AlF_3, which limit drastically the number of supports.

The common synthesis procedure as mentioned in the previous chapters consists of a two step process. Whereas the first step is not at all corrosive because the alkoxide and HF in stoichiometric ratios neutralize each other, the second "the post-fluorination" step involves HF. Hence, only such supports can be considered which are resistant against HF. Consequently, Al_2O_3-derived supports are the choice, because they meet more or less this requirement, especially α-Al_2O_3 among all the other Al_2O_3-modifications, is nearly inert against HF even at elevated temperature, but it has the disadvantage of small surface areas.

Accordingly, the specific goals of this chapter are (i) to demonstrate principally the preparation of HS-AlF_3 supported on Al_2O_3 and fluorinated γ-Al_2O_3 supports and (ii) to study the effects of synthesis parameters on the properties of supported HS-AlF_3. The main factors of influence to be tested are type and pre-treatment of support, amount of HS-AlF_3 loaded on the support, the aging of the supported wet HS-AlF_3 precursor, impregnation method, fluorination temperature, and concentration of the fluorination agent. All these factors have been varied and tested for their influence on the properties of supported HS-AlF_3 measured in terms of surface area and catalytic activity. In addition, texture properties using N_2 adsorption-desorption method, and acidity studies measuring NH_3-TPD as well as evaluation of the catalytic activity will be discussed in details in section 6.4.

6.2 Modification and characterization of the supports

It is well known that the surface of γ-Al_2O_3, as well as of all other meta-stable Al_2O_3, unless highly dried, is covered with hydroxyl groups formed by chemisorption of water (desorption starts at 300 and proceeds up to 800 °C) [111-112]. Therefore, in the early stage of this work, it was necessary to know at which temperature and to which degree surface hydroxyl groups are removed from the surface of the γ-Al_2O_3 support.

For this purpose, the supports were calcined at 400, 500, 700, and 1000 °C for 12 h in air. Then, the dehydroxylation of γ-Al_2O_3 (γ-$Al_2O_3^s$, γ-$Al_2O_3^a$) as well as α-Al_2O_3 was studied by monitoring the weight loss at these temperatures followed by phase analysis using XRD and surface area determination. The results are shown in Tables 6.1a and 6.1b.

Weight loss: Table 6.1a shows the effect of calcination temperature on the weight loss, i.e., removal of water adsorbed and/or formed from hydroxyl groups from the support surfaces, texture and phase composition of γ-$Al_2O_3^a$, γ-$Al_2O_3^s$, and α-Al_2O_3.

Table 6.1a: Effect of calcination temperature on the weight loss and the surface area of the supports

Calcination temperature (°C)	γ-$Al_2O_3^s$		γ-$Al_2O_3^a$		α-Al_2O_3	
	% Wt. loss	S_{BET} (m^2/g)	% Wt. loss	S_{BET} (m^2/g)	% Wt. loss	S_{BET} (m^2/g)
23	0	102	0	218	0	4.6
400	5.97	100	7.96	217	0.08	4.6
500	6.26	95	8.81	201	0.09	4.6
700	7.71	87	9.60	169	0.12	4.5
900	7.75	62	10.01	149	0.13	4.3
1000	7.77	58	10.06	121	0.13	3.9

V_p– BJH desorption cumulative pore volume, d_p– average pore diameter by BET

γ-$Al_2O_3^s$– supplied from Strem Chemicals, pellet, 3 mm

γ-$Al_2O_3^a$– supplied from Alfa Aesar, pellet, 3 mm, α-AlF_3– Saint-Gobain, pellet, 1 mm

For γ-$Al_2O_3^s$, the weight loss was relatively strong up to 400 °C and above this temperature it became much smaller. Above 700 °C, almost no further weight loss was observed. With respect to γ-$Al_2O_3^a$, up to 400 °C, the weight loss was also strong. Above

900 °C, no further insignificant weight loss was observed. The weight loss observed up to 400 °C corresponds to the removal of physically adsorbed water, whereas the weight loss above 400 °C and up to 900 °C is due to the removal of chemically bonded water (hydroxyl groups) [113-114]. α-Al_2O_3 showed almost constant weight loss over the whole temperature range.

Surface area: As for the surface areas (Table 6.1a), calcination up to 1000 °C was found to have minor effect on the surface area of α-Al_2O_3. In contrast, γ-$Al_2O_3^s$ and γ-$Al_2O_3^a$ with an initial surface area of 102 and 218 m^2/g, respectively, underwent substantial reduction in the surface area to 58 and 121 m^2/g, respectively, when calcined up to 1000 °C.

XRD: The XRD phase of α-Al_2O_3 retained, expectedly, unchanged upon heating (Table 6.1b). For γ-$Al_2O_3^s$, γ-Al_2O_3 was the only phase present up to 700 °C. Upon increasing the calcination temperature to 900 °C and above, phase transformation to α-Al_2O_3 took place. In case of γ-$Al_2O_3^a$, calcination up to 900 °C caused only sharpening of the γ-Al_2O_3 lines and no detectable traces of α-Al_2O_3 were observed. At 1000 °C, in addition to γ-Al_2O_3, traces of α-Al_2O_3 phase were also found.

Table 6.1b: XRD studies: Effect of calcination temperature on the structure of the supports

Calcination temperature (°C)	XRD phases		
	γ-$Al_2O_3^s$	γ-$Al_2O_3^a$	α-Al_2O_3
23	γ-Al_2O_3	γ-Al_2O_3	α-Al_2O_3
400	γ-Al_2O_3	γ-Al_2O_3	α-Al_2O_3
500	γ-Al_2O_3	γ-Al_2O_3	α-Al_2O_3
700	γ-Al_2O_3	γ-Al_2O_3	α-Al_2O_3
900	α-Al_2O_3	γ-Al_2O_3	α-Al_2O_3
1000	α-Al_2O_3	γ-Al_2O_3 + α-Al_2O_3	α-Al_2O_3

Based on the observations regarding texture, weigh loss, and XRD phases (Tables 6.1a-b), for the preparation of supported HS-AlF_3, unless otherwise stated, γ-$Al_2O_3^a$ and α-Al_2O_3 were always calcined at 900 °C, whereas γ-$Al_2O_3^s$ was calcined at 700 °C. In addition, partially fluorinated γ-$Al_2O_3^a$ (donated γ-$Al_2O_3^a$-F) was prepared by calcination of

γ-Al_2O_3[a] at 400 °C for 4 h, followed by fluorination with a mixture of HF (2 ml/min) and N_2 (20 ml/min) for 2 h at 120 °C. The resulting γ-Al_2O_3[a]-F had a surface area of 120 m^2/g, a pore volume of 0.26 cm^3/g and average pore size of 117 Å.

6.3 Preparation of supported HS-AlF_3

The preparation of supported HS-AlF_3 consisted of two steps: (1) the first preparation step is the formation of supported dry Al-F-gel (supported dry precursor) by impregnation of the pre-calcined/modified support in $Al(O^iPr)_3/^iPrOH$ followed by addition of HF/Et_2O solution. In general, the support was added to 0.4 mol/l aluminum isopropylate ($Al(O^iPr)_3$) dissolved in water free isopropanol. After that, the stoichiometric amount of HF dissolved in organic solvent was added to the mixture while stirring. The supported wet Al-F-gel (supported wet precursors) obtained was then subsequently dried under vacuum at 70 °C to produce supported dry precursor. The relative amount of precursor was adjusted to obtain HS-AlF_3 contents given in Table 6.2 to Table 6.5.

$$Al(OR)_{3(solv.)} + \text{support} \longrightarrow \text{support} / Al(OR)_3 + x\,HF \longrightarrow \underset{\textit{supported wet precursor}}{\text{support} / AlF_x(OR)_{3-x}.y\,ROH}$$

$$\downarrow \text{drying}$$

$$\underset{\textit{supported dry precursor}}{\text{support} / AlF_x(OR)_{3-x}.zROH}$$

(R= ^{i}Pr and z << y)

(2) The supported dry precursor was activated (fluorinated) to get the supported HS-AlF_3. Activation process was carried out in a continuous-flow fixed-bed tube-type reactor with an inner diameter of 5 mm under external heating. The supported material was loaded at the central position of the reactor onto a silver wool plug. $CHClF_2/N_2$ mixtures or HF/N_2 mixture were used as activating agents. The flow of gaseous reactants was controlled by mass flow controllers. Activation with $CHClF_2$ was examined by varying fluorination temperature and concentration of fluorination agent.

$$\underset{\textit{supported dry precursor}}{\text{support} / AlF_x(OR)_{3-x}\ .\ z\,ROH} \xrightarrow{\text{Fluorination}} \underset{(z << y),\ R= {}^i\text{Pr}}{\text{support} / \text{HS-}AlF_3}$$

In the following section, the influence of various synthesis parameters on the properties of the supported HS-AlF_3 will be discussed.

6.4 Results and discussion

Step 1: Supported dry precursor

This step aims at both the synthesis of the precursor of HS-AlF_3 and its deposition on the support, as discussed above.

Influence of γ-$Al_2O_3^a$ calcination temperature

Aluminas are known to exhibit surface hydroxyl groups, which might be present even after calcination at elevated temperatures [111-113]. Such surface hydroxyl groups could act as useful anchor groups in the process of depositing HS-AlF_3, e.g., via reaction with residual Al-OR groups of the precursor state. On the other hand, it is known from former investigations that the partial presence of oxo-(hydroxo-) groups may depress the Lewis acidity of HS-AlF_3 significantly [36]. Hence, the major objective of these investigations was to find out to what extent surface hydroxyl groups on a support can be tolerated in order to end up with highly Lewis acidic supported HS-AlF_3 sample.

In order to examine the influence of the γ-$Al_2O_3^a$ calcination temperature on the preparation of supported HS-AlF_3 and its catalytic properties, γ-$Al_2O_3^a$ was calcinated at 400 and 900 °C, respectively, this way decreasing the concentration of surface hydroxyl groups. The supported HS-AlF_3 was prepared as mentioned above, with various HS-AlF_3 loading, namely 5, 10, and 15 wt% HS-AlF_3.

The results presented in Table 6.2 reveal that HS-AlF_3 supported on γ-$Al_2O_3^a$ calcined at 900 °C had a higher catalytic activity for $CHClF_2$ dismutation (98-99% conversion even at 50 °C) than those samples supported on γ-$Al_2O_3^a$ calcined at 400 °C (66-74%), although the surface area of the former is lower.

Thus, the difference in the performance between HS-AlF_3 supported on γ-$Al_2O_3^a$ calcined at 400 °C or at 900 °C, respectively, is clearly not a result of the surface area. The effect of the calcination temperature of γ-$Al_2O_3^a$ on the properties of the resulting supported HS-AlF_3 can be explained as follows. Heating γ-$Al_2O_3^a$ at 400 °C removes all the water molecules, but relatively high number of OH groups remains [112-113]. In this case, during the coating of $AlF_x(OR)_{3-x}$ on γ-Al_2O_3 condensation reaction would be expected to

occur, forming Al-O-Al bonds. This leads to significant depression in the Lewis acidity of HS-AlF_3. With increasing calcination temperature of the γ-Al_2O_3[a] support, further dehydration is possible due to surface migration of individual hydroxyl groups at temperature above 650 °C, resulting in an almost fully dehydroxylated surface [111, 114, 116]. The crystal lattice of γ-Al_2O_3[a] undergoes rearrangement in the process and coordinately unsaturated aluminum ions (Al^{3+}_{cus}, Lewis acid sites) are formed. Consequently, after impregnation with $AlF_x(OR)_{3-x}$, Al-F-Al bonds are expected to form, enhancing the Lewis acidity of the supported HS-AlF_3.

Table 6.2: Effect of temperature of γ-Al_2O_3[a] calcination on properties of supported HS-AlF_3

Sample	Wt.% HS-AlF_3 loaded on the support		S_{BET} (m^2/g)	Conversion of $CHClF_2$ (%)		
	aimed	obtained		250 °C	100 °C	50 °C
γ-Al_2O_3[a] calcined at 400 °C						
HS-AlF_3/γ-Al_2O_3[a]	5	4.8	187	92	84	66
HS-AlF_3/γ-Al_2O_3[a]	10	9.8	192	93	88	70
HS-AlF_3/γ-Al_2O_3[a]	15	14.6	196	95	94	74
γ-Al_2O_3[a] calcined at 900 °C						
HS-AlF_3/γ-Al_2O_3[a]	5	4.8	138	98	98	98
HS-AlF_3/γ-Al_2O_3[a]	10	9.8	143	98	98	≈ 99
HS-AlF_3/γ-Al_2O_3[a]	15	14.7	146	99	99	99

γ-Al_2O_3[a]–BET surface area 149 m^2/g after calcination at 900 °C
γ-Al_2O_3[a]–BET surface area 206 m^2/g after calcination at 400 °C

Influence of preparation methods

In all standard experiments, the supported HS-AlF_3 was prepared by impregnation of the support with $Al(O^iPr)_3$ solution followed by fluorination with HF solution (method P1). In this case, $Al(O^iPr)_3$ in the solution penetrates into the support pores and covers the pores surfaces as well as the outer support surfaces. After fluorination with HF solution, the resulting $AlF_x(OR)_{3-x}$ is then fixed on the interior and exterior surface of the support particles. For comparison, in separate experiments the support was directly impregnated with pre-formed $AlF_x(OR)_{3-x}$ sol (method P2). Here, $AlF_x(OR)_{3-x}$ in the sol should become

deposited only on the walls of the larger pores which it passes. Therefore, after removal of the solvents, only the exterior of the support particles should be coated with $AlF_x(OR)_{3-x}$.

In Table 6.3, the amount of HS-AlF_3 deposited on the supports and catalytic activity of the supported HS-AlF_3 prepared by P1 or P2 are shown. It can be seen that the amount of HS-AlF_3 deposited according to P1 or according to P2 are almost identical. Again, the amount of HS-AlF_3 deposited on γ-$Al_2O_3{}^a$ with surface area of 149 m^2/g (4.8 wt%) was higher than that on α-Al_2O_3 (3 wt%).

In regard to the catalytic activity for both $CHClF_2$ dismutation and 1,2-DBP isomerization, the total conversions were quite similar for samples prepared according to P1 or according to P2. HS-AlF_3 /γ-$Al_2O_3{}^a$ showed the highest catalytic activity for 1,2-DBP isomerization (11% conversion).

Table 6.3: Effect of the preparation method on supported HS-AlF_3 properties

Catalyst	Wt.% HS-AlF_3 loaded on the support		S_{BET} (m^2/g)	Conversion of $CHClF_2$ (%)			1,2-DBP isomer. activity (%)
	aimed	obtained		250 °C	100 °C	50 °C	
P1) impregnation with $Al(O^iPr)_3$ solution / HF in ether							
HS-AlF_3 /α-Al_2O_3	5	2.9	4	98	97	90	> 1
HS-AlF_3 /γ-$Al_2O_3{}^s$	5	4.1	83	97	96	92	5
HS-AlF_3 /γ-$Al_2O_3{}^a$	5	4.8	143	98	98	98	11
P2) impregnation with $AlF_x(OR)_{3-x}$							
HS-AlF_3 /α-Al_2O_3	5	3.0	4	96	96	91	> 1
HS-AlF_3 /γ-$Al_2O_3{}^s$	5	4.0	85	96	95	90	3
HS-AlF_3 /γ-$Al_2O_3{}^a$	5	4.7	146	98	98	≈ 98	10

α-Al_2O_3– BET surface area 4.3 m^2/g after calcination at 900 °C

γ-$Al_2O_3{}^s$– BET surface area 87 m^2/g after calcination at 700 °C

γ-$Al_2O_3{}^a$– BET surface area 149 m^2/g after calcination at 900 °C

1,2-DBP isomer.– $CBrF_2CBrFCF_3$ isomerization

Since the amount of HS-AlF_3 deposited in P1 and P2 on the supports and their catalytic activity were of similar range, it seems that the processes of HS-AlF_3-precursor deposition are similar in the two methods.

Influence of type of support

The nature of the support can be crucial for the deposition of HS-AlF_3 and its catalytic properties. Therefore, besides γ-Al_2O_3 from different suppliers, α-Al_2O_3 and pre-fluorinated γ-$Al_2O_3^a$ (donated γ-$Al_2O_3^a$-F), whose characteristics are given in section 6.2.1, were used. The results are summarized in Table 6.4.

HS-AlF_3 loading on the supports: Comparisons of the affinity of the supports for adsorption of HS-AlF_3 were made by considering the HS-AlF_3 load obtained after impregnation at standard initial solvent concentration. From Table 6.4, it can be seen that the samples prepared with identical solvent concentration showed different HS-AlF_3 loadings from 3 wt% for α-Al_2O_3 (4.3 m^2/g) to 4.8 wt% for γ-$Al_2O_3^a$ (149 m^2/g). However, the loading did not directly correspond to the surface area of the support, indicating that the smaller pores of the supports have not been coated/filled with HS-AlF_3.

Catalytic activity: As it can be seen from Table 6.4, despite the large differences in the supported HS-AlF_3 surface areas, the differences in the catalytic activities for $CHClF_2$ dismutation between HS-AlF_3/γ-$Al_2O_3^a$, HS-AlF_3/γ-$Al_2O_3^s$, and HS-AlF_3/α-Al_2O_3 are marginal and appear only at lower temperature. At 250 °C, all the supported HS-AlF_3 samples showed about 97-98% conversion of $CHClF_2$. This means that the three catalysts (i) do not contain any considerable amounts of disturbing surface hydroxyl groups and (ii) are obviously totally covered by HS-AlF_3 and small differences are due to differences in the surface area of γ-$Al_2O_3^a$ (149 m^2/g), γ-$Al_2O_3^s$ (87 m^2/g), and α-Al_2O_3 (4.3 m^2/g).

Opposed to the supported HS-AlF_3 catalysts the pure supports behave, expectedly, differently in their catalytic activity for the dismutation of $CHClF_2$ (Table 6.4), γ-$Al_2O_3^a$ showed low initial reactivity at 250 °C, the conversion increased to 96% after 2 h on stream. After cooling the reactor, the catalytic activity started to decline and the conversion level of $CHClF_2$ remained 70% at 50 °C. However, HS-AlF_3/γ-$Al_2O_3^a$ exhibited under the same conditions almost 100% conversion. Hence, the impact of the support on the catalytic activity can be disregarded. This is even more evident considering that the pure support (although active in dismutation of $CHClF_2$) did not at all show any activity in the isomerization of 1,2-DBP. α-Al_2O_3 and γ-$Al_2O_3^s$, on the other hand, showed even at 250 °C only 0.5% and 32% conversion in the dismutation of $CHClF_2$, respectively. After decreasing the temperature to 50 °C, no catalytic activity was observed for the pure supports. Pre-fluorinated γ-$Al_2O_3^a$-F showed no catalytic activity for dismutation of

$CHClF_2$. For 1,2-DBP isomerization none of the pure support showed any catalytic activity.

Table 6.4: Effect of support type on supported HS-AlF_3 properties

Catalyst	Wt.% HS-AlF_3 loaded on the support		S_{BET} (m^2/g)	Conversion of $CHClF_2$ (%)			1,2-DBP isomer. activity (%)
	aimed	obtained		250 °C	100 °C	50 °C	
α-Al_2O_3	0	0	2.8	0.5	0	0	0
γ-$Al_2O_3^s$	0	0	72	32	8	0	0
γ-$Al_2O_3^a$-F	0	0	102	0	0	0	0
γ-$Al_2O_3^a$	0	0	110	96	89	70	0
HS-AlF_3 /α-Al_2O_3	5	3.0	4	98	97	90	> 1
HS-AlF_3 /γ-$Al_2O_3^s$	5	4.1	85	97	96	92	5
HS-AlF_3 /γ-$Al_2O_3^a$-F	5	4.7	102	97	97	95	6
HS-AlF_3 /γ-$Al_2O_3^a$	5	4.9	143	98	98	98	11

α–AlF_3– BET surface area 4.3 m^2/g after calcination at 900 °C

γ-$Al_2O_3^s$– BET surface area 87 m^2/g after calcination at 700 °C

γ-$Al_2O_3^a$– BET surface area 149 m^2/g after calcination at 900 °C

γ-$Al_2O_3^a$– F– pre-calcined γ-$Al_2O_3^a$ fluorinated with HF at 120 °C for 2 h (120 m^2/g)

1,2-DBP isomer.– $CBrF_2CBrFCF_3$ isomerization

Influence of type of alkoxides and of HS-AlF_3 loading

In chapter 4, it was shown that unsupported HS-AlF_3 prepared from $Al(O^tBu)_3$ exhibits slightly higher catalytic activity than that prepared from $Al(O^iPr)_3$. Therefore, supported HS-AlF_3 based on $Al(O^tBu)_3$ in butanol and HF in ether was also prepared under otherwise identical conditions, and its BET surface area and catalytic properties were determined. As it can be seen from Table 6.5, the conversion of $CHClF_2$ over HS-AlF_3/γ-$Al_2O_3^a$ starting from $Al(O^tBu)_3$ or $Al(O^iPr)_3$, respectively, are quantitatively comparable (98-99% conversion even at 50 °C). For the isomerization reaction, HS-AlF_3/γ-$Al_2O_3^a$ prepared from $Al(O^tBu)_3$ showed slightly higher catalytic activity (37% conversion) than that prepared from $Al(O^iPr)_3$, which showed 30% conversion.

Table 6.5: Influence of alkoxide types on HS-AlF_3 loading (wt %) on γ-Al_2O_3[a]

Sample	Wt. % $HSAlF_3$ loaded on the support		S_{BET} (m^2/g)	Conversion of $CHClF_2$ (%)			1,2-DBP isomer. activity (%)
	aimed	obtained		250 °C	100 °C	50 °C	
Al-alkoxide / Solvents:							
1) Al (O^iPr)$_3$ / isopropanol							
1	5	4.9	138	98	98	98	11
2	10	9.8	143	98	98	≈ 99	16
3	15	14.7	146	99	99	99	30
2) Al(O^tBu)$_3$ / *n*-butanol							
4	5	4.9	140	98	98	98	12
5	10	9.8	145	98	≈ 99	99	20
6	15	14.8	146	99	99	99	37

1,2-DBP isomer. – $CBrF_2CBrFCF_3$ isomerization

From the data in Table 6.5 it is also evident that the amount of HS-AlF_3 loading has a marked influence on the activity of HS-AlF_3/γ-Al_2O_3[a], but only with respect to 1,2-DBP isomerization. The conversion of 1,2-DBP was increased from 11 to 30% over HS-AlF_3/γ-Al_2O_3[a] prepared from Al(O^iPr)$_3$, and from 12 to 37% over those prepared from Al(O^tBu)$_3$ with increasing the HS-AlF_3 loading from 4.9 to 14.8 wt%. The increase of isomerization with loading can be rationalized by an increase of the number of most active sites at the catalyst, which might be mainly due to the fact that the influence of the support surface diminishes with increasing of the HS-AlF_3 loading. This means that with a certain loading the surface exclusively consists of HS-AlF_3. Contrary to that, an increase in HS-AlF_3 loading from 4.9, to 9.8, and to 14.7 wt%, respectively, does not significantly influence the $CHClF_2$ dismutation activity, since already 98% activity was achieved with 4.9 wt% loading. As this reaction is already catalyzed by medium strong Lewis acid sites, the amount of these is obviously optimum even with the lowest loading tested.

Effect of aging time

After preparation of HS-AlF_3/γ-Al_2O_3[a] (14 wt% HS-AlF_3) wet precursor, the wet supported HS-AlF_3 precursor was aged for 6, 24, and 48 h at room temperature. Reproducible results for $CHClF_2$ dismutation and 1,2-DBP isomerization were obtained irrespective of aging time studied as it indicates in Table 6.6. All samples showed 97-99% conversion for dismutation of $CHClF_2$ and 24-30% conversion for isomerization of 1,2-DBP. Hence, it can be concluded that there is no influence of aging time on the HS-AlF_3/γ-Al_2O_3[a] properties within these time limits.

Table 6.6 : Influence of aging time on supported HS-AlF_3 properties

Catalyst	Aging time (h)	S_{BET} (m^2/g)	Conversion of $CHClF_2$ (%) at 50 °C	1,2-DBP isomer. activity (%)
HS-AlF_3 /γ-Al_2O_3[a]	6	143	98	27
HS-AlF_3 /γ-Al_2O_3[a]	24	146	≈ 99	30
HS-AlF_3 /γ-Al_2O_3[a]	48	142	97	24

1,2-DBP isomer.– $CBrF_2CBrFCF_3$ isomerization

Step 2: Fluorination of the supported precursor

The fluorination step brings about the following transformations: removal of strongly adsorbed solvent and of the unconverted alkoxide groups of the precursor, whereby the latter are replaced by fluorine, resulting in the formation of HS-AlF_3. Accordingly, the activation parameters should have an effect on the final properties of supported HS-AlF_3 as known from chapter 4. So far, the precursor activation was carried out using $CHClF_2/N_2$ or HF/N_2 fluorination agent. All the experiments were performed with dry $AlF_x(OR)_{3-x}$/γ-Al_2O_3[a], since it has shown to result in the highest catalytic activity and the largest surface area.

Fluorination with $CHClF_2$

In general, the fluorination process is performed by passing a mixture of $CHClF_2$ and N_2 through the supported precursor placed in a heated metal reactor. The activation temperature is step-wise increased and held at each respective temperature until no changes

were observed in the GC. The reaction starts with liberation of ROH, however, with progressive fluorination, i.e., replacement of OR by F, the initially inactive supported precursor becomes an active catalyst by generation of Lewis acidic sites. Since $CHClF_2$ undergoes dismutation in the presence of a Lewis acid, the progress of the activation can be followed by monitoring the dismutation products by GC.

Effect of $CHClF_2$ concentration and fluorination temperature

To establish the appropriate conditions for activation with $CHClF_2$, the changes in catalytic properties and BET surface area of supported HS-AlF_3 were examined for varied $CHClF_2$:N_2 ratios and activation temperatures. These variables will be discussed for HS-AlF_3/γ-Al_2O_3[a] with HS-AlF_3 loading of 14 wt% only.

In order to examine the effect of activation temperature, the fluorination was carried out with $CHClF_2$:N_2 equal to 4:20 ml/min at maximum temperatures of 250, 300, and 350 °C. Whatever the final fluorination temperature, the dismutation of $CHClF_2$ was about 99% (Table 6.7). However, increasing the activation temperature above 250 °C reduced the surface area from 146 to 109 m^2/g and also caused coke formation. Although all the samples showed virtually the same dismutation activity, the sample behaviors in 1,2-DBP isomerization diverge. The conversion in the 1,2-DBP isomerization decreased from 30 to 2% with increasing fluorination temperature from 250 to 350 °C. These findings are obviously due to the fact that coke formed at the most active sites of the supported HS-AlF_3 surface blocks these sites and part of the pores, resulting in smaller surface area and lower catalytic activity for 1,2-DBP isomerization as measure for very strong Lewis acidity.

Table 6.7: Effect of fluorination temperature on HS-AlF_3/γ-Al_2O_3[a] properties

Sample	Final temp. (°C)	S_{BET} (m^2/g)	Conversion of $CHClF_2$ (%) at 50 °C	1,2-DBP isomer. activity (%)
1	250	146	99	30
2	300	125	≈ 100	13
3	350	109	≈ 99	2

V_p– BJH desorption cumulative pore volume, d_p– average pore diameter by BET

1,2-DBP isomer.– $CBrF_2CBrFCF_3$ isomerization

The effect of $CHClF_2$ concentration on the HS-AlF_3/γ-Al_2O_3[a] properties was studied at 250 °C by varying $CHClF_2$:N_2 ratio from 3:20 to 4:20 to 5:20 ml/min. Both high amount (5 ml/min) and low amount (3 ml/min) of $CHClF_2$ leads to drastic changes in the isomerization activity as well as coke formation. Despite only small differences in the BET surface areas, the time needed to complete the activation, i.e., to reach about 98-99% conversion of $CHClF_2$, varies. Low amount of $CHClF_2$ resulted in long fluorination time (8 h), as it can be seen from Table 6.8. These results are also in agreement with the results reported for unsupported-HS-AlF_3 (chapter 4).

Table 6.8: Effect of $CHClF_2$ concentration at 250 °C on HS-AlF_3/γ-Al_2O_3[a] properties

Sample	N_2 flow (ml/min)	$CHClF_2$ flow (ml/min)	Time needed to reach 98% dismutation activity (h)	S_{BET} (m^2/g)	1,2-DBP isomer. activity (%)
1	20	3	8	139	13
2	20	4	6	146	30
3	20	5	5	140	14

1,2-DBP isomer.– $CBrF_2CBrFCF_3$ isomerization

Activation with HF

Activation with HF was studied for HS-AlF_3/γ-Al_2O_3[a] with various HS-AlF_3 loading, namely, 4.9, 9.8, and 14.7 wt%. It was performed at flow rate ratio of 1:20 ml/min at 120 °C for 3 h. The resulting material was denominated HS-AlF_3-HF/γ-Al_2O_3[a].

In term of surface area, samples exhibited almost similar values as those prepared by activation with $CHClF_2$ (Table 6.9). However, the catalytic activity of the HS-AlF_3-HF/γ-Al_2O_3[a] samples for $CHClF_2$ dismutation was very low. Samples showed only 3% conversion in the dismutation of $CHClF_2$ at 250 °C and no conversion in 1,2-DBP to 2,2-DBP took place. This can be explained by assuming that HF is adsorbed on the strong Lewis acid sites. After heating the supported HS-AlF_3-HF in N_2 at 250 °C for 1 h, high dismutation activity for $CHClF_2$ (≈ 99%) was achieved even after cooling down to 50 °C. This is good evidence for the removal of the physically adsorbed HF by N_2 which is better proven by its activity for 1,2-DBP isomerization test where very strong Lewis acid sites are required.

Table 6.9: Fluorination with HF: Effect of loading

Catalyst	Wt. % HS-AlF_3 loaded on the support	S_{BET} (m^2/g)	Conversion of $CHClF_2$ (%)		1,2-DBP isomer. activity (%)
			250 °C	50 °C	
$HSAlF_3$-HF/γ-Al_2O_3[a] + N_2	4.9	138	98	98	3
$HSAlF_3$-HF/γ-Al_2O_3[a] + N_2	9.8	140	99	≈ 99	10
$HSAlF_3$-HF/γ-Al_2O_3[a] + N_2	14.7	143	99	≈ 100	22

1,2-DBP isomer.– $CBrF_2CBrFCF_3$ isomerization

In Table 6.9 are shown the data of catalytic activity for $CHClF_2$ dismutation and 1,2-DBP isomerization along with BET surface area of HF activated and N_2 treated (1 h at 250 °C). HS-AlF_3 supported on γ-Al_2O_3[a] showed high catalytic activity for $CHClF_2$ dismutation, reaching with 14.7% loading almost 100% conversion even at 50 °C. Furthermore, when the HS-AlF_3 loading was increased from 4.9 to 14.7 wt% the conversion in the 1,2-DBP isomerization reaction increased to 22 %.

6.5 Properties of supported HS-AlF_3

Texture properties

In the following section, a comparative discussion of texture properties (surface area, pore volume, pore size) of supported HS-AlF_3 samples, which were listed in Tables 6.2-6.9, will be made. The surface areas of HS-AlF_3 supported on various aluminas were determined using the BET method, while the pore volume distribution were attained from the desorption isotherm using the BJH method [78]. The results obtained are listed in Table 6.10. Among all the samples, the HS-AlF3/γ-Al_2O_3[a] exhibited a substantially higher surface area (146 m^2/g) and higher pore volume (0.56 cm^3/g) than the other three supports, whereas, HS-AlF_3/α-Al_2O_3 showed the lowest surface area (3.9 m^2/g) and pore volume (0.01 cm^3/g), due to the different surface areas of the parent supports.

Table 6.10: Texture properties of the supported catalysts

Catalyst	S_{BET} (m^2/g) of the support	Texture properties of supported HS-AlF_3		
		S_{BET} (m^2/g)	V_p (cm^3/g)	d_p (Å)
HS-AlF_3 / α-Al_2O_3	4.3	4	0.01	121
HS-AlF_3 / γ-$Al_2O_3^s$	87	85	0.25	73
HS-AlF_3 / γ-$Al_2O_3^a$ -F	120	102	0.23	100
HS-AlF_3 / γ-$Al_2O_3^a$	149	146	0.56	107
HS-AlF_3-HF / γ-$Al_2O_3^a$	149	138	0.54	117

V_p– BJH desorption cumulative pore volume, dp– average pore diameter by BET

α–AlF_3– BET surface area 4.3 m^2/g after calcination at 900 °C

γ-$Al_2O_3^s$– BET surface area 87 m^2/g after calcination at 700 °C

γ-$Al_2O_3^a$– BET surface area 149 m^2/g after calcination at 900 °C

γ-$Al_2O_3^a$– F–pre-calcined γ-$Al_2O_3^a$ fluorinated with HF at 120 °C for 2 h (120 m^2/g)

Surface acidity

NH_3-TPD was performed to determine the acidity of the HS-AlF_3 (14.7 wt%) supported on γ-$Al_2O_3^a$. To get more information about the acid strength distribution of HS-AlF_3/γ-$Al_2O_3^a$ sample, the experimental profiles were fitted by Gaussian functions using four peaks. The use of these peak fit profiles was not based on peak assignment to specific acid sites, but only to help to characterize the acid strength distribution. Figure 6.1a shows the fittings of desorption peaks for supported HS-AlF_3. The four peaks (deconvoluted peaks) with maximum at 240, 282, 352, and 500 °C can be assigned to ammonia desorbing from weak (240 °C), medium (282 and 352 °C) and strong (500 °C) acid sites, respectively, related to the maximum desorption temperature. These results indicate that the samples have weak and medium acid sites together with some strong acid sites, which are responsible for the isomerization activity.

In addition, in order to see if the support contributes to the surface acidity of the supported HS-AlF_3, TPD was also performed for the pure γ-$Al_2O_3^a$. Figure 6.1a-b compares the difference between the NH_3-TPD profiles of HS-AlF_3 supported on γ-$Al_2O_3^a$ and the pure γ-$Al_2O_3^a$ support. The intensity of the desorption peaks was normalized by weight.

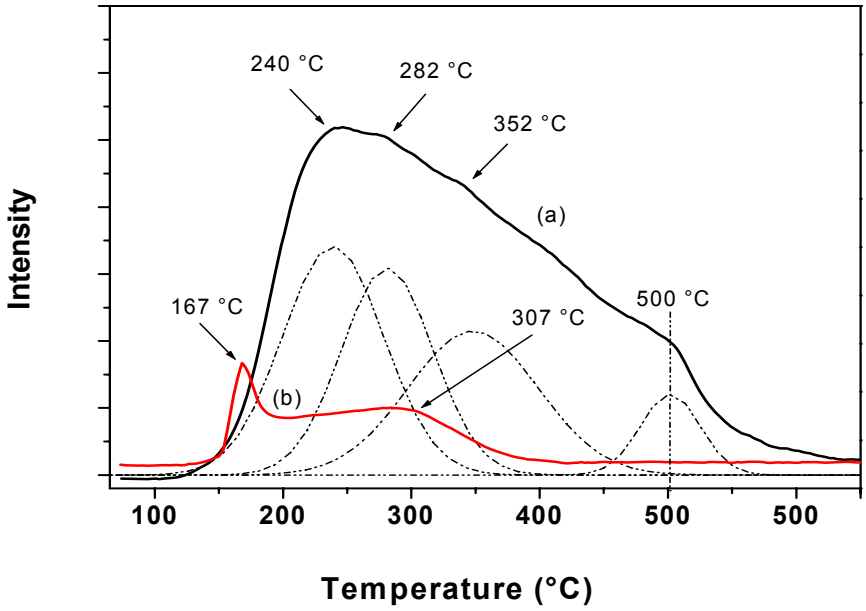

Figure 6.1 (a) NH_3-TPD curves and Gaussian fitting peaks of supported HS-AlF_3 and (b) NH_3-TPD curves pure γ-Al_2O_3[a] support.

The amount and the strength of the acidic sites are expectedly much lower in the case of support as Figure 6.1b shows. The TPD profile for pure γ-Al_2O_3[a] support shows two desorption peaks: one with maximum at 167 °C and one broader with a maximum at 307 °C, respectively, attributed to weak and medium acid sites. These desorption peaks of the pure support were replaced by new ones after coating the support with HS-AlF_3 (Figures 6.2a and 6.2b). These results indicate that γ-Al_2O_3[a] is completely covered with HS-AlF_3.

A comparison of NH_3-TPD of unsupported HS-AlF_3 and 14.7 % HS-AlF_3/γ-Al_2O_3[a], indicates that the acid sites of unsupported HS-AlF_3 are slightly stronger than those of supported HS-AlF_3. As it can be seen from Figure 6.2a-b, unsupported HS-AlF_3 shows four peaks with maximum at 227, 326, 392, and 500 °C (Figure 6.2a), assigned to weak (227 °C), medium (326 and 392 °C) and strong (500 °C) acidity, respectively, related to the maximum desorption temperature. Supported HS-AlF_3 shows an initial NH_3 desorption at slightly higher temperatures with maximum at 240 °C (Figure 6.2b), whereas the second and third desorption peaks are located at slightly lower temperature with maxima at 282 and 352 °C. Like the unsupported HS-AlF_3, a fourth desorption step with maximum at 500 °C is observed, attributed to strong acidity.

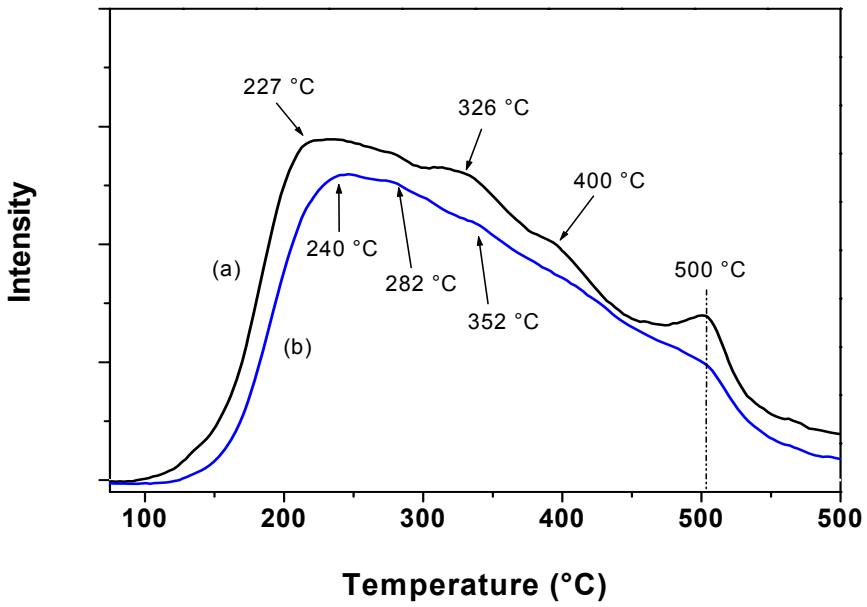

Figure 6.2 NH_3-TPD of supported (a) unsupported HS-AlF_3 and (b) HS-AlF_3/γ-Al_2O_3[a] support.

Catalytic properties

Catalytic activity of the supported HS-AlF_3 was discussed in section 6.3 (c.f. Tables 6.2-6.9). In the following section, comparative investigation of the catalytic activity of the supported HS-AlF_3 samples will be shown.

Dismutation and isomerization tests

The most interesting property of unsupported HS-AlF_3 is its very high Lewis acidity. This was proven by its high catalytic activity for dismutation of $CHClF_2$ (chapter 4, eq. 4.2) and for complete isomerization of $CBrF_2CBrFCF_3$ (chapter 4, eq. 4.3) at room temperature.

As it can be seen from Table 6.11, the highest conversion (98%) of $CHClF_2$ was obtained with HS-AlF_3/γ-Al_2O_3[a] even at 50 °C. The efficacy of the supported HS-AlF_3 with respect to $CHClF_2$ dismutation and isomerization falls in the sequence: HS-AlF_3/γ-Al_2O_3[a] ≥ HS-AlF_3/γ-Al_2O_3[a]-F ≥ HS-AlF_3/γ-Al_2O_3[s] ≥ HS-AlF_3/α–Al_2O_3 regardless of preparation method.

Table 6.11: Catalytic activity of the supported HS-AlF_3 catalysts

Catalyst	Conversion of $CHClF_2$ (%)		1,2-DBP isomer. activity (%)
	250 °C	50 °C	
HS-AlF_3 /α-Al_2O_3	98	90	>1
HS-AlF_3 /γ-$Al_2O_3^s$	97	92	5
HS-AlF_3 /γ-$Al_2O_3^a$-F	97	95	6
HS-AlF_3 /γ-$Al_2O_3^a$	≈ 99	99	30
HS-AlF_3 -HF/γ-$Al_2O_3^a$ + N_2	98	98	3

α–AlF_3– BET surface area 4.3 m^2/g after calcination at 900 °C

γ-$Al_2O_3^s$– BET surface area 87 m^2/g after calcination at 700 °C

γ-$Al_2O_3^a$– BET surface area 149 m^2/g after calcination at 900 °C

γ-$Al_2O_3^a$– F–pre-calcined γ-$Al_2O_3^a$ fluorinated with HF at 120 °C for 2 h (120 m^2/g)

1,2-DBP isomer.– $CBrF_2CBrFCF_3$ isomerization

Additionally, the 1,2-DBP isomerization activity was observed to increase with increasing HS-AlF_3 loading (Figure 6.3). Maximum isomerization activity was observed for 14.7 wt % HS-AlF_3/γ-$Al_2O_3^a$ with 30% conversion when HS-AlF_3 was prepared from $Al(O^iPr)_3$ and with 37 % conversion for supported HS-AlF_3 starting from $Al(O^iBu)_3$ (Table 6.5).

Although the conversions obtained in the isomerization reaction over HS-AlF_3/γ-$Al_2O_3^a$ samples (30-37%) are lower than those obtained for the unsupported HS-AlF_3 samples (≈ 100%, chapter 5), supported HS-AlF_3 is still strong Lewis acidic. This can be supported by the fact that even in the presence of SbF_5, elevated temperature (80 °C) is needed for the reaction and only in the presence of ACF this reaction is known to proceed at room temperature [39].

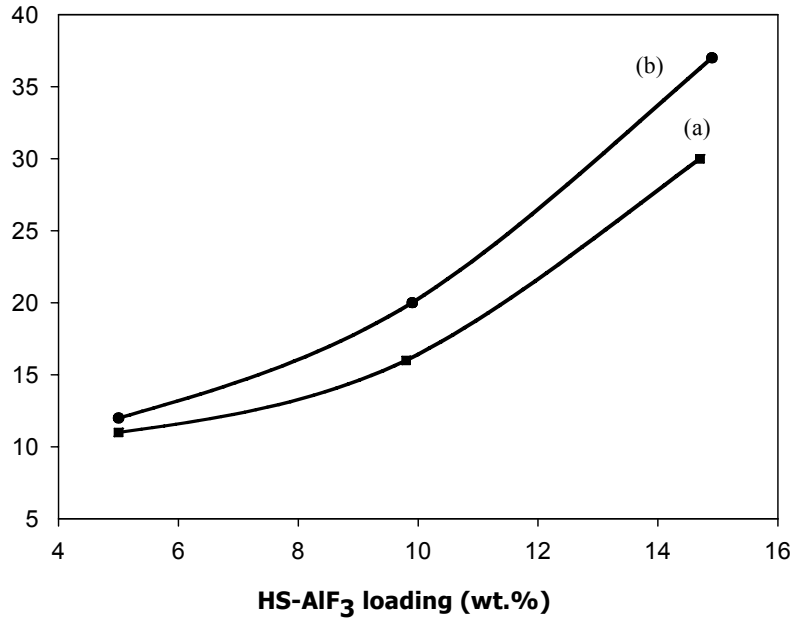

Figure 6.3 Catalytic performance of supported HS-AlF_3 as a function of HS-AlF_3 loading
(a) HS-AlF_3/γ-Al_2O_3[a], prepared starting from $Al(O^iPr)_3$
(b) HS-AlF_3/γ-Al_2O_3[a], prepared starting from $Al(O^iBu)_3$.

6.6 Summary

The preparation of supported HS-AlF_3 by impregnation method using various Al_2O_3 and modified Al_2O_3 was discussed. Two different routes to achieve coating of Al_2O_3 with HS-AlF_3 have been explored: (i) impregnation of the supports directly with aluminum alkoxide fluoride (precursor) and (ii) impregnation of the supports with $Al(O^iPr)_3$ solution then its fluorination with HF solution. It was found that both approaches have the same effect for the final properties of the supported HS-AlF_3.

HS-AlF_3 precursor deposition was carried out on γ-Al_2O_3[a] calcined at 400 °C and γ-Al_2O_3[a] calcined at 900 °C. HS-AlF_3 supported on γ-Al_2O_3[a] calcined at 900 °C showed higher catalytic activity (1,2-DBP isomerization and $CHClF_2$ dismutation) than those supported on γ-Al_2O_3[a] calcined at 400 °C.

The NH_3-TPD studies showed that the amount and strength of the acid sites on HS-AlF_3/γ-Al_2O_3[a] are slightly lower than those found on the unsupported HS-AlF_3.

Among all the supports used, HS-AlF_3/γ-Al_2O_3[a] showed the highest catalytic activity for $CHClF_2$ dismutation and $CBrF_2CBrFCF_3$ isomerization and the highest surface area.

Chapter 7

Preparation and Characterization of $_{aq.}HS\text{-}AlF_3$ and AlF_xO_y

7.1 Introduction

It was shown that HS-AlF_3 prepared under non-aqueous conditions exhibits an exiting strong Lewis acidity as well as very high surface area. Under non-aqueous conditions as the preferred fluorination route only fluoride ion acts as nucleophile. The fluoride ion is not able to undergo condensation reactions, however, can bridge different Al atoms thus forming three-dimensional networks. This way, an analogue behavior of fluorides like oxides in the sol-gel might be expected if the solvent can stabilize the wet gel thus preventing extended crystal formation. The substitution of an OR group by F can be regarded as fluorolysis. If water is in the system the question is if both reactions, hydrolysis and fluorolysis, compete to each other or if the fluorolysis is dominant. In an extreme scenario the presence of water might result in the formation of well crystallized AlF_3-phases like e.g., $AlF_3 \cdot 3H_2O$ [36].

fluorolysis: $\equiv M{-}OR + HF \longrightarrow \equiv M{-}F + ROH$ (M= Al)

hydrolysis: $\equiv M{-}OR + H_2O \longrightarrow \equiv M{-}OH + ROH$ (M= Al)

Thus, the question was whether total exclusion of water is a necessary precondition or if aqueous hydrogen fluoric acid can be used to get high surface area AlF_3 with similar properties. This way, the synthesis will be simplified and the overall preparation time reduced. Using e.g., 75 % HF, only minor amount of water (≈ 3%) would be present in the alcoholic reaction system under the conditions of the sol-gel synthesis route. Thus, water should not be a serious competitor due to its much weaker nucleophilicity. Even if there are some OH^- or O^{2-} groups in the framework, after post-fluorination in the gas phase they should be replaced by F^- yielding AlF_3.

Furthermore, by use of understochiometric amounts of HF, i.e., with HF/Al < 3, only partial fluorination will occur. On this basis it might be possible to form aluminum oxofluorides either by thermal decomposition of the alkoxofluoride or by selective hydrolysis of the remaining alkoxo-groups with the requested stoichiometric amount of water. The use of aqueous HF would combine the last path in a single reaction step. Thus, aluminum hydroxofluorides or aluminum oxofluorides might be accessible this way at low temperature. Oxyfluoride materials are known to have some special structure and catalytic properties in many acid-catalyzed reactions, high thermal and chemical stability, and semiconducting conductivity. Metal oxo/hydroxofluorides are prepared by fluorination of

metal oxides [30, 116-117], aluminum chloride fluoride [87], and aluminum bromide fluoride [118] at high temperature.

Therefore, in this chapter, high surface aluminum fluoride (denominated $_{aq.}HS\text{-}AlF_3$) and for the first time aluminum oxofluoride with high surface areas by soft-gel fluorination with 75% HF were prepared and studied by XRD, MAS-NMR, BET surface area, NH_3-TPD. Catalytic properties of the aluminum fluoride samples obtained were also tested in the $CHClF_2$ dismutation and isomerizations of $CF_3CFBrCF_2Br$ and CCl_2FCF_2Cl. As also discussed in chapter 4, the fluorination parameters have an effect on final properties of $_{aq.}HS\text{-}AlF_3$. Therefore the same parameters were also tested and the outcomes of these results were compared with $HS\text{-}AlF_3$.

7.2 Preparation of $_{aq.}HS\text{-}AlF_3$ and AlF_xO_y

In the following, $HS\text{-}AlF_3$ prepared with aqueous HF will be denominated $_{aq.}HS\text{-}AlF_3$. Basically, the sol-gel process for the preparation of aluminum oxyfluoride/aluminum fluoride consists of two steps (scheme 7.1):

(1) Synthesis of precursor ($_{aq.}$precursor) by reacting of $Al(O^iPr)_3$ dissolved in isopropanol with 75% HF ($HF:H_2O$ = 2.7:1) solution. The predicted amount of HF solution was then added to the pre-cooled Al $(O^iPr)_3$ solution under constant stirring. All samples were aged at room temperature for at least 24 h followed by drying under vacuum at 70 °C to produce $_{aq.}$precursor.

(2a) The post-fluorination (activation) of the $_{aq.}$precursor was performed exactly as described in chapter 4 (section 4.2) with $CHClF_2/N_2$ or HF/N_2.

(2b) In alternative experiments, the $_{aq.}$precursor was calcined in a flow-through tube furnace at various temperatures under a flow of Ar or air for 4 h to get aluminum oxyfluoride samples (AlF_yO_x).

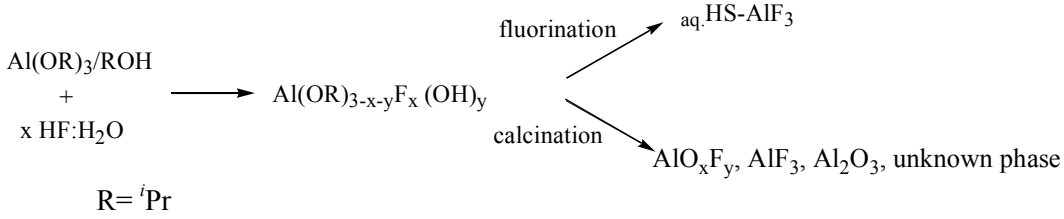

Scheme 7.1 Preparation of $_{aq.}HS\text{-}AlF_3$ and Al (F,O) samples.

7.3 Results and Discussion

7.3.1 $_{aq.}$HS-AlF_3

In the following section, parameters influencing the properties of $_{aq.}$HS-AlF_3 and its characterization will be presented and discussed.

Effect of HF/Al molar ratio: A series of $_{aq.}$precursor with various HF/Al ratios was prepared. The elemental analysis results of the samples are summarized in Table 7.1. As can be seen, the higher the HF/Al ratio the lower is the carbon content of the $_{aq.}$precursors. In addition, the remaining carbon contents in these samples are much lower than that of the corresponding HS-AlF_3 precursor (HF/Al = 3), prepared under non-aqueous conditions. The carbon content on the HS-AlF_3 precursor could be attributed to the residual -^{i}OPr groups and/or adsorbed organic solvents. The low carbon on the $_{aq.}$precursor can be explained as follows: (i) some hydrolysis of Al(^{i}OPr)$_3$/isopropanol introducing –OH groups in the framework takes place, (ii) water is adsorbed on the surface instead of alcohol, or (iii) both processes occur simultaneously.

Table 7.1: Effect of HF:Al(O*i*Pr)$_3$ molar ratio on $_{aq.}$HS-AlF_3 surface properties

Sample	Precursor		HS-AlF_3 properties		
	HF/Al (mol ratio) aimed	C Content (%)	C Content (%)	S_{BET} (m^2/g)	XRD
HS-AlF_3-3*	3	27	0.27	250	am
$_{aq.}$HS-AlF_3-1	1	34	0.13	132	am
$_{aq.}$HS-AlF_3-2	2	22	0.22	120	am
$_{aq.}$HS-AlF_3-3	3	15	0.20	171	am
$_{aq.}$HS-AlF_3-6	6	7	0.41	17	weakly crystalline

am– amorphous

*– HS-AlF_3 prepared under non-aqueous conditions

After fluorination with $CHClF_2/N_2$ (5:20 ml/min) at 300 °C, the results (Table 7.1) show for all but the highest HF amount comparatively moderate differences in $_{aq.}$HS-AlF_3 surface properties. Excessive HF led expectedly to smaller carbon content, i.e., smaller amount of organic constituents, of the $_{aq.}$precursor and, consequently, smaller surface area, and vice versa. Therefore, these samples were not further investigated.

Effect of alkoxide groups: $_{aq.}$HS-AlF_3 samples prepared starting from $Al(O^tBu)_3$ showed slightly higher surface area and higher catalytic activity for isomerization of 1,2-DBP than those prepared from $Al(O^iPr)_3$ (Table 7.2). These results indicate that the type of alkoxide has slight influence on the final properties of $_{aq.}$HS-AlF_3.

Table 7.2: $_{aq.}$HS-AlF_3 prepared from $Al(O^iPr)_3$ and $Al(O^tBu)_3$

Sample	HF.H_2O/Al (mol ratio)	C Content (%)		S_{BET} (m^2/g)	1,2-DBP isomer. activity (%)
		bf	af		
$Al(O^iPr)_3$	3	15	0.48	171	32
$Al(O^tBu)_3$	3	17	0.20	206	37

bf– before fluorination, af– after fluorination with $CHClF_2$

1,2-DBP isomer.– $CBrF_2CBrFCF_3$ isomerization

Post-fluorination

Fluorination with $CHClF_2$

Post-fluorination of the $_{aq.}$precursor with $CHClF_2$ was studied by varying fluorination temperature as well as $CHClF_2$ concentration. These variables will only be discussed for $_{aq.}$HS-AlF_3, prepared starting from $Al(O^iPr)_3$ with HF/Al ratio = 3.

The effect of fluorination temperature on the final properties of $_{aq.}$HS-AlF_3 was tested at 250, 300, and 350 °C and the results are shown in Table 7.3. At 250 °C, the low fluorine content (55.9%) in the sample indicates incomplete fluorination of the $_{aq.}$precursor. This implies that –Al–O–Al– units which may be formed during the decomposition of some of the remaining Al-alkoxide groups or –OH groups must have been present in the network, which can only be removed at higher fluorination temperature. With increasing the temperature of activation from 250 to 300 °C an increase in the fluorine content can be observed, approaching the value of AlF_3 (67.9%), whereas the carbon content decreased, indicating the removal of the remaining alkoxide groups.

In regard of catalytic activity for dismutation of $CHClF_2$, the dismutation started at 250 °C and reached 96-98% after short time. However, after cooling down the sample to 50 °C, the conversion of $CHClF_2$ decreased to 80%. At fluorination at 300 °C, the $CHClF_2$ conversion increased, reaching about 100% even after cooling the sample to 50 °C. Similarly, the conversion of 1,2-DBP over $_{aq.}$HS-AlF_3 increased with increasing the

fluorination temperature from 250 to 300 °C. The changes in the conversions (isomerization and dismutation) were negligible with further increase in the fluorination temperature to 350 °C, indicating that the optimum fluorination temperature is at 300 °C.

Table 7.3: Fluorination with $CHClF_2$: Effect of fluorination temperature on $_{aq.}HS\text{-}AlF_3$ properties

Sample	Final temperature (°C)	C Content (%)		F%	S_{BET} (m^2/g)	Conversion of $CHClF_2$ (%)		1,2-DBP isomer. activity (%)
		bf	af			98 °C	50 °C	
1	250	15	0.32	54.8	187	98	80	5
2	300	15	0.14	65.1	171	≈ 99	≈ 100	32
3	350	15	0.11	n.d.	159	≈ 99	≈ 100	29

bf– before fluorination, af– after fluorination with $CHClF_2$

1,2-DBP isomer.– $CBrF_2CBrFCF_3$ isomerization

The effect of $CHClF_2$ concentration was studied by fluorination of the $_{aq.}$precursor at 300 °C with $CHClF_2/N_2$ ratios of 3/20, 5/20, and 7/20 ml/min. Although, there are no differences in the residual carbon content and only slight differences in the surface area; the time needed for complete fluorination, i.e., for reaching a dismutation activity of 98-99% conversion, varies (Table 7.4). The $CHClF_2$ gas phase concentration also drastically influences the catalytic activity of $_{aq.}HS\text{-}AlF_3$ for 1,2-DBP isomerization. The highest conversion (32%) was obtained with the sample fluorinated with $CHClF_2/N_2$ ratio of 5/20 ml/min.

Table 7.4: Fluorination with $CHClF_2$: Effect of $CHClF_2$ concentration on $_{aq.}HS\text{-}AlF_3$ properties

Sample	$CHClF_2$ flow (ml/min)	N_2 flow (ml/min)	C Content (%)		Time needed for 98% dismutation	S_{BET} (m^2/g)	1,2-DBP isomer. activity (%)
			bf	af			
1	3	20	15	0.28	13	110	7
2	5	20	15	0.27	9	171	32
3	7	20	15	0.21	7	147	11

bf– before fluorination, af– after fluorination with $CHClF_2$

1,2-DBP isomer.– $CBrF_2CBrFCF_3$ isomerization

Fluorination with HF

Fluorination with HF was performed using a HF:N_2 ratio of 2:20 ml/min at 140 °C for 4 h of $_{aq.}$precursor prepared with HF/Al molar ratios equal to 1, 2, and 3. Samples fluorinated with HF were named $_{aq.}$HS-AlF_3-HF-1 (HF/Al = 1), $_{aq.}$HS-AlF_3-HF-2 (HF/Al = 2), and $_{aq.}$HS-AlF_3-HF-3 (HF/Al = 3) to differentiate them from those fluorinated with $CHClF_2$.

As shown in Table 7.5, $_{aq.}$HS-AlF_3-HF-1 and $_{aq.}$HS-AlF_3-HF-2 showed very high BET surface, low F%, and high carbon contents. The high carbon contents and the low F% indicate incomplete fluorination. In contrast, $_{aq.}$HS-AlF_3-HF-3 had very low carbon content (0.2%) and high F content (65%), which corresponds inside the experimental error, with that of AlF_3 (67.7%). This means that under these fluorination conditions, $_{aq.}$precursor with HF/Al = 3 is completely fluorinated and $_{aq.}$HS-AlF_3-HF-3 is formed.

Table 7.5: Fluorination with HF

Sample	HF/Al (mol ratio)	C Content (%)		F%	S_{BET} (m^2/g)	$CHClF_2$ conversion (%)	
		bf	af			250 °C	50 °C
$_{aq.}$HS-AlF_3-HF-1 +N_2	1	34	7.12	48.1	215	5	0
$_{aq.}$HS-AlF_3-HF-2 +N_2	2	22	4.80	58.3	199	32	2
$_{aq.}$HS-AlF_3-HF-3 +N_2	3	15	0.20	64.9	170	99	99

bf– before fluorination, af– after fluorination with HF

The catalytic activity for $CHClF_2$ dismutation of these $_{aq.}$HS-AlF_3-HF samples is analogous to that of HS-AlF_3-HF addressed in chapter 4. Briefly, HS-AlF_3-HF (HF/Al = 3) (see chapter 4) showed negligible conversion of $CHClF_2$ (4%), however, after purging the sample with N_2 for 3 h at 250 °C, considerable increase in the catalytic activity for $CHClF_2$ was achieved. Similarly, $_{aq.}$HS-AlF_3-HF-3 showed negligible conversion of $CHClF_2$ (2%), however, after purging the sample with N_2 for 3 h at 250 °C, the catalytic activity for $CHClF_2$ was increased, reaching 99% and remained 99% even at temperature as low as 50 °C. On the other hand, $_{aq.}$HS-AlF_3-HF-1 and $_{aq.}$HS-AlF_3-HF-2, as expected, showed a rather low catalytic activity for $CHClF_2$ dismutation even after prolonged heating in $CHClF_2/N_2$ flow (30-60 min).

Characterization

N_2 adsorption-desorption

The N_2 adsorption-desorption isotherms of $_{aq.}HS\text{-}AlF_3$-3 (171 m^2/g) and $_{aq.}HS\text{-}AlF_3$-HF-3 (178 m^2/g) samples are presented in Figure 7.1. All the isotherms are of type IV, which characterize mesoporous solids. The isotherms and hysteresis loops of $_{aq.}HS\text{-}AlF_3$-3 sample is slightly different from that of $_{aq.}HS\text{-}AlF_3$-HF-3.

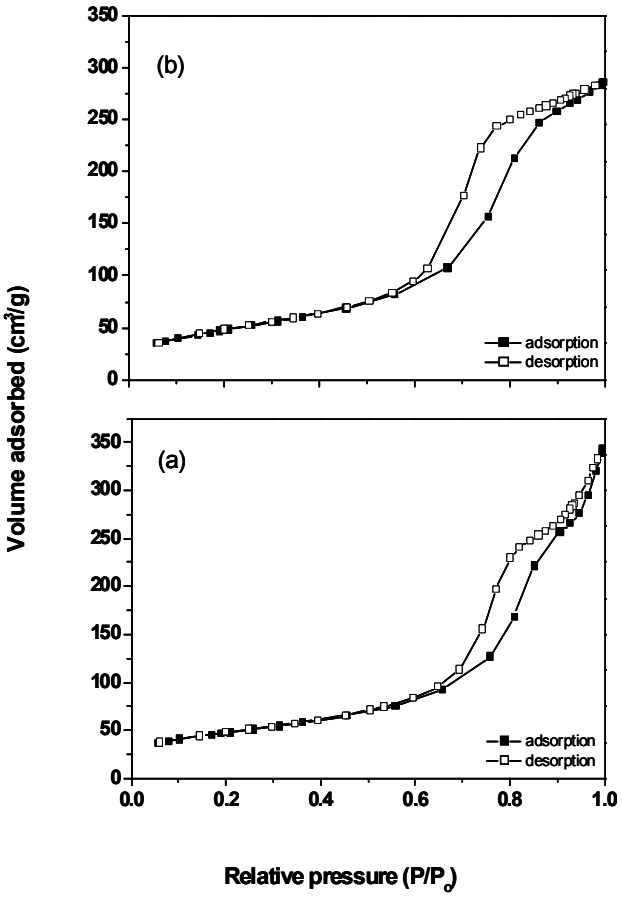

Figure 7.1 N_2 adsorption-desorption isotherms: (a) $_{aq.}HS\text{-}AlF_3$ and (b) $_{aq.}HS\text{-}AlF_3$-HF-3.

Large mesopores were found in the samples $_{aq.}HS\text{-}AlF_3$-3 (Figure 7.1a), whose loops close at around P/P_o = 0.6, whereas slightly narrower mesopores were found in $_{aq.}HS\text{-}AlF_3$-HF-3 (Figure 7.1b) indicated by a closing of the hysteresis loop at P/P_o values of *ca.* 0.5. The observed loops in Figure 7.1a-b imply that the types of pores formed are affected by the type of fluorination agent and fluorination time. The sharp step in the adsorption isotherm of $_{aq.}HS\text{-}AlF_3$-3 also indicates that these $_{aq.}HS\text{-}AlF_3$-3 samples have

relatively large pore distribution, almost similar to those observed for the well-organized mesoporous HS-AlF_3.

Figure 7.2 shows the pore size distributions of $_{aq.}$HS-AlF_3-3 and $_{aq.}$HS-AlF_3-HF-3. The pore diameter of $_{aq.}$HS-AlF_3-3 is slightly larger and more uniform with a maximum at 85 Å than that of $_{aq.}$HS-AlF_3-HF-3. $_{aq.}$HS-AlF_3-HF-3 exhibits pore size distribution with two maxima at about 59 Å and the other at about 71 Å.

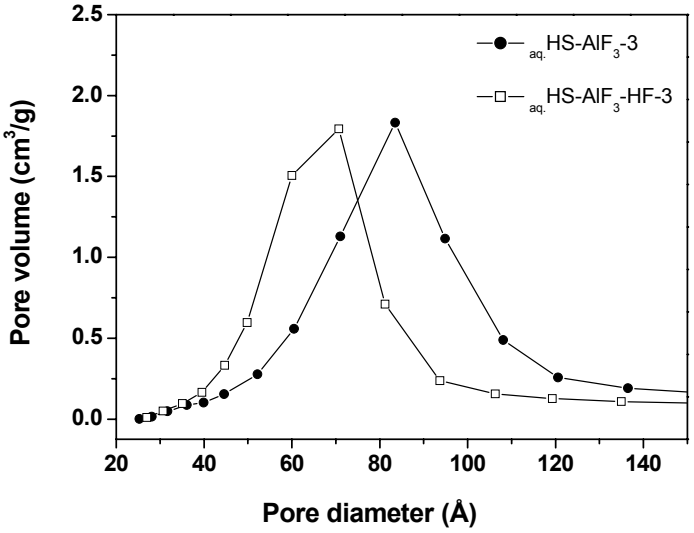

Figure 7.2 Pore size distributions of $_{aq.}$HS-AlF_3-3 and $_{aq.}$HS-AlF_3-HF-3.

Thermal analysis

The TG/DTA/MS of a representative $_{aq.}$HS-AlF_3-3 sample, prepared by fluorination of precursor (HF/Al=3) with $CHClF_2$, is shown in Figure 7.3A-B. A mass loss of 18% is observed over the whole temperature range, which is mainly due to the release of water {*m/z* peak at 18 (H_2O^+) for H_2O or 17 (OH^+)}. There are several sources for the appearance of water: (i) This sample was stored for about three months in a closed plastic container but access of moisture can not totally be excluded and this would be easily adsorbed on the surface due to its strong Lewis acidity. (ii) A more probable scenario is the formation of water from the decomposition of isopropanol which would form propene beside water. Since the typical fragments for isopropanol (*m/z* = 45) and propene (m/z = 41) appear exactly at the same temperature, this interpretation is the most obvious one for the effect observed at 170 °C. The effect at about 527 °C is most likely due to the condensation of isopropanol adsorbed on very strong Lewis acid sites. The distinct exothermic effect at 527 °C in the DTA curve indicates the crystallisation of the amorphous material forming

α-AlF_3. A mass loss is observed at about 532 °C, corresponding to the evolution of HF (*m/z* = 19) which may originate from either HF formed during the second fluorination step being still strongly adsorbed on the strong Lewis acid sites, or from hydrolysis reactions during removal of chemically formed water at high temperature (about 532 °C) leading to the formation of HF.

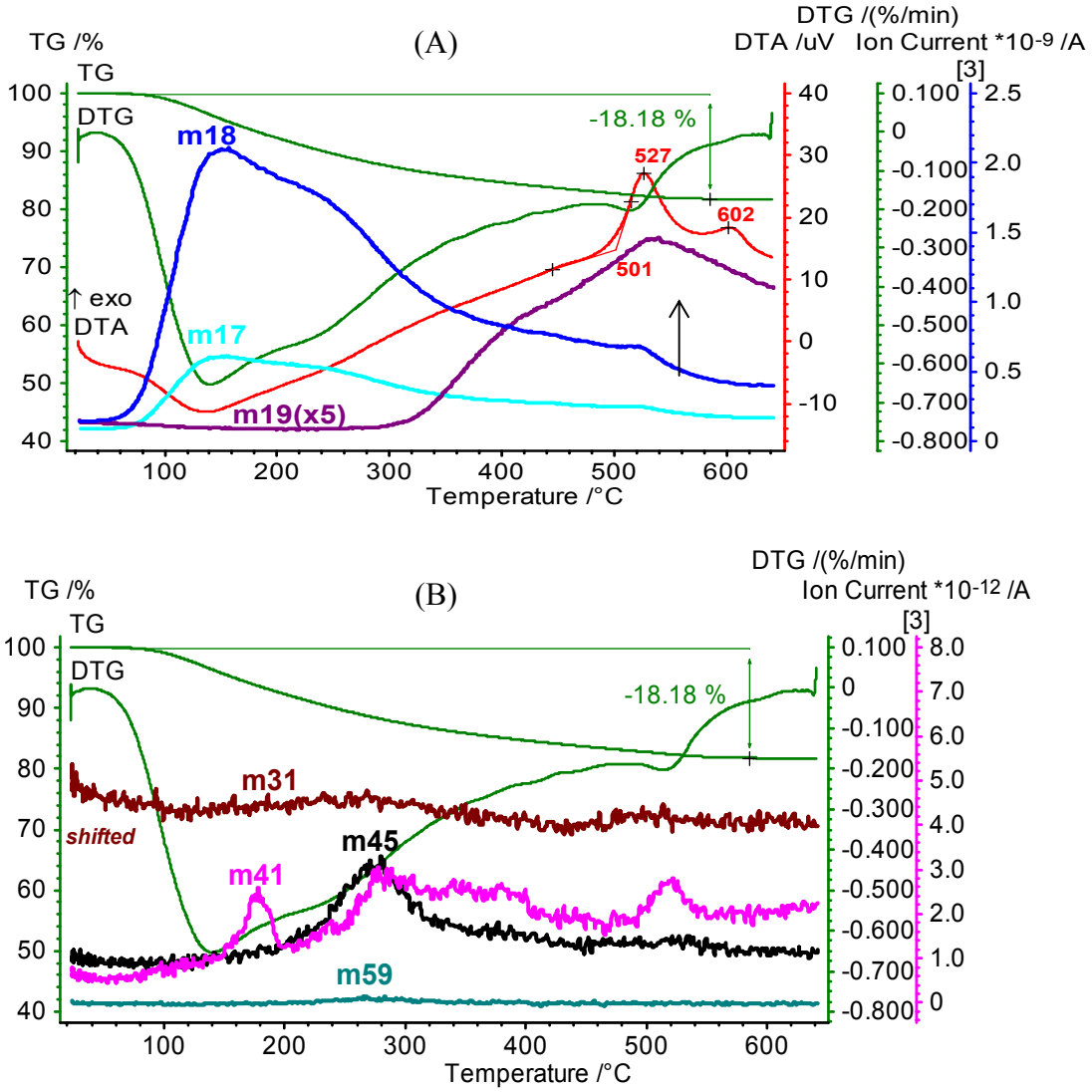

Figure 7.3 TG/DTA/MS of $_{aq.}HS$-AlF_3-3 with IC curves (A) for *m/z* 18 (H_2O^+), *m/z* 17 (OH^+), *m/z* 19 (F^+) and (B) for *m/z* 41 ($C_3H_5^+$), *m/z* 45 ($C_2H_5O^+$), and *m/z* 31 (CH_3O^+).

In any case, at the crystallization temperature any compound being still adsorbed will be evolved and can evaporate. Moreover, hydrolysis products possibly formed may become re-fluorinated by the released HF. Thus, the second exothermic effect at 602 °C may be due to the transformation of the re-fluorinated material to α-AlF_3; the final residue was α-AlF_3 (PDF file number 77-252).

FTIR studies

To further investigate the framework of the $_{aq.}HF\text{-}AlF_3$ samples and $_{aq.}HF\text{-}AlF_3\text{-}HF$ and to clarify whether AlF_3 is the only phase present or OH^- is also present in the network, FTIR was performed.

The transmission IR spectra of $_{aq.}HS\text{-}AlF_3\text{-}3$, and $_{aq.}HS\text{-}AlF_3\text{-}HF\text{-}3$ are presented in Figure 7.4a-b. For comparison, Figure 7.4c gives the spectrum of $HS\text{-}AlF_3$. As it can be seen from Figure 7.4a-c, no bands due to the presence of hydroxyl groups ($\nu_{O\text{-}H}$ = 3700 cm^{-1}) or alkoxy groups ($\nu_{C\text{-}H}$ = 2800-3000 cm^{-1} and $\nu_{C\text{-}O}$ = 950-1300 cm^{-1}) were observed in the IR spectra of $_{aq.}HS\text{-}AlF_3\text{-}3$ (Figure 7.4b) and $_{aq.}HS\text{-}AlF_3\text{-}HF\text{-}3$ (Figure 7.4c) and only the bands due to AlF_3 were observed in the IR spectra. The highest-frequency bands in the spectra of $_{aq.}HS\text{-}AlF_3\text{-}3$ are due to the stretching vibration modes (366 cm^{-1}) and the bands at 361 and 366 cm^{-1} are due to bending vibration modes. The broadness of the two IR peaks is due to the high degree of disordering in the samples [119-120].These results are similar to those found for $HS\text{-}AlF_3$ as Figure 7.4c shows.

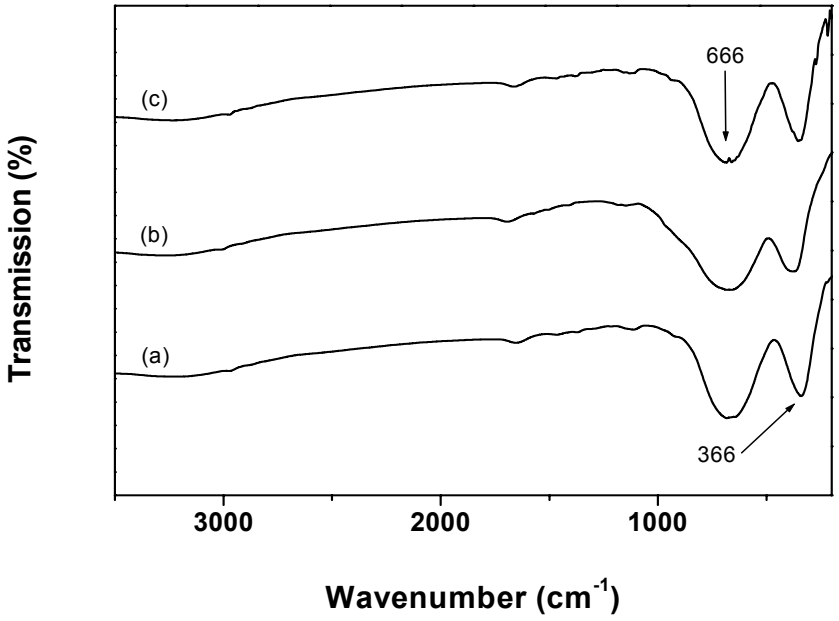

Figure 7.4 FTIR spectra of (a) $_{aq.}HS\text{-}AlF_3\text{-}3$, (b) $_{aq.}HS\text{-}AlF_3\text{-}HF\text{-}3$, and (c) $HS\text{-}AlF_3$.

MAS NMR

MAS NMR was used to probe the local environment of Al and F in the $_{aq.}HF\text{-}AlF_3$. MAS-NMR measurements were performed only on $_{aq.}HF\text{-}AlF_3\text{-}1$ and $_{aq.}HF\text{-}AlF_3\text{-}3$.

^{27}Al MAS NMR

Figure 7.5a-b illustrates the ^{27}Al MAS NMR spectra obtained for $_{aq.}HF\text{-}AlF_3$-1 and $_{aq.}HF\text{-}AlF_3$-3 samples. Only one signal at -15.9 ppm is present in the ^{27}Al MAS NMR spectrum (Figure 7.5a) of $_{aq.}HF\text{-}AlF_3$-3, which can be assigned to AlF_6 polyhedra and no contributions from other phases were found. The ^{27}Al chemical shift observed for $_{aq.}HF\text{-}AlF_3$-3 is close to that arising from crystalline AlF_3 and similar to that observed for $HS\text{-}AlF_3$ [121, 37]. The ^{27}Al MAS-NMR spectrum of $_{aq.}HF\text{-}AlF_3$-1 shows a signal at -16.1 ppm and an additional weak resonance at 54.1 ppm due to aluminum coordinated to oxygen in tetrahedral environments (AlO_4, Figure 7.5b). There is also a very weak signal at 10.1 ppm, typical for AlO_6 polyhedra. Thus, it seems there are minor mixed phases, in which aluminum is coordinated to fluorine and to oxygen.

The asymmetric lineshapes of the ^{27}Al peaks (Figure 7.5a-b) illustrate the contribution of ^{27}Al quadrupole parameters in the $_{aq.}HF\text{-}AlF_3$-1 and $_{aq.}HF\text{-}AlF_3$-3 samples. The presence of a large sideband manifold spreading over more than 6000 ppm in both samples and their shape indicate the local disorder at the aluminum sites.

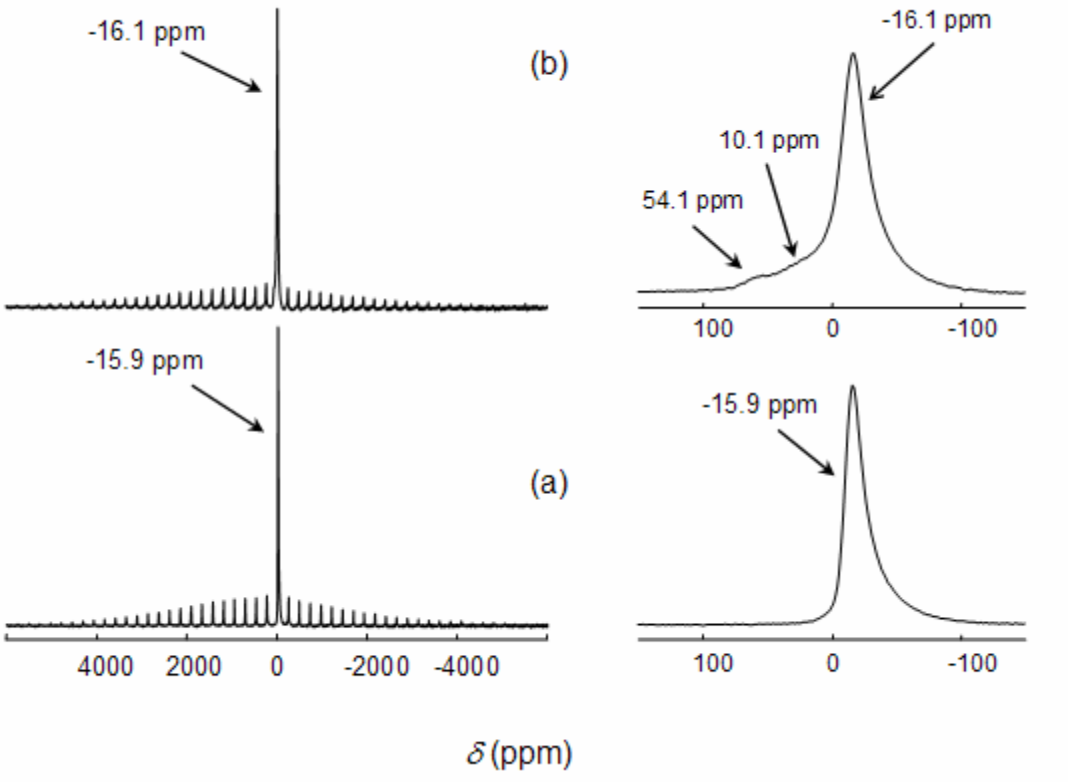

Figure 7.5 ^{27}Al MAS-NMR of (a) $_{aq.}HS\text{-}AlF_3$-3 and (b) $_{aq.}HS\text{-}AlF_3$-1 (ν_r = 25 kHz).

^{19}F MAS NMR

^{19}F MAS NMR spectra obtained for $_{aq.}HF\text{-}AlF_3$-1 and $_{aq.}HF\text{-}AlF_3$-3 are given in Figure 7.6a-b.

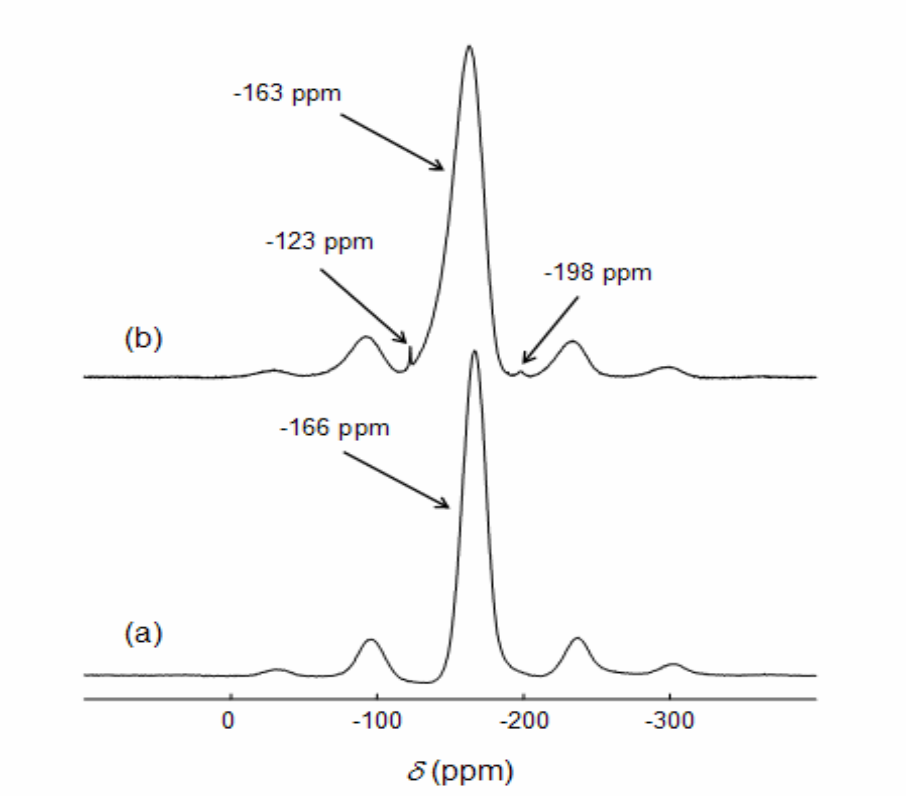

Figure 7.6 ^{19}F MAS-NMR of (a) HS-AlF_3-3 (b) HS-AlF_3-1 (ν_r = 25 kHz).

The spectra show the main signal at -163 and -166 ppm, respectively, which is consistent with an octahedral AlF_6 environment and also observed for amorphous and crystalline phases [29, 34, 116, 122]. Sample $_{aq.}HF\text{-}AlF_3$-1 showed two additional weak signals at -123 and -198 ppm (Figure 7.6b).The signal at -198 ppm is caused by terminal fluorine atoms bound to only one aluminum atom (F-Al species) at a distance of about 1.7 Å [123]. The origin of the other signal (-123 ppm) is not clear at the moment and further investigations are still needed. According to Chupas et al, the signal at -123 ppm can be due to either an $AlO_{6-x}F_x$ ($x \approx 2$) environment or to terminal fluorine atom at the surface [121].

TEM measurements

In order to observe the morphology of the elemental particles of $_{aq.}HS\text{-}AlF_3$, the sample was observed by TEM. Figure 7.7 shows a representative TEM micrograph of $_{aq.}HS\text{-}AlF_3$ (171 m^2/g). Irregular shapes of particles (around 10 nm) are observed, which have low

contrast and are probably agglomerates of much smaller particles. The selected-area electron diffraction patterns of the particles show some crystalline and some amorphous parts, which indicate that the particles are microcrystalline. Because the particles are very small, in XRD pattern of this sample, only broad peaks are observed. The lattice distances measured from the diffraction rings (*d* values = 3.6 nm) is similar to those found in aluminum fluorides and similar to those found in HS-AlF_3 [35].

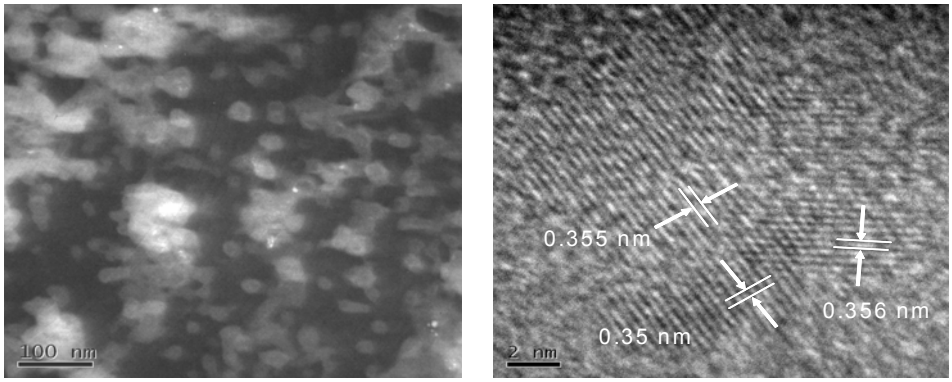

Figure 7.7 High resolution TEM image of $_{aq.}HS\text{-}AlF_3$.

NH_3-TPD

In order to determine and to compare the acid strength distribution of the obtained HS-AlF_3-1, HS-AlF_3-2, and HS-AlF_3-3 samples, temperature programmed desorption of ammonia was performed and the experimental TPD profiles were fitted by Gaussian deconvolution using four peaks fitting (Figure 7.8a-c). The area under each of these peaks were named weak (A), medium (B and C) and strong (D) related to maximum desorption at low, medium and high temperatures, respectively. Figure 7.8a-c shows the desorption profiles and the Gaussian deconvoluted peaks of $_{aq.}HS\text{-}AlF_3$-1 (Figure 7.8a), $_{aq.}HS\text{-}AlF_3$-2 (Figure 7.8b), and $_{aq.}HS\text{-}AlF_3$-3 (Figure 7.8c) samples.

$_{aq.}HS\text{-}AlF_3$-1 sample shows four deconvoluted peaks, namely at 201, 227, 323, and 497 °C. $_{aq.}HS\text{-}AlF_3$-2 shows an initial NH_3 desorption at 200 °C. The second and third desorption peak are located at a slightly higher temperatures with maxima at 253 and 354 °C, respectively. Like $_{aq.}HS\text{-}AlF_3$-1, a fourth step of desorption has a maximum at 497 °C (Figure 7.8b). The low temperature desorption peak of NH_3 (A) for $_{aq.}HS\text{-}AlF_3$-1 and $_{aq.}HS\text{-}AlF_3$-2, is assigned to ammonia desorbing from weak acid sites, the second and the third is due to ammonia desorbing from medium acid sites, and the fourth maximum occurring at roughly 497 °C (D) is attributed to desorption of NH_3 from strong acid sites.

Obviously, the weaker ones are dominant. $_{aq.}HS\text{-}AlF_3$-3 (Figure 7.8c) displays distinctly four deconvoluted peaks; two of them are located at similar positions to the proceeding ones and a third and a forth located at intermediate temperatures, 361 and 426 °C, respectively, defined as medium acidity (B and C). The peaks at 361 °C and 488 °C, are the dominant ones. These results suggest that $_{aq.}HS\text{-}AlF_3$-3 has stronger acid sites than $_{aq.}HS\text{-}AlF_3$-1 and $_{aq.}HS\text{-}AlF_3$-2.

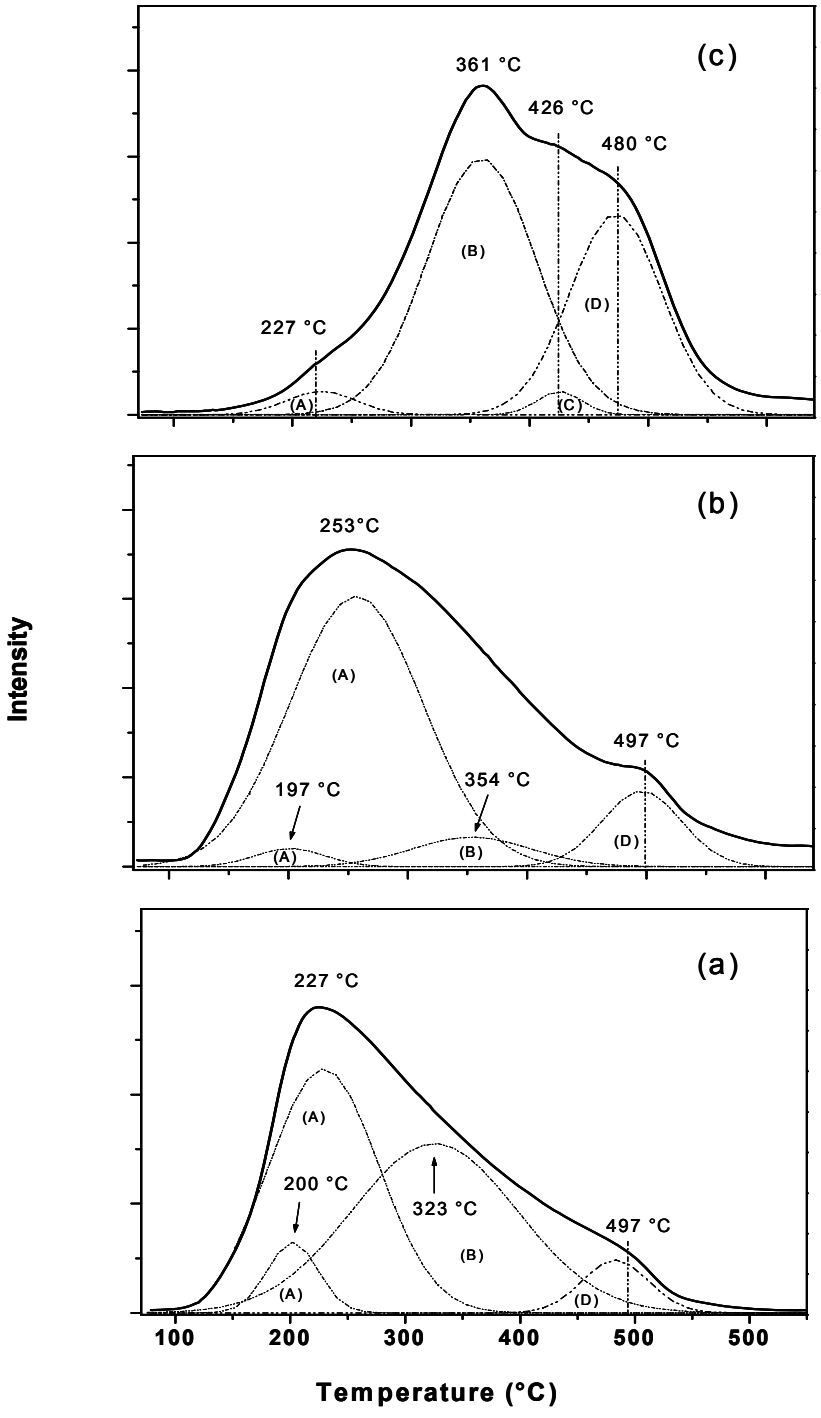

Figure 7.8 NH_3-TPD spectra on (a) $_{aq.}HS\text{-}AlF_3$-1; (b) $_{aq.}HS\text{-}AlF_3$-2, (c) $_{aq.}HS\text{-}AlF_3$-3.

A comparison of NH_3-TPD of $_{aq.}HS\text{-}AlF_3$-3, and HS-AlF_3 prepared under non-aqueous conditions (HF/Al = 3), indicates that the strength of acid sites on $_{aq.}HS\text{-}AlF_3$ is almost similar to those found on HS-AlF_3, but their concentration is much lower (Figure 7.9a-b). HS-AlF_3 shows four peaks with maximum at 227, 326, 392, and 500 °C (Figure 7.9a), assigned to weak (227 °C), medium (326 and 400 °C) and strong (500 °C) acidity, respectively. Like HS-AlF_3, $_{aq.}HS\text{-}AlF_3$-3 shows an initial NH_3 desorption at 227 °C (Figure 7.9b), whereas the second and third desorption peaks are located at slightly higher temperatures, the fourth desorption step at somewhat lower temperature, corresponding to a somewhat lower maximum acidity.

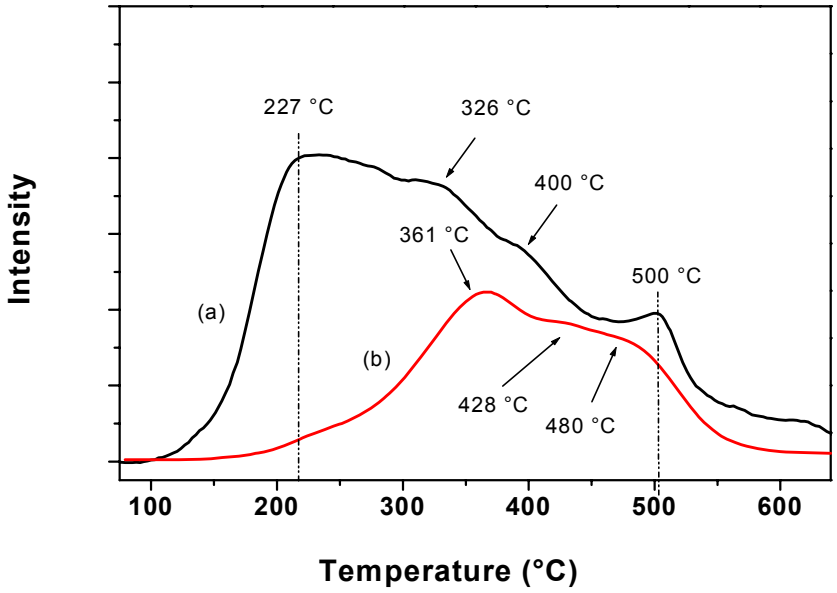

Figure 7.9 NH_3-TPD spectra on (a) HS-AlF_3-1 and (b) $_{aq.}HS\text{-}AlF_3$-3.

Catalytic behavior

$CHClF_2$ dismutation and $CF_3CBr_2CF_3$ and CCl_2FCClF_2 isomerizations (eq. 4.2 to 4.4, chapter 4) were used to probe the surface acid properties of $_{aq.}HS\text{-}AlF_3$ samples. The results obtained in the dismutation of $CHClF_2$ at 300, 150, and 50 °C over $_{aq.}HS\text{-}AlF$ samples prepared by different precursors as well as $_{aq.}HS\text{-}AlF_3$-3-HF + N_2 are shown in Table 7.6.

The conversion of the $CHClF_2$ over the $_{aq.}HS\text{-}AlF_3$ samples was always about 99 % even after cooling the reactor to temperature as low as 50 °C (Table 7.6). $_{aq.}HS\text{-}AlF_3$ prepared with HF/Al = 3 ratio showed slightly higher catalytic activity, reaching about 100% at 50 °C. The major products of dismutation of $CHClF_2$ are CHF_3 and $CHCl_3$ (eq. 4.2).

Table 7.6: Catalytic activity for $CHClF_2$ dismutation

Sample	HF/Al (mol ratio)	S_{BET} (m^2/g)	Conversion of $CHClF_2$ (%)		
			300 °C	150 °C	50 °C
$_{aq.}HS\text{-}AlF_3$-1	1	113	99	99	99
$_{aq.}HS\text{-}AlF_3$-2	2	120	99	99	≈ 99
$_{aq.}HS\text{-}AlF_3$-3	3	171	99	≈ 100	≈ 100
$_{aq.}HS\text{-}AlF_3\text{-}HF + N_2$	3	187	99	≈ 99	≈ 99
$_{aq.}HS\text{-}AlF_3$-3*	3	192	99	≈ 100	≈ 100

*– $HS\text{-}AlF_{3(aq.)}$ prepared using $Al(O^tBu)_3$

Table 7.7 gives the catalytic activities of $_{aq.}HS\text{-}AlF_3$ samples for $CF_3CBr_2CF_3$ and CCl_2FCClF_2 isomerizations. A good reproducibility could be obtained with experimental error of less than 4% for each experiment. Obviously, the highest activity for isomerization of 1,2-DBP (eq. 7.3) was attained on $_{aq.}HS\text{-}AlF_3$-3 (32%), and decreased in the order $_{aq.}HS\text{-}AlF_3$-2 (10%) > $_{aq.}HS\text{-}AlF_3$-1 (9%). Similarly, CCl_2FCClF_2 isomerization (eq.7.3) over $_{aq.}HS\text{-}AlF_3$-3 was higher (42%) than those observed for $_{aq.}HS\text{-}AlF_3$-1 (9 %) and $_{aq.}HS\text{-}AlF_3$-2 (10%). $_{aq.}HS\text{-}AlF_3$ prepared from $Al(O^tBu)_3$ showed slightly higher catalytic activity.

Table 7.7: Catalytic activity for $CF_3CBr_2CF_3$ and CCl_2FCClF_2 isomerizations

Sample	HF/Al (mol ratio)	Isomerization of $CF_3CBr_2CF_3$ (%)	Isomerization of CCl_2FCClF_2 (%)
		2 h	2 h
$_{aq.}HS\text{-}AlF_3$-1	1	9	10
$_{aq.}HS\text{-}AlF_3$-2	2	10	11
$_{aq.}HS\text{-}AlF_3$-3	3	32	42
$_{aq.}HS\text{-}AlF_3\text{-}HF\text{-}3 + N_2$	3	19	23
* $_{aq.}HS\text{-}AlF_3$-3	3	37	45

*– $_{aq.}HS\text{-}AlF_3$ prepared using $Al(O^tBu)_3$

The change of activity of these catalysts corresponds to the observed difference in acidity and surface area. As discussed in section 7.3, $_{aq.}HS\text{-}AlF_3$-1 and $_{aq.}HS\text{-}AlF_3$-2

samples have much less strong acid sites and about 20% less surface area than $_{aq.}HS\text{-}AlF_3$-3. Because the reaction takes place on the surface and for the isomerization reactions, very strong acid sites are pre-requisite for these reactions to take place, the difference in their catalytic behavior can be related to the higher porosity of $_{aq.}HS\text{-}AlF_3$-3 (171 m^2/g), which exposes a higher number of strong Lewis acid sites, thus, higher catalytic activity than $_{aq.}HS\text{-}AlF_3$-1 (132 m^2/g) and $_{aq.}HS\text{-}AlF_3$-2 (120 m^2/g).

7.3.2 AlF_xO_y

This part will demonstrate that the aimed introduction of –OH groups – beside F^- by using aqueous hydrofluoric acid during the precursor synthesis can result in the formation of aluminium oxyfluorides. This gives access to a new compound class, AlO_xF_{3-x}, which may be of interest for several purposes. Only some preliminary results will be presented in the following section.

Preparation

Aluminium oxyfluoride/aluminium fluoride (AlOF, i.e., $_{aq.}$precursor) with various HF/Al molar ratios was prepared as demonstrated in section 7.2. The samples were then placed in platinum crucible and calcined under Ar or in air for 4 h at various calcination temperatures and with various heating rates. Samples were denoted in the following way: AlFO-1 (HF/Al = 1), AlFO-3 (HF/Al = 3), and AlFO-6 (HF/Al = 6).

Characterization

Thermal analysis

Thermal analysis was performed for AlFO-1 (HF/Al = 1) and AlFO-3 (HF/Al = 3). The measurements were carried out under N_2.

AlFO-1: TG/DTA/MS diagrams of thermal analysis of a representative AlFO-1 (HF/Al = 1) is shown in Figures 7.10A-C. A mass loss of about 25% is observed which occurs in two steps; both are endothermic. The first one (22% loss, 170 °C) is attributable to removal of H_2O, loosely bound isopropanol, and water, which is adsorbed on the surface when the sample was exposed to air during preparation (Figure 7.10A-B), as detected by MS (*m/z* peak at 45).

The second step (at 240 °C) is endothermic with a mass decrease of about 7% due to the loss of water, indicated by *m/z* peak at 18 (H_2O^+) for H_2O, and propene (peak at 41) (Figure 7.10A-B). Water and propene can result from (i) the condensation of the remaining Al-O^{i}R groups (5.1 and 5.2) or (ii) from condensation of alcohol, which is adsorbed on the surface, as demonstates in 5.3.

At higher temperature (up to 350 °C) no further mass change occurs; the final decomposition residue is X-ray amorphous. A steady horizontal TG line after 400 °C shows no further weight loss (Figure 7.10C). At 598 °C, an exothermic reaction takes place without any additional weight loss due to transformation of the amorphous phase to crystalline α-AlF_3. A second exothermic DTA effect occurs at 785 °C. The residue of the thermal analysis was α-AlF_3 as was identified from XRD (PDF No: 77-252). Thus, the second exothermic peak may be due to crystallization of the remaining amorphous AlF_xO_y to α-AlF_3. The residual Al_2O_3 obviously is still amorphous.

AlFO-3: The thermal behavior of a (representative) AlFO-3 sample prepared with high HF/Al molar ratio (HF/Al = 3) is shown in Figures 7.11A-B. The TG/DTA/MS diagram of the sample reveals a clear different picture than that of AlFO-1 sample. The overall mass loss of about 27% extended over the whole temperature range from 50 to 950 °C. In Figure 7.11A the weight loss of about 22 % (up to 350 °C) corresponds to removal of water (from moisture air), isopropanol, probably from Lewis acid sites on aluminum, and to the condensation of Al-O^{i}R groups or alcohol to give propene and water, indicated by *m/z* peak at 18 (H_2O^+) for water and *m/z* peak at 41 for propene. Again, the residue of the thermal analysis was X-ray amorphous. At 479 °C (Figure 7.11B), an exothermic process takes place probably due to phase transformation of the amorphous AlFO-3 sample to α-AlF_3. XRD was not measured at this point, however, at 700 °C phase transformation to α-AlF_3 was confirmed from XRD. Above 850 °C, a weight loss of *ca.* 4 % occurs, probably due to the sublimation of AlF_3. The final decomposition residue is α-AlF_3.

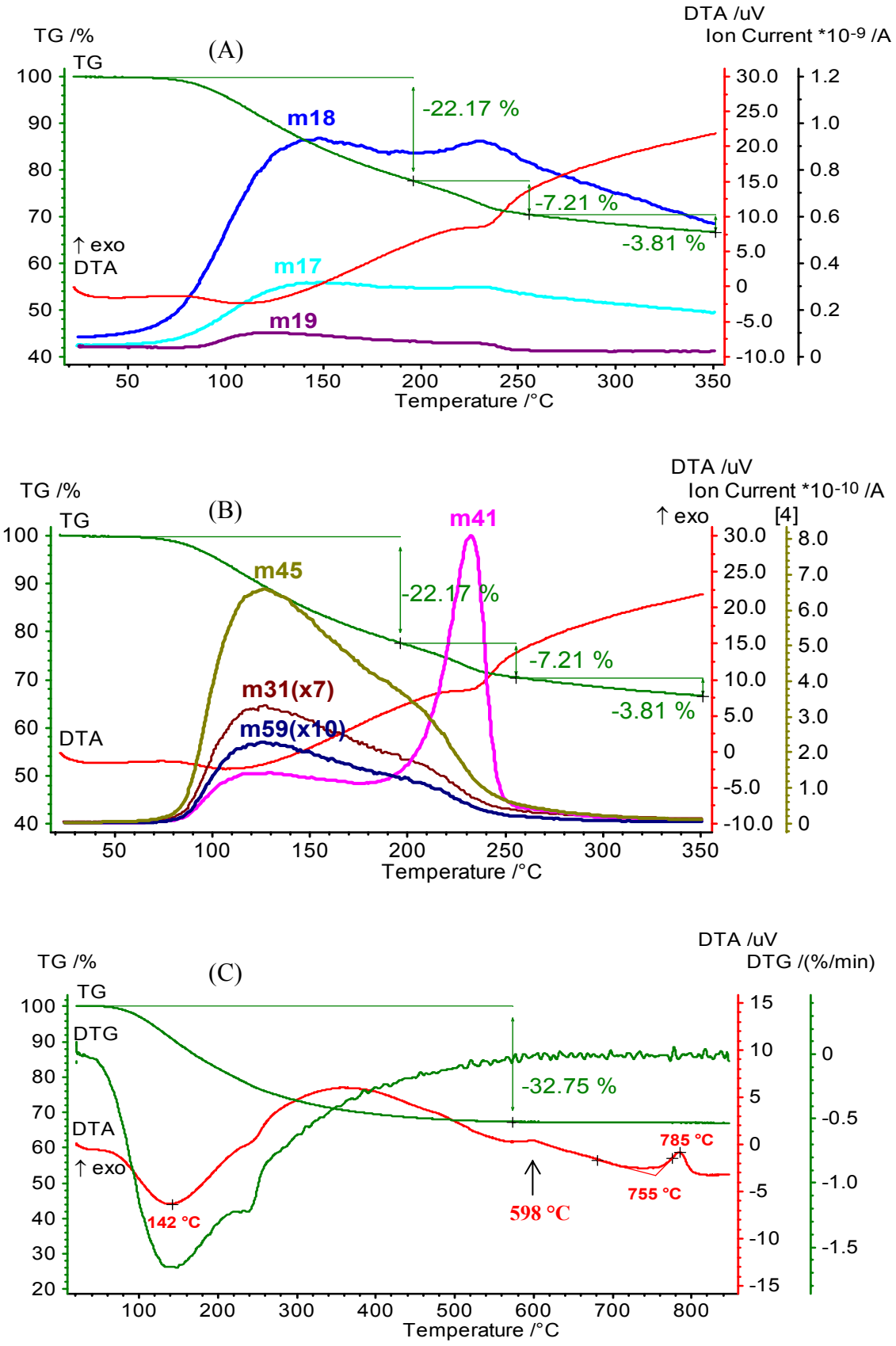

Figure 7.10 TG\DTA\MS of AlFO-1 $_{aq.}$precursor measured up to 350 °C with IC curves for **(A)** *m/z* 18 (H_2O^+), *m/z* 17 (OH^+), **(B)** *m/z* 59 ($C_3H_7O^+$), *m/z* 41 ($C_3H_5^+$), *m/z* 45 ($C_2H_5O^+$), and **(C)** TG\DTA of AlFO-1 $_{aq.}$precursor measured up to 850 °C.

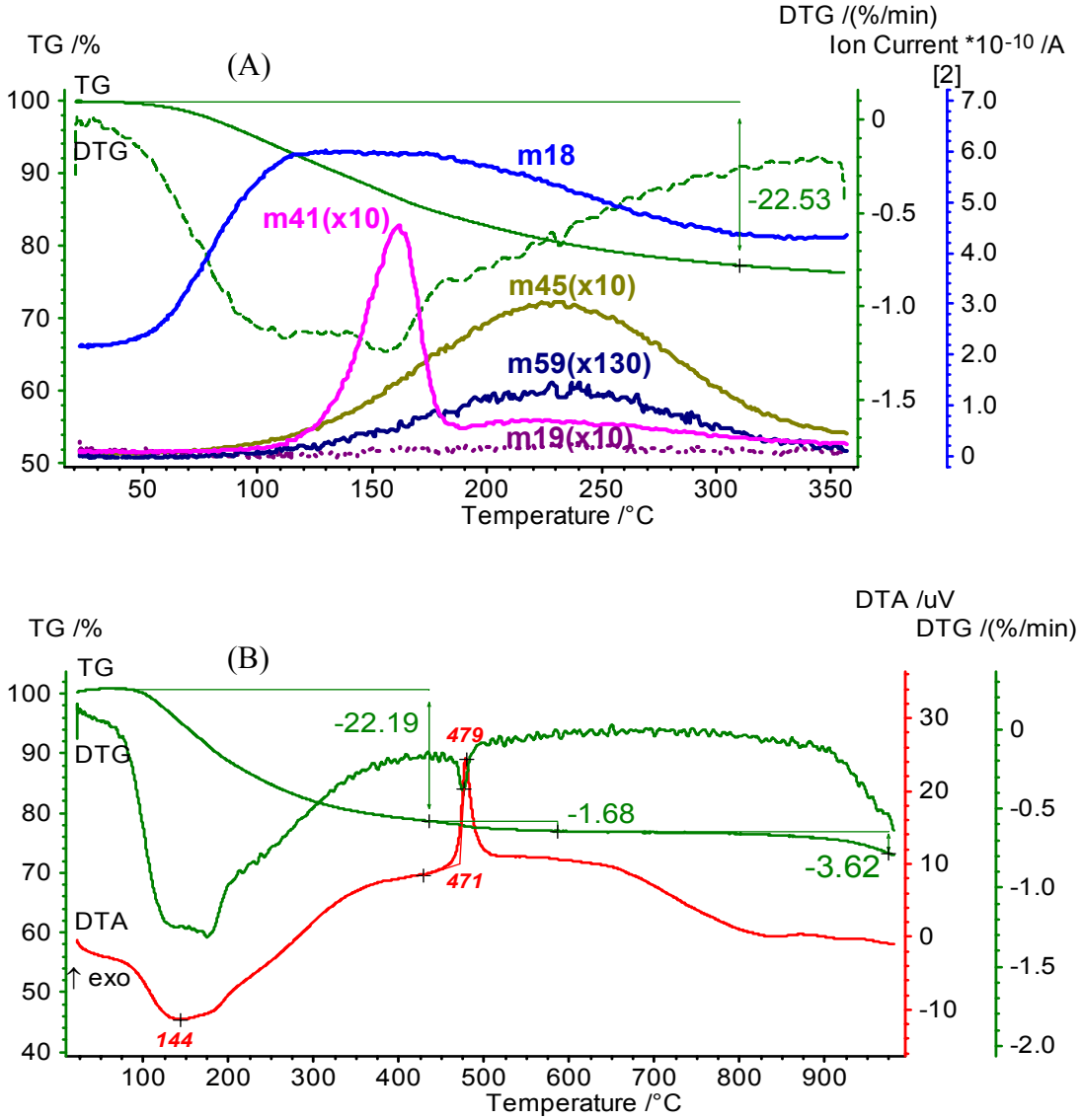

Figure 7.11 **(A)** TG/MS of AlFO-3 $_{aq.}$precursor measured up to 350 °C with IC curves for *m/z* 18 (H_2O^+), *m/z* 17 (OH^+), *m/z* 59 ($C_3H_7O^+$), *m/z* 41 ($C_3H_5^+$), *m/z* 45 ($C_2H_5O^+$), *m/z* 19 (F^+) and **(B)** TG/DTA of AlFO-3 measured up to 1000 °C.

Heating in dry-air: Thermal analysis was also performed in dry air. This variable will be discussed for the AlFO-1 sample only.

As shown in Figure 7.12, the thermal analysis of AlFO-1 samples in dry air is similar to that measured in N_2. The overall weight loss of about 54% extends over a broad temperature region from about 40 to 290 °C and may be divided up to two steps. Again the first one probably corresponds to the endothermic removal of water and weakly bound isopropanol. The second step is due to the decomposition of the remaining alkoxide. The residue of the thermal analysis is α-AlF_3. Since there must be still some oxide in the solid probably X-ray amourphous Al_2O_3 is also present but not detected.

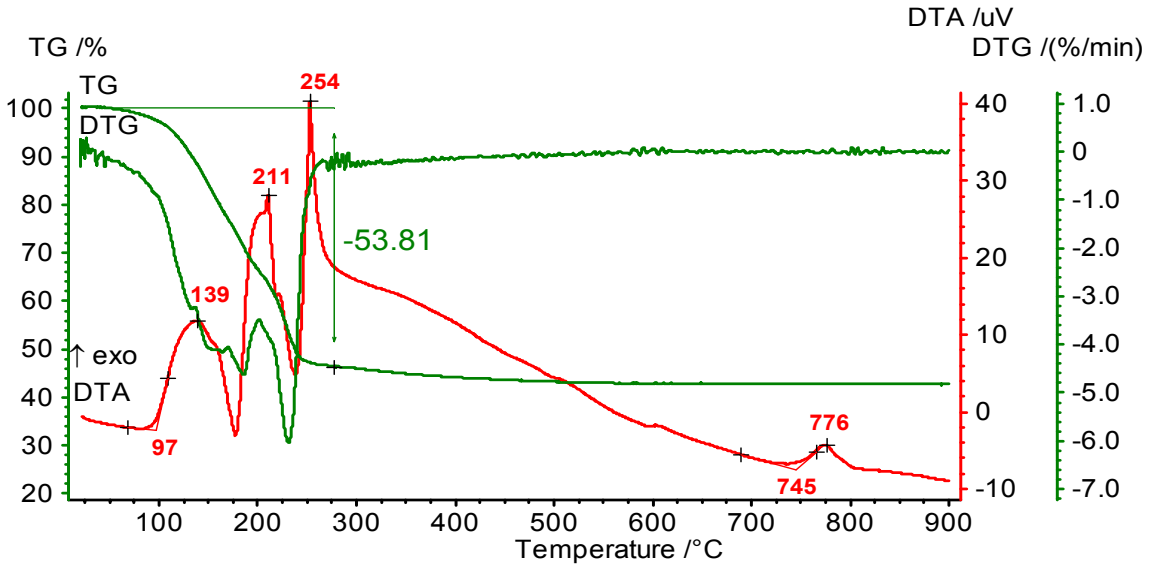

Figure 7.12 TG\DTA of AlFO-1 $_{aq.}$precursor measured up to 900 °C in dry-air.

Based on our pre-investigation and thermal analysis results, it was found that heating rate, heating atmosphere, i.e., heating under inert atmosphere (such as Ar) or in air, and calcination temperature have a large effect on the texture properties and crystallization behavior of the resulting material. Therefore, the effect of heating rate, calcination temperature, duration, and calcination atmosphere on the AlFO-1 (HF/Al molar ratio = 1), AlFO-3 (HF/Al molar ratio = 3), and AlFO-6 (HF/Al molar ratio = 6) samples were studied in more depth.

In the following section, some selected results obtained from calcination under Ar and in air are reported.

Heating under Ar

Data of the F contents, C contents, and surface areas of AlFO samples calcined for 4 h at various temperatures with heating rate of 5 °C/min are listed in Table 7.8. Heating the samples up to 350 °C resulted in removal of all the residual organic constituents (C% = 0). At 700 °C, the absence of carbon and the high F contents of AlFO-3 and AlFO-6 samples (65%), reaching the theoretical value of AlF_3 (67.7%), indicate complete transformation of AlFO-3 and AlFO-6 into AlF_3. In contrast, AlFO-1 had only F content of about 30%. The absence of carbon and low F% indicate that there is not or not only AlF_3, but other phase(s) must be present in the sample.

At 350 °C, AlFO-1 has the highest surface area (241 m^2/g), whereas AlFO-6 has the lowest surface area (11 m^2/g). Further increase in the calcination temperature to 700 °C induced a significant drop in the surface area. It is obvious that some ordering processes took place at high calcination temperature. These results indicate that the porous structures of the sol-gel made samples are very sensitive to calcination temperature. Note the surface area of AlFO-1 was about 20 times higher than that of AlFO-6 calcined at the same temperature and under the same conditions.

When the samples were calcined with heating rate of 20 °C/min, no remarkable influence on the carbon contents, fluorine contents, or BET surface area were observed (Table 7.8).

Table 7.8: characterization of AlFO samples after calcination under Ar at various temperatures and various heating rate

Sample	HF/Al (mol ratio)	C content before calcination (%)	Heating rate					
			5 °C/min			**20 °C/min**		
			F%	C%	S_{BET} (m^2/g)	F%	C%	S_{BET} (m^2/g)
Calcination: 1) at 350°C								
AlFO-1	1	34	29.8	0.0	241	29.9	0.0	229
AlFO-3	3	15	61.1	0.0	82	60.6	0.0	79
AlFO-6	6	7	62.6	0.0	11	62.1	0.0	n.d.
2) at 700 °C								
AlFO-1	1	34	30.9	0.0	102	30.8	0.0	98
AlFO-3	3	15	64.7	0.0	8	62.9	0.0	6
AlFO-6	6	7	64.9	0.0	3	n.d.	0.0	3
3) at 900 °C								
AlFO-1	1	34	30.1	0.0	77	29.1	0.0	n.d.
AlFO-3	3	15	58.9	0.0	2	57.6	0.0	≈ 2
AlFO-6	6	7	n.d.	0.0	n.d.	n.d.	0.0	n.d.

n.d.– not determined

XRD: In order to study the phase development with increasing the calcination temperature, the above samples were calcined under Ar for 4 h at various temperatures with heating rate of 5 °C, followed by phase analysis using XRD.

Figures 7.13a-c and 7.14a-c presents the XRD patterns of AlFO-1, AlFO-3, and AlFO-6 calcined at 350 and 700 °C, respectively, with a heating rate of 5 °C/min and dwell time of 4 h.

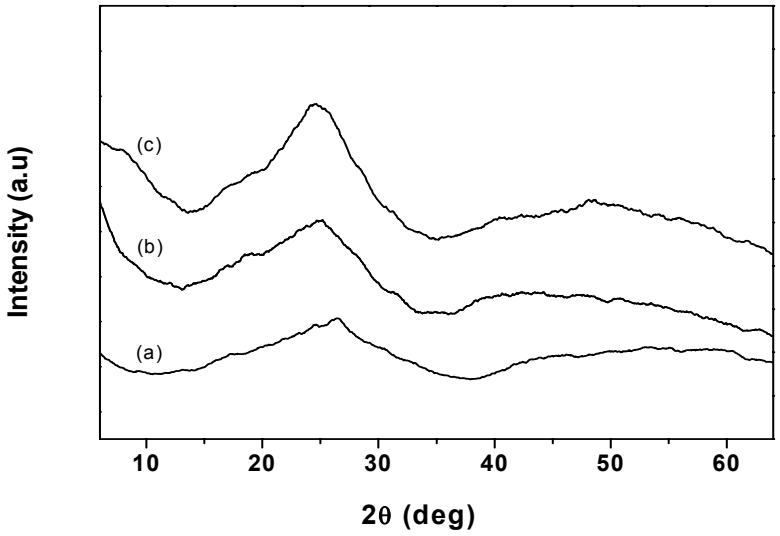

Figure 7.13 XRD patterns of (a) AlFO-1, (b) AlFO-3, (c) AlFO-6 calcined under Ar at 350 °C for 4 h.

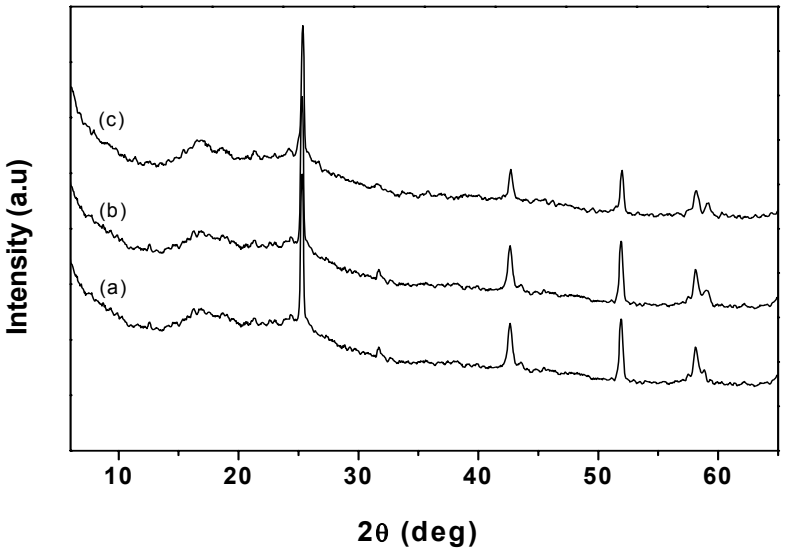

Figure 7.14 XRD patterns of (a) AlFO-1, (b) AlFO-3, (c) AlFO-6 calcined under Ar at 700 °C for 4 h.

As it can be seen from Figure 7.13a-c, the calcined samples remained amorphous up to 350 °C. The amorphous like materials transformed to α-AlF_3 (PDF file number 77-252) after further heat treatment at 700 °C (Figure 7.14a-c). At 900 °C, only diffraction patterns due to α-AlF_3 were observed and no traces of other phases were found, suggesting that heating AlFO-3 and AlFO-6 samples under Ar at high temperature lead to the formation of aluminum fluoride. AlFO-1 (F content 31%) gave also the same line pattern even after calcination at 900 °C, indicating that some other material or phase(s) should be present in the amorphous state. It seems that these amorphous phases (presumably aluminum oxyfluoride), do not crystallize under these calcination conditions.

Similar results were obtained even when the samples were calcined with 20 °C/min, indicating that upon calcination under Ar heating rate has no influence on the final structure of AlFO samples (Figures are shown here).

MAS NMR: Because of the short range ordering of AlFO samples calcined at 350 °C, it was not possible to identify their structure from XRD (only amorphous like materials were obtained (Figure 7.13a-c)). Therefore, MAS NMR was used to probe the local structure of the calcined AlFO samples after calcination at 350 °C. Only results concerning AlFO-1 (HF/Al = 1) are reported.

Figures 7.15 and 7.16 show the ^{27}Al MAS NMR and ^{19}F MAS NMR spectra, respectively, of AlOF-1 sample obtained by calcination of AlOF-1 at 350 °C with heating rate of 5 °C/min for 4 h.

^{27}Al MAS NMR: In the ^{27}Al MAS NMR spectra of AlOF-1 calcined at 350 °C (Figure 7.15), three signals at around -4.61, 30, and 60 ppm can be observed. These three signals correspond to the different local electron densities at the aluminum nucleus produced by the neighboring atoms. The signal with a maximum at -4.6 ppm is characteristic of octahedral aluminum species AlF_xO_y. The assignment of this signal is quite consistent with the corresponding ^{19}F MAS NMR result. The signal with a maximum at 60 ppm is typical for tetrahedrally coordinated Al (AlO_4) and the weak signal at 30 ppm corresponds to an aluminum nucleus surrounded by atoms that produce an electron density larger than that produced by an oxygen tetrahedron but smaller than the one produced by an oxygen octahedra (pentacoordinated aluminum, AlO_5) [124].

^{19}F MAS NMR: The ^{19}F MAS NMR spectrum of AlOF-1 sample shows only one single peak appeared at approximately -153 ppm (Figure 7.16). The signal, assigned to a broad

line, covers many possible fluorine species, which may be statistically distributed, is attributed to AlF_xO_y; $x \geq 3$ (oxygen may come from oxo or hydroxyl group, fluorine may come from bridge or terminal coordinating fluorine species) coordination species in octahedrally coordinated Al sphere [121, 125-126].

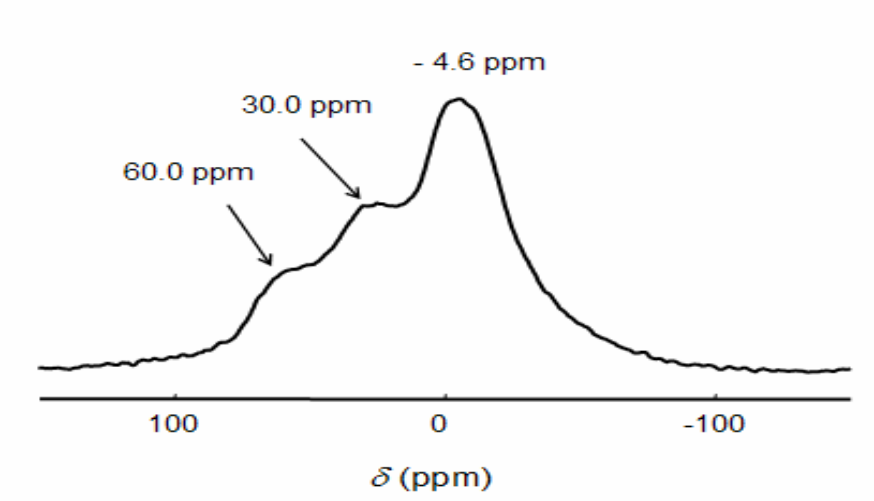

Figure 7.15 ^{27}Al MAS NMR for AlOF-1 (HF:Al = 1) calcined for 4 h at 350 °C (MAS=25 kHz) heating rate 5 °C/min.

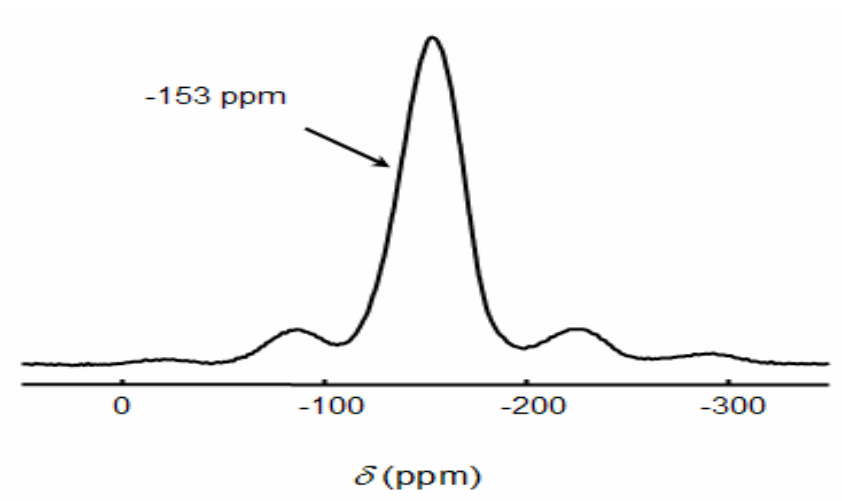

Figure 7.16 ^{19}F MAS NMR of AlOF-1 (HF/F=1) calcined at 350 °C (MAS = 25 kHz).

Calcination in air

AlFO-1, AlFO-3, and AlFO-6 samples were heated in air at various temperatures with heating rate of 5 and 20 °C/min and the results are shown in Table 7.9. Heating AlFO-1, AlFO-3, and AlFO-6 samples in air with heating rate of 5 °C/min resulted also in removal of the organic constituents/solvents (C% = 0), however, the BET surface areas were also to a greater extent reduced compared to Ar (Table 7.8). With increasing calcination

temperature, F contents dropped significantly. As it can be seen the amount of fluorine contents retained in the samples after calcination at 900 °C are quite small (0.5 - 3.9%). This unexpected significant loss in the F content is obviously a result of pyrohydrolyis taking place under these conditions and resulting in removal of HF and the formation of Al_2O_3 or AlF_xO_y.

Table 7.9: characterization of AlFO samples after calcination in air at various temperatures and various heating rate

Sample	HF/Al (mol ratio)	C content before calcination (%)	Calcination atmosphere					
			5 °C/min			**20 °C/min**		
			F%	C%	S_{BET} (m^2/g)	F%	C%	S_{BET} (m^2/g)
Calcination: 1) at 350 °C								
AlFO-1	1	34	29.8	0	220	29.1	0	192
AlFO-3	3	15	60.6	0	102	60.1	0	61
AlFO-6	6	7	62.1	1.2	21	62.6	0	11
	2) at 700 °C							
AlFO-1	1	34	6.9	0	132	3.3	0	56
AlFO-3	3	15	6.7	0	52	3.7	0	8
AlFO-6	6	7	9.3	0	7	6.3	0	3
	3) at 900 °C							
AlFO-1	1	34	0.5	0	101	0.5	0	73
AlFO-3	3	15	3.9	0	8	1.5	0	6
AlFO-6	6	7	6.9	0	n.d.	5.3	0	≈ 2

Samples calcined with a heating rate of 20 °C/min had even lower F contents than those calcined with lower heating rate (Table 7.9). This somehow unexpected behaviour could be explained considering that in case of a high heating rate the formation of H_2O from different sources as explained above is delayed. Consequently, the Al-F-bonds will be attacked by water at higher temperatures thus resulting in a higher degree of hydrolysis reaction resulting in the evolution of HF and the formation of Al_2O_3. Hence, the hydrolysis process and the removal of HF are faster.

XRD: XRD was used for characterization of AlFO samples after calcination in air at different temperatures and with various heating rate.

Low heating rate: Figures 7.17a-c and 7.18a-c present the XRD patterns of AlFO-1, AlFO-3, and AlFO-6 samples after calcination at 700 °C and 900 °C in air with heating rate of 5 °C/min.

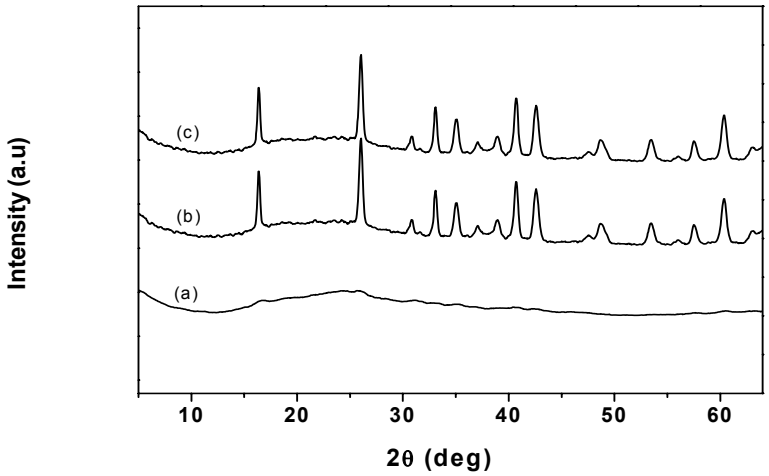

Figure 7.17 XRD patterns of (a) AlFO-1, (b) AlFO-3 (unknown phase(s)), (c) AlFO-6 (unknown phase(s)) after calcination at 700 °C in air at 5 °C/min for 4 h.

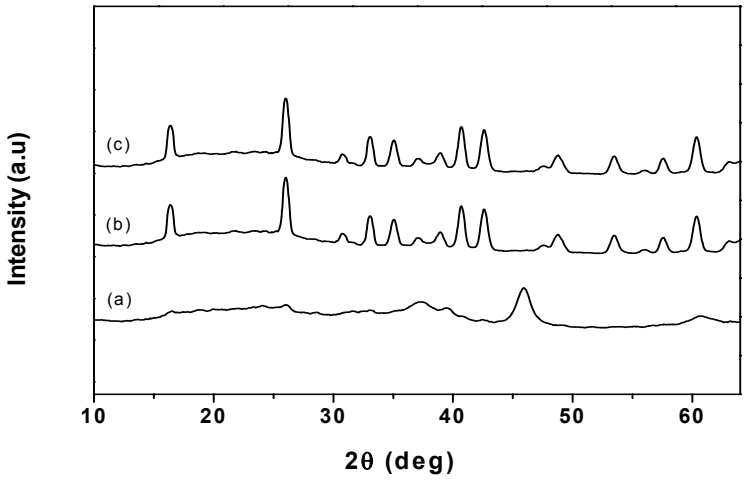

Figure 7.18 XRD patterns of (a) AlFO-1 (γ-Al_2O_3), (b) AlFO-3 (unknown phase(s)), (c) AlFO-6 (unknown phase(s)) after calcination at 900 °C in air at 5 °C/min for 4 h.

At 700 °C, AlFO-3 (Figure 7.17b), and AlFO-6 (Figure 7.17c) showed crystalline phases. All the reflection of the XRD pattern belongs to new phases. The XRD patterns of the newly formed species (AlFO-3 and AlOF-6 samples) are quite different from AlF_3, Al_2O_3 or AlOOH phases and do not match with any of the aluminum species listed in the

PDF databank [72], which indicates the presence of new crystalline phases after calcination. In contrast, AlFO-1 remained amorphous up to 700 °C (Figure 7.17a), however, at 900 °C, broad characteristic peak at 2θ of 46° and broad much weaker diffraction peaks intensity around 2θ of 26, 37, and 61° are observed (Figure 7.18a), which were assigned to γ-Al_2O_3 (supported by MAS NMR, Figure 7.21a). It seems that some special species formed during the first fluorination step preserved the structure during the calcination.

For AlFO-3 and AlOF-6 samples, after calcining at 900 °C, the typical unknown diffraction lines observed after calcination at 700 °C of AlFO-3 and AlOF-6 samples remained practically constant (Figure 7.18b-c). It must be also noted that when the AlFO-1 samples were calcined under the same condition but at 1100 °C, the same typical unknown diffraction lines as they were observed for AlFO-3 and AlOF-6 samples were also found for AlFO-1 samples (not shown here).

Fast heating rate: With fast heating rate (20 °C/min and higher) at 900 °C with dwell time of 4 h, AlFO-1 (Figure 7.19a) showed XRD pattern similar to those obtained at slow heating rate (5 °C/min), whereas AlFO-3 (Figure 7.19b) and AlOF-6 (Figure 7.19c) showed the distinctly different pattern of α-Al_2O_3 (corundum). The presence of this α-Al_2O_3 was confirmed by MAS-NMR (Figure 7.21c). It is interesting to note that even after heating AlOF-3 at 900 °C for only an hour dwell time, α-Al_2O_3 was also obtained. These results imply that upon calcination different heating rates have an important effect on the formation of crystalline phases from AlOF-3 and AlOF-6 framework but not on AlFO-1.

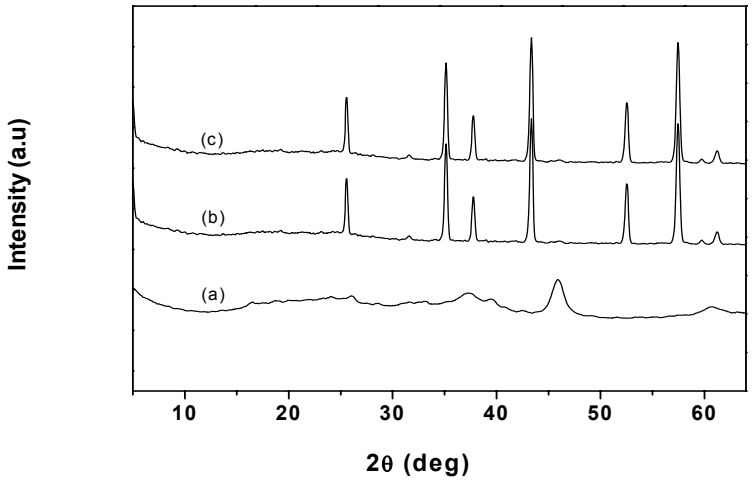

Figure 7.19 XRD patterns of (a) AlFO-1 (γ-Al_2O_3), (b) AlFO-3 (α-Al_2O_3), (c) AlFO-6 (α-Al_2O_3) after calcination at 900 °C in air at 20 °C/min for 4 h.

Formation of α-Al_2O_3: To test if it is possible to obtain α-Al_2O_3 at a temperature below 900 °C, AlOF-3 and AlOF-6 were calcined at 800 °C in air for 4, 20, and 50 h. In all cases, in addition to α-Al_2O_3 phase (marked with *), a κ- Al_2O_3 phase is present (PDF No: 26-31) even after heating the samples at 800 °C for 50 h in air (Figure 7.20a-e). Similar results were obtained when the samples were calcined in air at 850 °C with the same heating rate and duration. Obviously, 900 °C is needed for complete phase transformation to α-Al_2O_3.

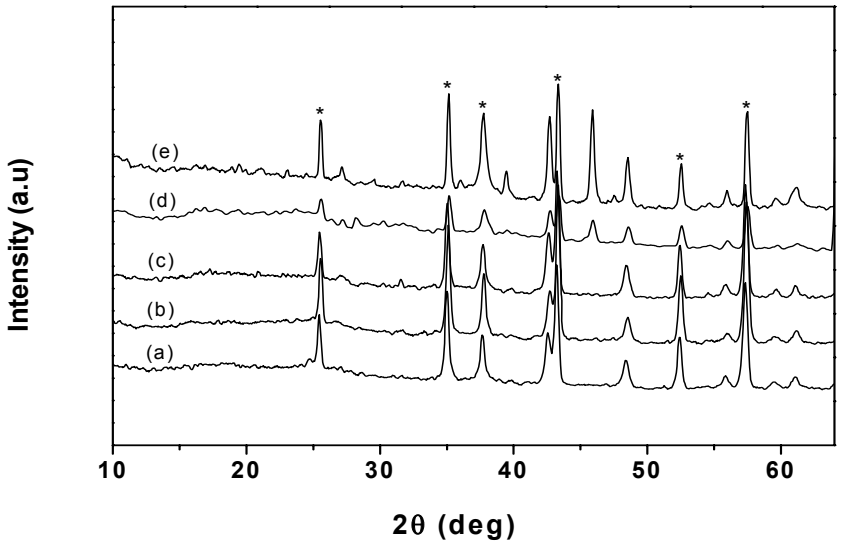

Figure 7.20 XRD patterns of dry AlFO-gel calcined in air at 800 °C at 20 °C/min: (a) AlFO-3 for 4 h, (b) AlFO-3 for 20 h, (c) AlFO-3 for 50 h, (d) AlFO-6 for 4 h, (e) AlFO-6 for 50 h, (* for α-Al_2O_3 phase).

^{27}Al MAS-NMR

The ^{27}Al MAS NMR spectra of samples derived from AlFO-1 and AlOF-3 (calcined at 900°C with heating rate of 5 °C/min for 4 hour) and AlOF-3 (calcined under same conditions but with heating rate of 20 °C/min), collected at spinning rate of 25 kHz are shown in Figure 7.21 a-c.

AlFO-1 samples (Figure 7.21a) shows two signals at 60 and 4.9 ppm. The broad asymmetric resonance at 4.9 ppm is due to the octahedrally coordinated aluminum atoms (AlO_6), while the tetrahedrally coordinated aluminum atoms are responsible for the signal at about 60 ppm. Both signals are consistent with Al atom in the of γ-Al_2O_3 phase (supported by XRD, Figure 7.18a).

When the HF/Al molar ratio was increased from 1 to 3 (AlOF-3, Figure 7.21b), the resonances at 4.9 and 60.9 ppm were no longer present in the spectra, which is probably

caused by ion rearrangement and the phase transformation to new phases. Two new signals, with line shapes broadened by the second-order quadrupoles interactions new signals appeared. The signal at 46.8 ppm is assigned AlO_4 polyhedra and the one at 0.7 ppm can be attributed to AlO_6 or AlF_xO_y (not confirmed).

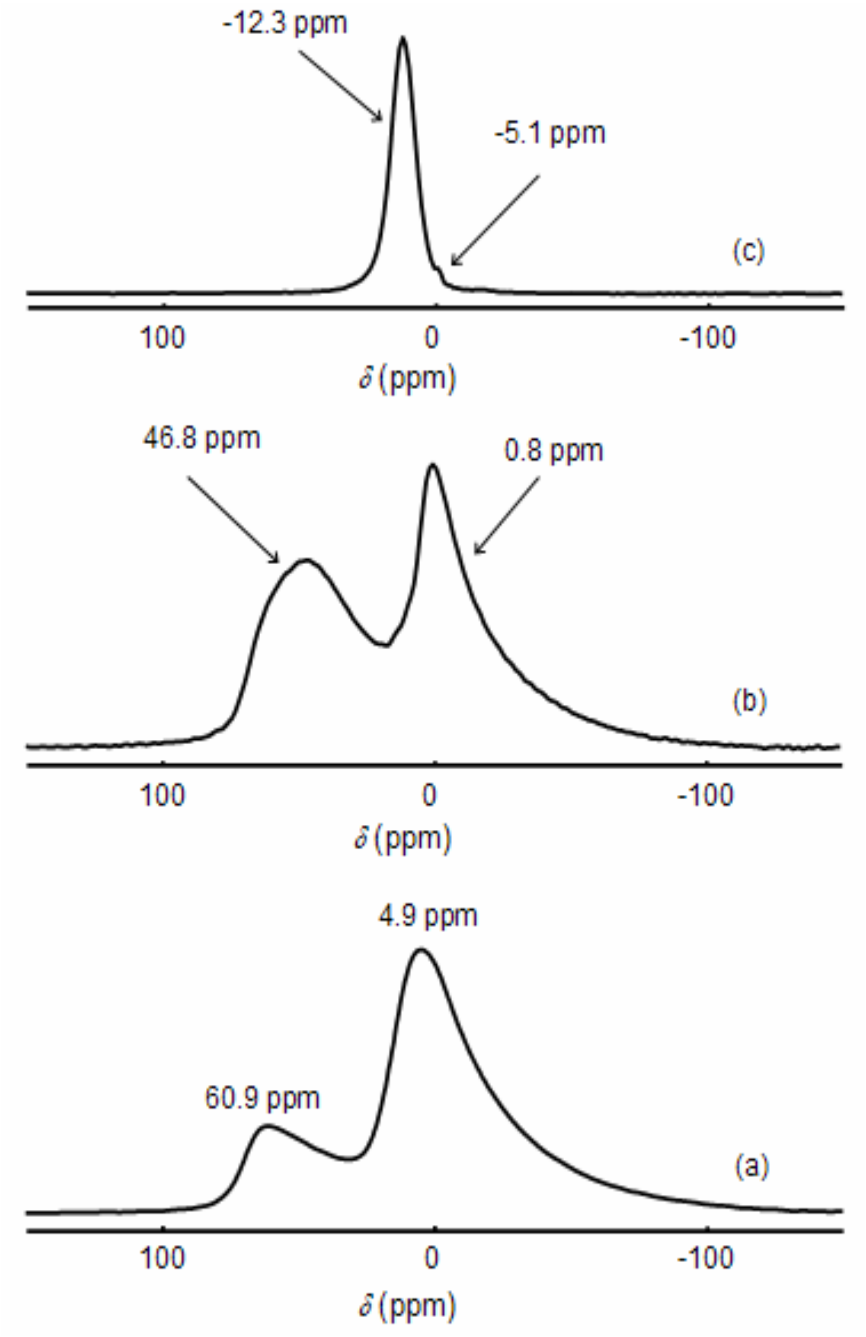

Figure 7.21 ^{27}Al MAS-NMR (MAS = 25 kHz) of AlFO samples calcined at 900°C
(a) AlFO-1 calcined with a heating rate of 5 °C/min,
(b) AlFO-3 calcined with a heating rate of 5 °C/min,
(c) AlFO-3 calcined with a heating rate of 20 °C/ min.

Calcination of AlFO-3 with higher heating rate (20 °C/min, Figure 7.21) led also to the formation of another phase. One main signal at -12 ppm was observed for AlOF-3 calcined under the same conditions but with higher heating rate (20 °C/min) attributes to AlF_6 polyhedral. There is also a small shoulder at about -5 ppm, which can be assigned to AlF_xO_y. These results indicate that the calcination temperature and HF/Al molar ratio markedly altered the structure of AlFO samples.

^{19}F MAS NMR

The state of F and its changes with the calcination temperature have been studied by ^{19}F MAS NMR of the sample obtained from AlOF-1 (HF/Al=1) calcined at 900 °C in air (heating rate 5 °C/min) only. The results obtained from ^{19}F MAS NMR of AlFO-3 with heating rate of 20 °C/min and ^{19}F MAS NMR of AlFO-3 with heating rate of 5 °C/min are not shown and will not be considered, since some of the signals are similar with those obtained from the rotor cape. Thus, no reliable information can be deduced form the spectra.

Figure 7.22 shows the ^{19}F MAS NMR spectrum of AlOF-1 sample calcined at 900 °C in air.

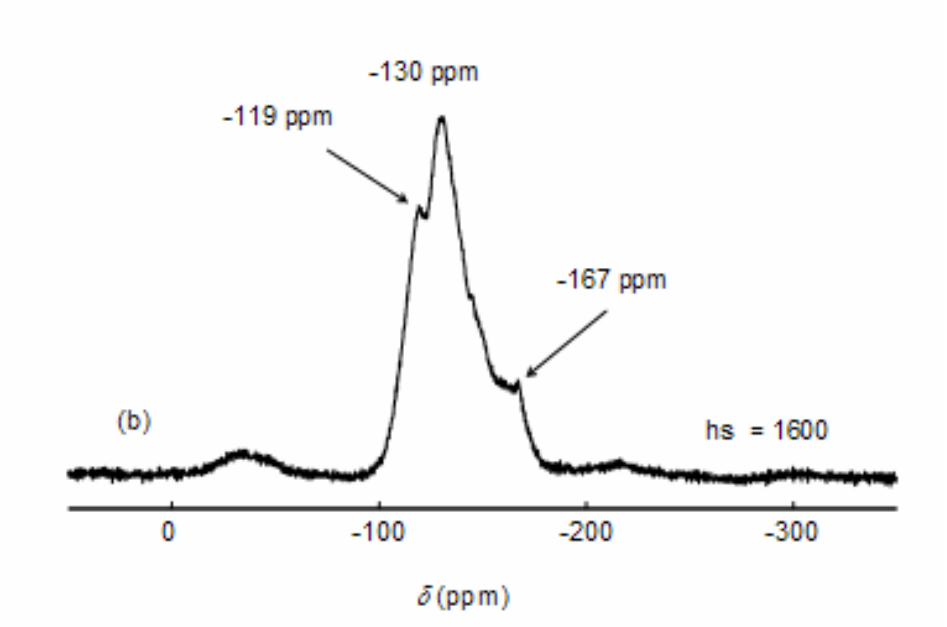

Figure 7.22 ^{19}F MAS-NMR of AlOF-1 (HF/F=1) calcined at 900 °C (MAS = 25 kHz) in air, number of accumulation (hs) = 1600.

One signal and two shoulders appeared at -129.9, -119.2, and -167.1 ppm, respectively. The intensities of these new signals are 50 times smaller than that calcined at 350 °C under

Ar (Figure 7.16), indicating that the F content is very small (F content 0.5% from elemental analysis). The shoulder at -167 ppm comes from the rotor. According to the literature [122], the signal at -130 ppm and shoulder at -119 ppm should be due to octahedral aluminium oxyfluoride groups such as AlF_xO_{6-x}. The ^{19}F chemical shift of -119 ppm was observed for bridging fluorine (Al–F–Al) in AlO_5F_1 while the chemical shift at -130 ppm was observed for terminal fluorine [121, 125-126].

Characterization of AlF_xO_y ($x \geq 3$)

NH_3-TPD

Figure 7.23 shows the NH_3-TPD and the Gaussian deconvoluted peaks of a AlF_xO_y sample, prepared by calcining AlFO (HF/Al = 1) at 350 °C under Ar (5 °C/min). The sample shows four deconvoluted peaks at 200, 232, 290, and 396 °C. The low temperature desorption peak of NH_3 (at 200 and 232 °C), are assigned to ammonia desorbing from weak acid sites, the third (290 °C) and the fourth (400 °C) are due to ammonia desorbing from medium acid sites. Obviously, the medium sites are dominant.

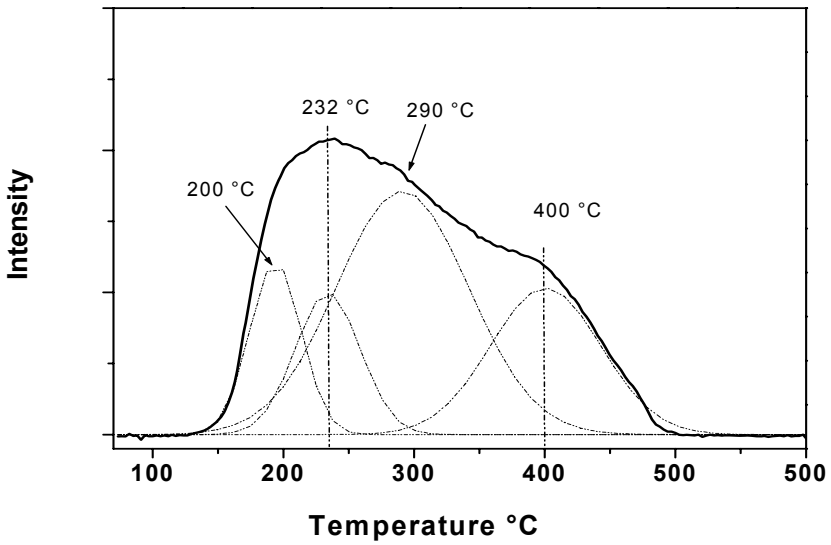

Figure 7.23 NH_3-TPD profile of AlF_xO_y.

The amount of ammonia desorbing from AlF_xO_y is much lower than those desorbing from HS-AlF_3 as it can be seen in Figure 7.24a-b. Also, the desorption temperature in case of AlF_xO_y is lower indicating weaker acid sites than in HS-AlF_3 which exhibits also four desorption temperatures, however, located at higher temperature.

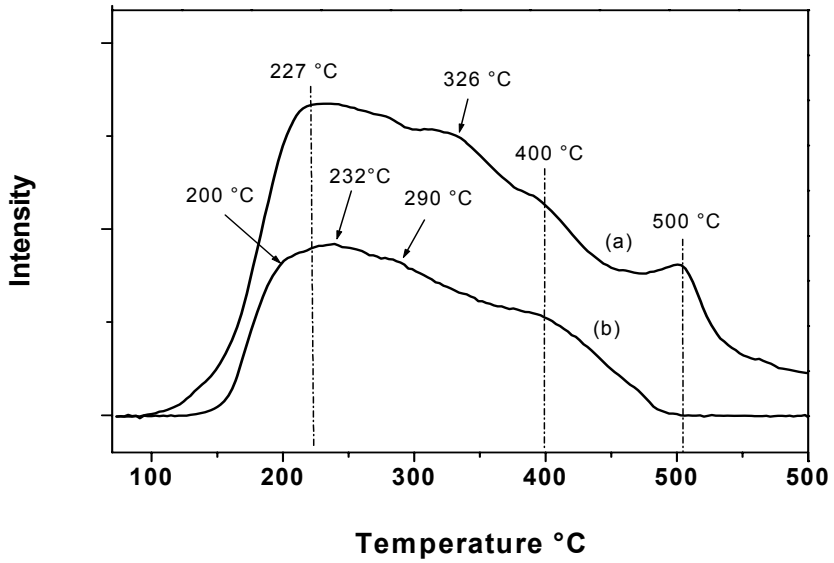

Figure 7.24 NH_3-TPD of (a) HS-AlF_3 and (b) AlF_xO_y.

IR-PAS studies

The IR-PAS of pyridine (Py) adsorbed on AlF_xO_y was measured to differentiate between Lewis and Brønsted acid sites and to probe the strength of these acid sites. The IR-PAS spectrum of Py adsorbed on AlF_xO_y is shown in Figure 7.25.

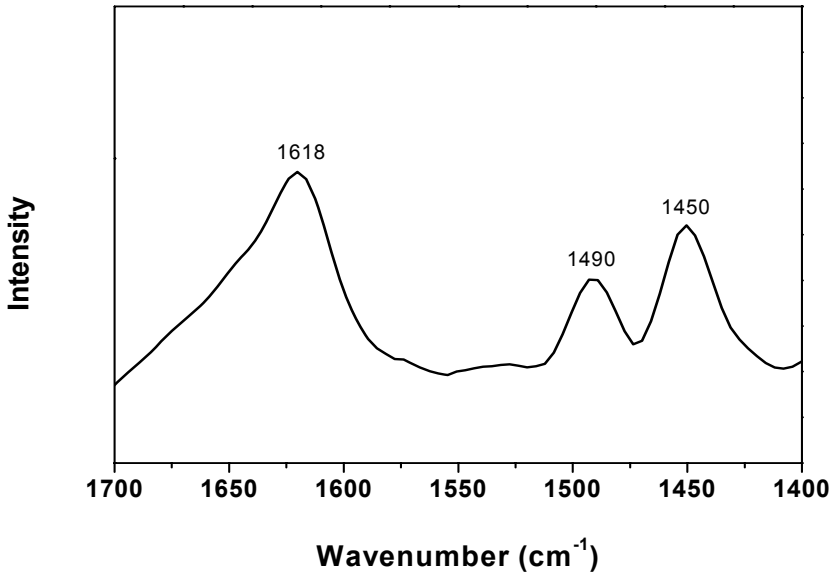

Figure 7.25 IR-PAS of pyridine adsorbed on AlF_xO_y.

There are three bands at 1450, 1490, and 1618 cm^{-1}. These bands correspond to coordinatively bonded Py to Lewis acid sites between 1620 and 1600 cm^{-1} (ν_{8a} mode) and at around 1450 cm^{-1} (ν_{19b} mode). No evidence was found for a band at 1540 cm^{-1} on the AlF_xO_y indicating that if there are any Brønsted acid sites on the surface, they are too weak to ineract with pyridine.

Is the changed structural motif of the calcined AlFO samples a consequence of HF/Al molar ratio, heating atmosphere, or heating rate?

Experimental results demonstrate that depending on the HF/Al molar ratio, calcination temperature, atmosphere, and duration, and heating rate, different phases can be developed.

The calcination of AlFO-3 samples in air under appropriate conditions led to the formation of α-Al_2O_3, whereas AlFO-1 samples formed γ-Al_2O_3. In both cases a hydrolysis has occurred. Higher heating rate enables the hydrolysis of the AlFO to go faster. HF is liberated and Al_2O_3 phases are formed. Calcination of AlFO-3 and AlFO-6 at 700 °C or 900 °C at low heating rate (5 °C/min) led to formation of new phases, which were not possible to identify from XRD data bank or MAS NMR. These new phases still contain some F contents which still remain in AlFO-3 and AlFO-6 even after calcination at 900 °C (3.9% and 6.9%, respectively) but no carbon. For these reasons, these resulting materials might be crystalline aluminum oxyfluoride, but more experiments are needed to verify this conlusion. This means that heating rate has a significant influence on the resulting materials.

Interestingly enough, heating under Ar reveal clearly a different picture. At about 700 °C and higher, $_{aq.}$precursor prepared with higher HF/Al ratio ($_{aq.}$precursor ≥ 2) when calcined at 700 °C resulted in the formation of pure α-AlF_3 with surface area of about 8 m^2/g. On the other hand, samples with a HF/Al ratio equal to 1, when heated under Ar at 350 °C lost most of the organic substituents and gave rise for the first time to the formation of amorphous aluminum oxyfluorides (AlF_xO_y). The resulting AlF_xO_y has high surface area together with strong Lewis acid sites as was demonstrated above from Pyridine IR-PAS and NH_3-TPD. However, the strength and the amount of these acid sites present on AlF_xO_y are lower than those found for $HS\text{-}AlF_3$ or $_{aq.}HS\text{-}AlF_3$ as NH_3-TPD results showed (Figures 7.23 and 7.24). Oxyfluoride compounds are known to have interesting properties, thus, AlF_xO_y might be promising materials for optical and other applications such as glass compounds.

Surprisingly, heating rate 5, 20 °C/min or higher, has no influence on the final structure of the AlFO samples calcined under Ar. In all cases, calcination up to 700 °C and higher led to phase transformation to α-AlF_3 (XRD, Figure 7.14).

Although the experimental results at this early stage do not allow to present a definite picture about processes going on, a speculative description will be briefly given at this place:

(i) Heating atmosphere: Although both calcinations processes (in Ar and in air) were performed with the same starting materials, even in case of highly fluorinated precursors in air a nearly total loss of fluorine was observed in all the cases. Obviously the thermohydrolysis reaction in air is drastically favoured resulting in a dramatic loss of fluorine (in form of HF) but at the same time enabling rearrangement processes in the solid, which lead to the formation of crystalline α-Al_2O_3 at interestingly low temperatures. This does not happen with samples of lower fluorine contents. A plausible explanation is that most of the (less) fluorine evolves from the solid before the suitable temperature for the phase transformation into α-Al_2O_3 can occur. In dry Argon atmosphere, obviously the hydrolysis is suppressed, meaning the gas phase does not provide a suitable H_2O-partial pressure for the hydrolysis reaction. In order to test this hypothesis, in further experiments similar experiments should be performed using wet Argon and dried air. If the hypothesis stated above is true, the opposite behaviour should be observed.

(ii) Heating rate: The same argumentation as above might be used to explain this behavior. At fast heating the formation of α-Al_2O_3 is accelerated with nearly total loss of fluorine whereas at lower heating rate the remaining F-content is higher and no α-Al_2O_3-formation is observed. The explanation is probably that at fast heating rate, the evolution of fluorine (as HF) is delayed resulting in the situation that at higher temperature there is still a somehow higher F-content in the solid. Consequently, this provides better conditions for the rearrangement processes in the solid and, hence, the formation of α-Al_2O_3 is more likely in this case than at low heating rate at which the evolution of HF can occur more completely.

Nevertheless, these finding could be the basis for the formation of corundum at lower temperatures than known so far.

7.5 Summary

The results obtained can be summarized as follows:

Nano-aluminum fluoride was prepared from the reaction of aqueous HF ($HF:H_2O$ = 2.7:1) with an alcoholic $Al(O^iPr)_3$ solution followed by drying in vacuum. The resulting material is then post-fluorinated to obtain the $_{aq.}HS\text{-}AlF_3$. Under the appropriate preparation conditions aluminum fluoride ($_{aq.}HS\text{-}AlF_3$) with specific surface area up to *ca.* 171 m^2/g and high Lewis acidity is obtained. The Bulk structure of $_{aq.}HS\text{-}AlF_3$ samples are highly distorted as MAS-NMR and FTIR indicated.

$_{aq.}HS\text{-}AlF_3$ and its precursor are X-ray amorphous, but their thermal analysis revealed the exothermic formation of a crystalline phase at 527 °C identified by XRD as α-AlF_3. TEM analysis showed that $_{aq.}HS\text{-}AlF_3$ samples are composed of irregularly shaped micrographs and well-defined domains of about 20 nm diameter AlF_3 grains. The lattice plane distances of ≈ 3.6 Å were estimated for $_{aq.}HS\text{-}AlF_3$, which are typical for aluminium fluorides.

Calcination brings information about the following transformations: decomposition of the AlFO compound and formation of oxide or oxyfluoride species depending on the heating rate and calcination temperature. The effect of HF/Al molar ratio, dwell time and heating rates were found to have a profound effect on phase formation of calcined AlFO powders. Heating AlFO-3 sample (HF/Al = 3) in air at just 900 °C for only an hour yielded α-Al_2O_3, whereas γ-Al_2O_3 was formed by heating AlFO-1 sample (HF/Al = 1) in air at the same temperature.

The ^{27}Al MAS NMR spectra of the AlOF samples prepared using different 75% HF/Al molar ratios in the synthesis medium indicate that the Al/F ratio has an important effect on the isomorphic incorporation of −OH groups in the AlOF framework.

Heating of $_{aq.}$precursor under moderate conditions provides a new and convenient route for the preparation of aluminum oxyfluoride with high surface area. Amorphous AlF_xO_y with high surface area (241 m^2/g) was synthesized by calcining AlFO-1 sample (HF /Al = 1) under Ar at 350 °C.

Chapter 8

Discussion andConclusion

Discussion

HS-AlF_3

Based on the investigations performed in this thesis, a more comprehensive reflection about the reaction path ways during sol-gel synthesis of AlF_3 in detail but of nano-metal fluorides in general can be developed. The most important point is that according to the 2-step reaction path in the sol-gel synthesis of metal oxides starting from metal alkoxide precursors according Eq. 1 and 2:

$$\text{-M-OR} + H_2O \longrightarrow \text{-M-OH} + \text{ROH} \quad (1)$$

$$\text{-MOH} + \text{HO-M-} \longrightarrow \text{-M-O-M-} + H_2O \quad (2a)$$

$$\text{-MOH} + \text{RO-M-} \longrightarrow \text{-M-O-M-} + \text{ROH} \quad (2b)$$

The sol-gel synthesis of nano-metal fluorides parallels somehow this reaction path. Whereas in case of metal oxides synthesis the first step consist of the controlled hydrolysis of a suitable precursor (mostly an alkoxide), in case of metal fluorides the first step consists of a fluorolysis reaction according Eq. 3:

$$\text{-M-OR} + \text{HF} \longrightarrow \text{-M-F} + \text{ROH} \quad (3)$$

Most importantly is to prevent a possible competitive hydrolysis reaction, there, water free reactions have to be established by using anhydrous HF. Since fluoride is well know to bridge metal atoms in polymeric solids, the next step is the bridging of small units formed according Eq.3. Both sol-gel routes, therefore, have many in common as there is to prevent the formation of a regular three-dimensional polymeric solid. Since both types of reactions are performed in alcoholic reaction systems, by the alcohol acting as electron donor and by varying the pH the sols become electrostatically stabilizes, thus preventing further precipitation. As a result a voluminous gel can be obtained. Furtheron, in case of sol-gel synthesis of metal fluorides the OR against F exchange is – depending on the metal – incomplete, as it can also be observed for metal oxides. However, in case of metal oxides this is not a problem because any remaining or-groups still present in the resulting dry gel will be easily transformed into oxide upon final calcinations:

$$2\ \text{–M-OR} \longrightarrow \text{-M-O-M-} + \text{R-O-R} \quad (4)$$

In case of metal fluoride, however, this would be a worth scenario since it would not allow to end up with pure metal fluorides. Since most of the dry sols of metal fluorides contain varying amount of un-converted alkoxide groups, another reaction procedure has to be established. This is, the obtained dry metal fluoride alkoxide precursor has to be post-fluorinated by suitable gaseous fluorinating agents in order to ensure a complete transformation of the remaining M-OR units into M-F units.

As it is shown inside this thesis, especially this final gas-phase fluorination is the most decisive stage in the preparation of nano-metal oxides especially if the target property is Lewis acidity. Lewis acidity is one (but not the only one) of the most interesting properties of the nano-metal fluorides obtained this way. Especially HS-AlF_3 is a superior substance because its Lewis acidity is almost as good as that of the strongest known Lewis acid SbF_5. However, the advantage of HS-AlF_3 is that is does not undergo hydrolysis reactions at ambient temperature whereas SbF_5 and all the other known strong Lewis acids like $AlCl_3$ or $FeCl_3$, easily become hydrolysed. The main reason why HS-AlF_3 differs that much is its high surface of up to 400 m^2/g in comparison to just about 30 to 50 m^2/g in case of classically prepared AlF_3-phases. This high surface corellates very well with a extremely high degree of distortion in the bulk of HS-AlF_3, and hence, is the basic for the appearance of many fife and four-fold coordinated Al-sites in the surface which represent the very high Lewis acidity of this phase. The high degree of distortion is confirmed by extensive MAS NMR, XANES, EXAFS, XAFS, AFM and TEM investigations. Furthermore, the excitingly high Lewis acidity was proved by special probe reactions which can otherwise only be performed with SbF_5 and aluminium chloride fluoride (ACF) as catalysts. Detailed CO-adsorption measurements proofed the existence of strong Lewis sites which were never detected for any other solids before.

Inside of this thesis it was also shown that this very Lewis acidic and catalytically very active HS-AlF_3 can be deposited of suitable supports. Due to the reaction with HF, only supports can be used which are somehow resistant against HF. It was shown that γ-Al_2O_3 can be a good support if it is pre-calcined under appropriate conditions, e.g., up to 900°C. Thus it was found that surface hydroxyls – although they are though to be a good anchor group for binding the active phase chemically – suppress the formation of the strongest Lewis surface sites in HS-AlF_3. Thus, the present thesis also developed a route towards supported very active HS-AlF_3 materials which is the basic for any possible technical application of this new kind of catalysts.

It was argued above that the absence of water is an important precondition to prevent hydrolysis reaction which could favour the competitive formation of hydroxide/oxide. On the other hand, the formation of an Al-F-bond should be thermodynamically favoured. Therefore it was also tested if certain amounts of water in the reaction system can be tolerated. If this is the case, the synthesis would be more simple because then instead of anhydrous HF (gas) hydrofluoric acid (liquid) could be sued. It was found that in fact, some hydroxyls are formed but to a low extend. Since the final treatment for the preparation of highly Lewis acidic HS-AlF_3 is a gas phase fluorination of the dry precursor, hydroxyl groups formed in the first step become fully fluorinated. Thus, even in this case, very active materials can be obtained based on a significant more convenient synthesis route especially if any technical application is aimed.

$AlO_{x/2}F_{3-x}$

As a result of the investigations by using hydrofluoric acid another synthesis strategy was also briefly aimed at the end of this thesis. The question was is possible just by using a certain stoichiometric ratio of Al to F to OH to end up with phases of the general formula $AlO_{x/2}F_{3-x}$. Also these are preliminary results , it was evidently shown – especially based on MAS NMR investigations – that under appropriate conditions starting from just partly fluorinated precursors the formation of aluminium oxyfluoride phases can be achieved, a substance group which is not known so far. It is up to further investigations to fully develop and characterise this new substance class which might offer some interesting new field of applications.

Finally, the present thesis was concentrated on understanding the parameters influencing the properties of nano aluminum fluoride, HS-AlF_3. The results obtained allow a comprehensive use of this exciting substance especially for catalytic applications. Moreover, the correlations between synthesis parameters and properties obtained for HS-AlF_3 are of great value for the synthesis of other metal fluorides according to the new sol-gel synthesis route for metal fluorides. Although in detail they may differ, the general synthesis is very similar for many other metal fluorides too.

Conclusion

The sol-gel fluorination route under non-aqueous conditions has proved to give access to aluminium fluoride with extraordinary properties. Thus, HS-AlF_3 prepared this way has a very high surface area, is amorphous, and exhibits Lewis acidity, which is documented by its catalytic activity. Depending on the nature of fluorination agent, fluorination temperature, and duration, aluminum fluorides with surface areas up to 420 m^2/g can be prepared. Even by using aqueous HF (75%), aluminum fluoride with high surface area and high Lewis acidity can also be prepared.

It was found that CCl_2F_2/N_2 or $CHClF_2/N_2$ as fluorination agents are more advantageous over more hydrogen rich fluorocarbon compounds (HFCs). HF/N_2 can also be used successfully provided the HF which is adsorbed at the Lewis acid sites of HS-AlF_3 or $_{aq.}$HS-AlF_3 is in an additional step removed by, e.g., heating in nitrogen flow.

Fluorination temperature and duration have a significant impact on the surface area of the resulting high surface area aluminum fluoride. HS-AlF_3 samples have surface areas of about 300 m^2/g when made using the sol-gel process as described in this thesis when finally fluorinated with $CHClF_2$ at about 250 °C. At 350 °C, a collapse of the porous structure and crystallization during the high fluorination temperature leads to the surface area loss (155 m^2/g). The fluorination temperature has also strong effect on the HS-AlF_3 sample activity. Fluorination above 250 °C leads to decrease in the activity. Long fluorination time also causes the activity and surface area losses.

The AlF_6 octahedra in HS-AlF_3 and $_{aq.}$HS-AlF_3 are highly distorted even more than the crystalline phase β-AlF_3 as was confirmed by MAS NMR and FTIR, which is most likely the reason for the catalytic activity obtained.

HS-AlF_3 supported on γ-$Al_2O_3{}^a$ prepared by impregnation method is nearly as Lewis acidic as unsupported HS-AlF_3 is, that is high catalytic activity in the catalytic probe reactions employed was achieved. It was found that the type of support used, calcination temperature of γ-Al_2O_3 support, and the activation conditions (temperature and $CHClF_2/N_2$ ratio) have an effect on supported HS-AlF_3 properties. According to the results obtained in this study, the best catalyst was HS-AlF_3 supported on γ-$Al_2O_3{}^a$.

Many attempts have been carried out in the literature to develop aluminum oxyfluoride (AlF_xO_y). This work demonstrated that using the sol-gel process and aqueous HF (75%), AlF_xO_y can be prepared. This AlF_xO_y is an amorphous material and has high surface area.

Heating atmosphere and heating rate have an influence on the structure of the resulting material. By heating the AlFO, i.e., $_{aq.}$precursor (HF/Al = 3), in air α-Al_2O_3 can be obtained at only 900 °C (20 °C/min), whereas heating under Ar at the same temperature resulted in the formation of α-AlF_3.

Chapter 9

Summary and Outlook

Summary

HS-AlF_3 was developed in our group in 2003 [35-36]. The preparation of HS-AlF_3 is shown schematically in Scheme 9.1.

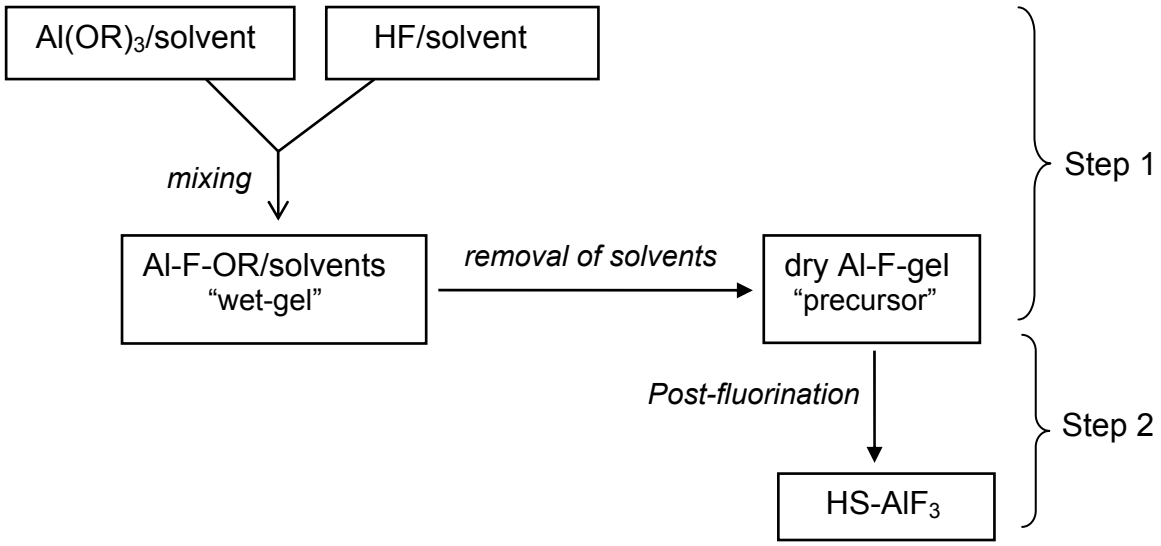

Scheme 9.1 Schematic representation of HS-AlF_3 synthesis.

In this thesis, the effect of synthesis parameters on the properties of HS-AlF_3 was examined in detail in order to optimize the preparation conditions. This includes the use of various solvents, alkoxides, fluorination agents, and fluorination regime. The surface and bulk structure of HS-AlF_3 were investigated using various chemical and spectroscopic methods.

The first step of preparation of HS-AlF_3 is the fluorolysis of an aluminum alkoxide in an organic solvent with anhydrous HF to get the wet Al-F-gel (aluminum alkoxide fluoride), an amorphous and strongly distorted material. After removing volatiles at 70 °C in vacuum, a white solid powder is obtained (precursor). The resulting precursor, in the dry state, exhibits a very high surface area (≈ 600 m^2/g) and a carbon content up to 30%; however, it is catalytically inactive because it still contains unconverted OR-groups. Thus, a second fluorination step is applied to exchange these remaining OR-groups against F. This step involves the treatment of the precursor with a gaseous fluorination agent such as CCl_2F_2 and $CHClF_2$ at temperatures up to 300 °C, but below the crystallization temperature of AlF_3. First the adsorbed alcohol is split off, then the Al–OR groups are replaced by fluoride. Using HF as fluorination agent, the fluorination process can be performed at lower temperature, up to 150 °C. The resulting material (HS-AlF_3-HF) has very high

surface area (≈ 420 m^2/g), however, the Lewis acidity and catalytic activity of HS-AlF_3-HF prepared via HF fluorination is lower than that of HS-AlF_3 samples prepared via CFC or HCFC treatment. However, upon heating in a N_2 stream up to 280 °C, the strongly adsorbed HF is completely removed and high catalytic activity is obtained.

Utilization of aqueous HF instead of anhydrous HF in organic solvent conditions yields also high surface aluminum fluoride (denominated $_{aq.}$HS-AlF_3). Firstly, $Al(O^iPr)_3$ in isopropanol was reacted with aqueous HF (75% HF) to get aluminum hydroxyofluoride ($_{aq.}$precursor). Thus, a second gas phase fluorination was applied to get $_{aq.}$HS-AlF_3. The $_{aq.}$HS-AlF_3 obtained had a ratio of fluorine to aluminum of about three and the carbon content was less than 0.2%. Most remarkably, the aluminum fluoride prepared this way had also high surface area of up to 178 m^2/g and showed a very high catalytic activity in $CHClF_2$ dismutation (100% conversion) and $CF_3CBr_2CF_3$ (32-37% conversion) and CCl_2FCClF_2 (42-45% conversion) isomerizations.

HS-AlF_3 and the precursor as well as $_{aq.}$HS-AlF_3 are X-ray amorphous and only by heating above 527 °C crystallization occurs resulting in α-AlF_3. SEM micrographs of amorphous HS-AlF_3 as well as its precursor comprises disordered aggregated particles, which are mesoporous ones, most likely are agglomerates of much smaller particles of irregular size. In TEM micrographs well-defined domains of about 10 nm diameter can be seen, some of which are regular, i.e., lattice planes could be seen of regions. For both HS-AlF_3 and $_{aq.}$HS-AlF_3 lattice plane distances of ≈ 3.6 Å were estimated, which are typical for aluminum fluorides [35].

The bulk structure of HS-AlF_3 (or $_{aq.}$HS-AlF_3) is highly distorted unlike those of crystalline AlF_3, which is the reason for its extraordinary properties, i.e., strong Lewis acidity and high surface area. Several spectroscopic and chemical methods can support these findings. The bulk structure of HS-AlF_3 and $_{aq.}$HS-AlF_3 contain ^{27}Al and ^{19}F resonance in the range that is attributable to octahedral AlF_6 environments.

HS-AlF_3 and $_{aq.}$HS-AlF_3 are mesoporous with pore size distribution of about 68 and 85 Å and specific surface area around 250 m^2/g. Aluminum fluoride prepared using aqueous HF has lower specific surface (171 m^2/g), respectively. Similarly, HS-AlF_3-HF and $_{aq.}$HS-AlF_3-HF have high surface areas reaching almost 420 m^2/g.

Adsorption of probe molecules on differently prepared HS-AlF_3 revealed differences in their surface acid properties. When pyridine was adsorbed on HS-AlF_3 and HS-AlF_3-HF+N_2 only bands indicative of pyridine adsorbed on Lewis acid sites were observed. However, adsorption of pyridine on a HF-post-fluorinated sample, HS-AlF_3-HF,

confirmed the presence of Brønsted acid sites, whereas HS-AlF_3 precursor showed in principal Lewis acidic sites, however, with low concentration. These results were supported by IR-CO.

This thesis also reports on an extensive investigation of the formation of HS-AlF_3 coatings on alumina. These coatings, aiming at depositing HS-AlF_3 on a support, are challenging because of the need for having strong Lewis acidic catalyst with certain shape and certain mechanical stability that can be used for industrial applications. With the HS-AlF_3 deposited on a support; there is for the first time an extremely strong Lewis acidic solid catalyst available for practical applications.

The experimental realization of the corresponding investigation required the exploration of a suitable route of the synthesis including appropriate supports. The detailed steps of this approach concern various aspects of this investigation. One of these aspects is that the support employed must meet some requirements. These are in brief: (i) surface area, (ii) chemical nature of the support, and (iii) calcination temperature of the support. Other aspects are the process of deposition and the preparation method. A number of aluminum oxides and modified γ-Al_2O_3 were examined with respect to their surface area by BET and to the presence of hydroxyl groups by weight loss analysis.

HS-AlF_3 supported on alumina and partially fluorinated γ-Al_2O_3 with different HS-AlF_3 loadings were prepared by impregnation method. The first preparation step results in the formation of supported dry Al-F-gel (precursor). Al ($O^iPr)_3$ dissolved in water free isopropanol reacts with anhydrous HF dissolved in organic solvent either before coming in contact with the support surface or after impregnation of the support. The resulting $AlF_x(OR)_{3-x}$ (precursor) is deposited on the surface of the pre-calcined support. After removal of the solvents, the dried precursor is fluorinated in a second step with $CHClF_2$ or HF. The influence of various synthesis parameters on the properties of the supported HS-AlF_3 was thoroughly investigated. These factors of influence are type and pre-treatment of support, amount of HS-AlF_3 loaded on the support, the aging of the supported wet HS-AlF_3 precursor, impregnation method, fluorination temperature, and concentration of the fluorination agent.

This thesis reports also on the preparation of aluminum oxyfluoride (AlF_xO_y). It was that by heating AlFO-1, i.e, the $_{aq.}$precursor with HF/Al = 1, under Ar at 350 °C with a heating rate of 5 °C/min Al_xO_y is formed. The obtained AlF_xO_y is XRD amorphous, has high surface area, and is highly distorted as was confirmed from MAS NMR. From the NH_3-TPD, the existence of weak and medium acid sites can be inferred. The acid sites

present on the surface are mainly Lewis acid site as was indicated from IR-PAS. The amount and the strength of these acid sites are much lower than those found for HS-AlF_3 and $_{aq.}$HS-AlF_3.

Furthermore, the effect of HF/Al molar ratio, calcination temperature, dwell time, and heating rates on the structure of the calcined AlFO samples were investigated. It was found that heating AlFO-3 sample (HF/Al = 3) in air with fast heating rate (20 °C/min and higher) at just 900 °C for only one hour gave a rise to α-Al_2O_3, whereas γ-Al_2O_3 is formed by heating AlFO-1 sample (HF/Al = 1) in air at the same temperature. After calcination of the AlFO samples (HF/Al > 1) at 700 °C with low heating rate (5 °C/min) a new phase(s) were formed, which were not possible at the time of the study to identify from the XRD data bank.

All the samples prepared in this thesis were catalytically probed by for $CHClF_2$ dismutation and $CF_3CBr_2CF_3$ and CCl_2FCClF_2 isomerizations. HS-AlF_3, $_{aq.}$HS-AlF, and HS-AlF_3-HF + N_2 showed very high catalytic activity in the probe test reactions used. Table 9.1 gives a brief summary of catalytic behaviour of different samples.

Table 9.1 Summary of the catalytic behaviour of various samples in $CHClF_2$ dismutation and $CF_3CBr_2CF_3$ and CCl_2FCClF_2 isomerizations

Samples	$CHClF_2$ conversion (%)	$CF_3CBr_2CF_3$ conversion (%) at 25 °C	CCl_2FCClF_2 conversion (%) at 25 °C
Precursor	No activity	No activity	No activity
Precursor heated in N_2	No activity	No activity	No activity
HS-AlF_3	98	> 90 - 100	17-71 (≈ 100 at 50 °C)
HS-AlF_3-HF + N_2	99	56	13
$_{aq.}$Precursor	No activity	No activity	No activity
$_{aq.}$HS-AlF_3	99	32-37	42-45
$_{aq.}$HS-AlF_3-HF + N_2	99	19	23
HS-AlF_3/γ-Al_2O_3	98	30-37	5
AlF_xO_y	No activity	No activity	No activity

Outlook

The research presented in this thesis has opened a number of research lines that should be explored in the future. For instance, the catalytic activity of HS-AlF_3 samples for

propane oxidation has to be further explored. The novel HS-AlF_3 and supported HS-AlF_3 samples prepared was tested for the oxidation of propane and have shown high selectivity for the propan oxidation.

Moreover, metal oxyfluorides are of interest because they expected to have useful optical, magnetic, and catalytic properties. Therefore, many attempts were made to produce metal oxyfluorides. As stated earlier, amorphous/crystalline AlF_xO_y can be prepared via sol-gel process by using aqueous HF (75%). Only some preliminary tests were conducted and more thoroughly investigation of this route of preparation is needed.

In addition, through this sol-gel preparation route, it was possible to prepare α-Al_2O_3 at just 900°C. However, the mechanism involve in the formation of α-Al_2O_3 is not clear and more experiments are required to understand the influence of HF/Al molar ratio, calcination temperature, and heating rate on the formation of α-Al_2O_3.

References

1 M. E. Turner, T. J. Trentler, V. L. Colvin, *Adv. Mater.* 13 (2001) 180-183.

2 J. Aguado, D. P. Serrano, J. M. Escola, E, Garagorri, J. A. Fernandez, *Polymer Degradation and Stability*, 69 (2000) 11-16.

3 P. Gronchi, A. Kaddouri, P. Centola, R. Del Rosso, *J. Sol-Gel Sci. Tech.* 26 (2003) 843-846.

4 L. Khelifi and A. Ghorbel, *J. Sol-Gel Sci Tech.* 19 (2000) 643-646.

5 H. Meixner, U. Lampe, J. Gerblinger, M. Fleische, *Fresenius J Anal. Chem.* 348 (1994) 536-541.

6 R. A. Bennett and N.D. McCavish, *Topics in Catalysis* 36 (2005) 11-19.

7 Chemistry of Advanced Materials: An Overview, *Wiely-VCH, Inc, Canada*, 1998, Chapt. 9, *Molecular Precursor Routes to Inorganic Solids,* 389–448.

8 G. C. Righini and S. Pelli, *J. Sol-Gel Sci. Tech,* 8 (1997) 991–997.

9 S. Fujihara, M. Tada, T. Kimura, *J. Sol-Gel Sci. Tech.,* 19 (2000) 311–314.

10 R. Thielsch and H. Bottcher, *Chem. Phys. Lett.* 189 (1992) 226 -230.

11 R. A. Jackson, M. E. G. Valerio, M. A. C. dos Santos, *Dalton Trans.* (2004) 3098-3100.

12 M. Dejneka, E. Snitzer, R.E. Riman, *J. Non-Cryst. Solids* 202 (1996) 23-34.

13 R. E. Riman, M. Dejneka, J. Eamsiri, E. Snitzer, A. Mailhot, A. Leaustic, *J. Sol-Gel Sci. Tech.,* 2 (1994) 849–853.

14 P. A. Sermon and R. Badheka, *J. Sol-Gel Sci. Tech.,* 32 (2004) 149–153.

15 Z. Mazej, A. Tressaud, J. Darriet, *J. Fluorine Chem.* 110 (2001) 139-143.

16 A. Moerkerken, B. Behr, M. A. Noordeloos-Mass, C. Boelhouwer, Academic Press, Inc. Lab. Chem. Tech., University of Amsterdam (1971) 177-180.

17 I. Grohmann, A. Hess, E. Kemnitz, W. Fentrup, E. S. Unger, J. Wong, M. Rowen, T. Tanka, M. Föba, *J. Mater. Chem.* 8 (1998) 1453-1457.

18 M. Vecchio and G. Groppelli, *J. Fluorine Chem.* 4 (1974) 117-139.

19 H. dao Quan, H.Yang, M. Tamura, A. Sekiya, *J. Fluorine Chem.* 125 (2004) 1169-1172.

20 A. Sekiya, H. dao Quan, M. Tamura, R. X. Gao, J. Murata, *J. Fluorine Chem.* 112 (2001) 145-148.

21 H. dao Quan, M. Tamura, T. Takagi, A. Sekiya, *J. Fluorine Chem.* 99 (1999) 167-170.

22 O. Boese, E. S. Wolfgang, E. S. Unge, Kemnitz, S. Schroeder, *Phys. Chem. Chem. Phys.* 4 (2002) 2824-2832.

23 G. B. Mc.Vivker, C. J. Kim, J. J. Eagert, *J. Catal.* 80 (1983) 315-327.

24 C. H. Barclay, H. Bozorgadeh, E. Kemnitz, M. Nickkho-Amiry, D. E. M. Ross, T. Skapin, J. Thomson, G. Webb, J. M. Winfield, *J. Chem. Soc., Dalton Trans.* (2002) 40-47.

25 H. J. Reitsma and C. Boelhouwer, *J. Catal.* 33 (1974) 39-46.

26 C. G. Krespan and D. A. Dixon, *J. Fluorine Chem.* 77 (1996) 117-126.

27 J. M. Sanginer, N. A. Sanchez, J. O. Flores, *J. Fluorine Chem.* 88 (1998) 117-125.

28 T. Skapin and E. Kemnitz, *Catalysis Lett.* 40 (1996) 241-247.

29 P. J. Chupas, M. F. Ciraolo, J. C. Hanson, C. P. Grey, *J. Am. Chem. Soc.* 123 (2001) 1694-1702.

30 A. Hess and E. Kemnitz, *J. Catal. 149* (1994) 449-457.

31 A. Hess, E. Kemnitz, A. Lippitz, W.E. S. Unge, D. H. Menz, *J. Catal.* 148 (1994) 270-280.

32 C. Alonso, A. Morato, F. Mendina, F. Guirado, Y. Cesteros, P. Salare, J. E. Sueiras, *Appl. Catal. B: Environ.* 40 (2003) 259-269.

33 C. Alonso, A. Morato, F. Mendina, F. Guirado, Y. Cesteros, P. Salare, J. E. Sueiras, *Chem. Mater.* 12 (2000) 1148-1155.

34 J. L. Delattre, P. J. Chupas, C. P. Grey, A. M. Stacey, *J. Am. Chem. Soc.* 123 (2001) 5364-5365.

35 Kemnitz, U. Groß, St. Rüdiger, C. Shekar, *Angew. Chem. Int. Ed.* 42 (2003) 4251-4254.

36 St. Rüdiger, U. Groß, M. Feist, H. A. Prescott, SC. Shekar, S. I. Troyanov, and E. Kemnitz, *J. Mater. Chem.* 15 (2005) 588-597.

37 St. Rüdiger, G. Eltanany, U. Groß, E. Kemnitz, *J. Sol-Gel Sci. Tech.* 41 (2007) 299–311.

38 K. O. Christe, D. A. Dixon, D. McLemore, W. W. Wilson, J. A Sheehy, J. A. Boatz, *J. Fluorine Chem.* 101 (2000) 151-153.

39 V. A. Petrov, C. G. Krespan, B. E. Smart, *J. Fluorine Chem.* 89 (1998) 125-130.

40 J. K. Murthy, U. Gross, St. Rüdiger, V. V. Rao, V. V. Kumar, A. Wander, C. L. Bailey, N. M. Harrison, E. Kemnitz, *J. Phys. Chem. B.* 110 (2006) 8314-8319.

41 D. J. Suh, T.-J Park, *Chem. Mater.* 14 (2002) 1452–1454.

42 K. Niesz, P. Yang, G.A. Somorjai, *Chem. Commun.* (2005) 1986–1987.

43 http://optoweb.fis.uniroma2.it/opto/solgel.

44 R. J. P: Corriu, D. Leclercq, P. H. Mutin, L. Sarlin, A. Vioux, *J. Mater. Chem.* 8 (1998) 1827-1833.

45 G. K. Chuah, S. Jaenicke, B. K. Pong, *J. Catal.* 175 (1998) 80-92.

46 J. A. Wang, X. Bokhimi, A. Morales, O. Novaro, *J. Phys. Chem. B* 103 (1999) 299-303.

47 J. Sanchez-Valente, X. Bokhimi, F. Hernandez, *Langmuir* 19 (2003) 3583-3588.

48 J. A. Wang, A. Cuan, J. Salmones, N. Nava, S. Castillo, M. Moran-Pineda, F. Rojas, *Appl. Sur. Sci.* 230 (2004) 94-105.

49 R. Diaz, S. Macias, E. Cazares, *J. Sol-Gel Sci. Tech.,* 35 (2005) 13–20.

50 Z. J. Li, H. A. Prescott, J. Deutsch, A. Trunschke, H. Lieske, E. Kemnitz, *Catal. Lett.* 92 (2004) 175-180.

51 A. F. Bedilo and K. J. Klabunde, *J. Catal.* 176 (1998) 448-458.

52 R. A. Comelli, C. R. Vera, J. M. Parera, *J. Catal.* 151 (1995) 96-101.

53 W. Stichert and F. Schüth, *J. Catal.* 174 (1998) 242-245.

54 H. Bozorgzadeh, E. Kemnitz, M. Nickkho-Amiry, T. Skapin, J. M. Winfield, *J. Fluorine Chem.* 110 (2001) 181-189.

55 A. A. Rywak and J. M. Burlitch, *Chem. Mater.* 8 (1996) 60-67.

56 S. Fujihara, T. Kato, T. Kimura, *J. Mater. Sci Lett.* 20 (2001) 687-689.

57 D. J. Talyor and H. M. Meyer, *J. Mater. Sci Lett.* 40 (2005) 2655-2658.

58 J. K. Murthy, U. Groß, St. Rüdiger, E. Ünveren, E. Kemnitz, *J. Fluorine Chem.* 125 (2004) 937-949.

59 J. K. Murthy, U. Groß, St. Rüdiger, E. Kemnitz, *Appl. Catal. A: General* 278 (2004) 133-138.

60 J.K. Murthy, U. Groß, St. Rüdiger, E. Kemnitz, and J.M. Winfield, *J. Solid State Chem.* 179, (2006) 739-746.

61 M. Ahrens, G. Scholz, M. Feist, and E. Kemnitz, *Solid State Sci.* 8 (2006) 798-806.

62 J.K. Murthy, U. Groß, St. Rüdiger, E. Ünveren, W. Unger, and E. Kemnitz, *Applied Catal. A* 282 (2005) 85-91.

63 R. Hoppe and D. Kissel, *J. Fluorine Chem.* 24 (1984) 327-340.

64 A. La Bail, C. Jacobni, M. Leblanc, R. De Pape, H. Duroy, J. L. Fourquet, *J. Solid State Chem.* 77 (1988) 96-101.

65 E. Kemnitz and D. Menz, *Prog. Solid St. Chem.* 26 (1998) 97-153.

66 Y. R. Chen, V. Perebeinos, P. B. Allen, *Phys. Rev. B* 69 (2004) 054109-1- 054109-5.

67 Ph. Daniel, A. Bulou, M. Rousseau, J. Nouet, J. L. Fourquet, M. Leblanc, R. Burriel, *J. Phys. Condens. Matter.* 2 (1990) 5663-5677.

68 A. Wander, B. G. Searle, C. L. Bailey, N. M. Harrison, *J. Phys. Chem. B* 109 (2005) 22935-22938.

69 A. Wander, C. L. Bailey, S. Mukhopadhyay, B. G. Searle, N. M. Harrison, *J. Mater. Chem.* 16 (2006) 1906-1910.

70 A. Wander, C. L. Bailey, B. G. Searle, S. Mukhopadhyay, N. M. Harrison, *Phys. Chem. Chem. Phys.* 7 (2005) 3989-3993.

71 N. Herron, D. L. Thorn, R. L. Harlow, G. A. Jones, J. B. Parise, J. A. Fernandez-Baca, T. Vogt. *Chem. Mater.* 7 (1995) 75-83.

72 N. Herron and W. E. Farneth. *Adv. Mater.* 8 (1996) 959-968.

73 A. La Bail, J. L. Fourquet, U. Bentrup, *J. Solid State Chem.* 100 (1992) 151-159.

74 *Römpp Lexikon Chemie, Version 2.0 [CD-ROM];* Georg-Thieme Verlag: Stuttgart/New York, 1999.

75 P. Lidstroem, J. Tierney, B. Wathey, Westman, *Tetrahedron* 57 (2001) 9225-9283.

76 M. S. Corbillon, M. P. Carril, J. M. Madariaga, I. Uriate, *Analyst,* 120 (1995) 2227–2231.

77 S. Brunauer, P. H. Emmett, E. Teller *J. Am. Chem. Soc*. 60 (1938) 309-319.

78 E. P. Barrett, L. G. Joyner, P. P. Halenda, *J. Am. Chem. Soc.* 73 (1951) 373-380.

79 *PCPDFWIN, Version 1.30 [CD-ROM],* International Centre of Diffraction Data: Newtown Square, Pennsylvania, USA, 1997.

80 C. J. Powell, *Appl. Surf. Sci.* 89 (1995) 141-149.

81 E. Kemnitz, U. Groß, and St. Rüdiger, EP 04008229.9.

82 L. L. Hench and J. K. West, *Chem Rev*. 90 (1990) 33-72.

83 M. Molina and F. S. Rowland, *Nature* 249 (1974) 810-812.

84 V. K. Pecharsky and P. Y. Zavalij, *Fundamentals of Powder Diffraction and Structural Characterization,* Springer, 2005, Chapt. 2, *Fundamentals of Diffraction,* 99–167.

85 C. Morterra, G. Cerrato, P. Cuzzato, Masiero, M. Padovan, *J. Chem. Soc. Faraday Trans.* 88 (1992) 2239-2250.

86 P. J. Chupas, M. F. Ciraolo, J. C. Hanson and C. P. Grey, *J. Am. Chem. Soc.* 123 (2001) 1694 – 1702.

87 T. Krahl, R. Stösser, E. Kemnitz, G. Scholz, M. Feist, G. Silly and J.-Y. Buzare, *Inorg. Chem.* 42 (2003) 6474-6483.

88 D. E. Sayers, E.A. Stern, F.W. Lytle, *Phys. Rev. Lett.,* 27 (1971) 1204-1207.

89 C. D. Wagner, D. E. Passoja, H. F. Hillery, T. G. Kinisky, H. A. Six, W. T. Jansen, J. A. Taylor, *J. Vac. Sci. Technol.* 21 (1982) 933-944.

90 J. A. Taylor, *J. Vac. Sci. Technol.* 20 (1982) 751-755.

91 P. A. Webb and C. Orr, *Analytical Methods in Fine Particle Technology,* Micromeritics Instrument Corp. 1997.

92 G. Leofani, M. Padovan, G. Tozzola, B. Venturelli, *Catal. Today* 41 (1998) 207–219.

93 M. R. Basila, T. R. Kantner, K. H. Rhee, *J. Phys. Chem.* 68 (1964) 3197-3207.

94 C. Morterra and G. Cerrato, *Langmuir* 6 (1990) 1810-1812.

95 M. M. Mohamed, *Spectochimica Acta.* 51A (1995) 1-9.

96 F. E. Klviai and L. Petrakis, *J. Phys. Chem.* 77 (1973) 1232-1239.

97 T. Fransen, O. Van der Meer, P. Mars, *J. Phys. Chem.* 80 (1976) 2103-2106.

98 T. R. Hughes and H. M. White, *J. Phys. Chem.* 71 (1967) 2192-2201.

99 E. Perry, *J. Catal.* 2 (1963) 371-379.

100 C. Morterra, S. Coluccia, A. Chiorino, F. Boccuzzi, *J. Catal.* 54 (1978) 348–364.

101 C. H. Kline Jr. and J. Turkewich, *J. Chem. Phys.* 12 (1944) 300-309.

102 T. H. Ballinger and J. T. Yates Jr., *Langmuir* 7 (1991) 3041-3045.

103 C. Motrerra and G. Magnacca, *Catal. Today* 27 (1996) 497-532.

104 C. Motrerra, G. Cerrato, P. Cuzzato, A. Masiero, M. Padovan, *J. Chem. Soc. Faraday Trans.* 88 (1992) 2239–2250.

105 N. Katada, H. Igi, J. H. Kim, M. Niwa, *J. Chem. Phys. B* 101 (1997) 5969-5977.

106 A. Satsuma, Y. Kamiya, Y. Westi, T. Hattori, *Appl. Catal. A: General* 194-195 (2000) 253-263.

107 H. G. Karge, V. Dondur, J. Weitkamp, *J. Phys. Chem.* 95 (1991) 283-288.

108 H. G. Karge and V. Dondur, *J. Phys. Chem.* 94 (1990) 765-772.

109 M. Niwa, N. Katada, M. Sawa, Y. Murakami, *J. Phys. Chem.* 99 (1995) 8812-8816.

110 M. Blanchard, L. Wendlinger, P. Canesson, *Appl. Catal.* 59 (1990) 123-128.

111 J. B. Peri, *J. Phys. Chem.* 69 (1965) 220-230.

112 J. B. Peri, *J. Phys. Chem.* 69 (1965) 211-219.

113 A. A. Tsyganeko and P. P. Mardilovich, *J. Chem. Soc. Faraday Trans.,* 92 (1996) 4848-4852.

114 J. B. Peri and R. B. Hannan, *J. Phys. Chem.* 64 (1960) 1526-1530.

115 A. Zamora and A. Cordoba, *J. Phys. Chem.* 82 (1978) 584-588.

116 E. Kemnitz, A. Hess, G. Rother, S. Troyanov, *J. Catal.* 159 (1996) 332–339.

117 B. Adamczyka, O. Boesea, N. Weiherb, S.L.M. Schroederb, E. Kemnitz, *J. Fluorine Chem.* 101 (2000) 239-246.

118 T. Krahl, E. Kemnitz, *Angew. Chem. Int. Ed.* 43 (2004) 6653–6656.

119 R. Peacock, D. J. Sharpe, *J. Chem. Soc.* (1959) 2762-2766.

120 U. Groß, St. Rüdiger, E. Kemnitz, K. W. Brzezinka, S. Mukhopadhyay, C. Bailey, A. Wander, N. Harrison, *submitted to Spectroscopy.*

121 P. J. Chupas, D. R. Corbin, N. V. M. Rao, J. C. Hanson, C. P. Grey, *J. Phys. Chem. B* 107 (2003) 8327-8336.

122 P. J. Chupas and C. P. Grey, *J. Catal.* 224 (2004) 69-79.

123 B. Bureau, G. Silly, J.Y. Buzare, J. Emery, *Chem. Phys.* 249 (1999) 89–104.

124 W. Zhang, M. Sun, R. Prins, *J. Phys. Chem. B* 106 (2002) 11805-11809.

125 E. Dumas, F. Taulelle, G. Ferey, *Solid State Sci.* 3 (2001) 613-621.

126 P. J. Chupas and C. P. Grey, *J. Phys. Chem. B* 107 (2003) 8327-8336